



Search for single production of vector-like T quarks decaying into Ht or Zt in pp collisions at $\sqrt{s} = 13$ TeV with the ATLAS detector

The ATLAS Collaboration

This paper describes a search for the single production of an up-type vector-like quark (T) decaying as $T \rightarrow Ht$ or $T \rightarrow Zt$. The search utilises a dataset of pp collisions at $\sqrt{s} = 13$ TeV collected with the ATLAS detector during the 2015–2018 data-taking period of the Large Hadron Collider, corresponding to an integrated luminosity of 139 fb^{-1} . Data are analysed in final states containing a single lepton with multiple jets and b -jets. The presence of boosted heavy resonances in the event is exploited to discriminate the signal from the Standard Model background. No significant excess above the Standard Model expectation is observed, and 95% CL upper limits are set on the production cross section of T quarks in different decay channels. The results are interpreted in several benchmark scenarios to set limits on the mass and universal coupling strength (κ) of the vector-like quark. For singlet T quarks, κ values above 0.53 are excluded for all masses below 2.3 TeV. At a mass of 1.6 TeV, κ values as low as 0.35 are excluded. For T quarks in the doublet scenario, where the production cross section is much lower, κ values above 0.72 are excluded for all masses below 1.7 TeV, and this exclusion is extended to κ above 0.55 for low masses around 1.0 TeV.

1 Introduction

The discovery of a new particle consistent with the Standard Model (SM) Higgs boson by the ATLAS [1] and CMS [2] experiments at the Large Hadron Collider (LHC) represents a milestone in high-energy physics. A comprehensive programme of measurements of the Higgs boson’s properties to unravel its nature is underway at the LHC, so far yielding results compatible with the SM predictions. However, a pressing question remains as to why the electroweak mass scale (and the Higgs boson mass along with it) is so small compared to the Planck scale, a situation known as the hierarchy problem. Naturalness arguments [3] require that quadratic divergences that arise from radiative corrections to the Higgs boson mass are cancelled out by some new mechanism in order to avoid fine-tuning. To that effect, several explanations have been proposed in theories beyond the SM (BSM theories).

One such solution involves the existence of a new strongly interacting sector, in which the Higgs boson would be a pseudo Nambu–Goldstone boson (pNGB) [4] of a spontaneously broken global symmetry. The Composite Higgs [5–7] model is a particular realisation of this scenario, which also addresses additional open questions in the SM, including the hierarchy in the mass spectrum of the SM particles. A key prediction is the existence of new fermionic resonances referred to as vector-like quarks (VLQs), which are also common in many other BSM scenarios [8–11]. Vector-like quarks are defined as colour-triplet spin-1/2 fermions whose left- and right-handed chiral components have the same transformation properties under the weak-isospin SU(2) gauge group [12, 13]. Assuming an unchanged scalar sector with respect to the Standard Model, theoretical constraints on renormalisability and gauge completeness restrict the SU(2) representation of the vector-like quarks to seven possible multiplets: singlets ($T^{2/3}$) or ($B^{-1/3}$), doublets ($X^{5/3} T^{2/3}$) or ($T^{2/3} B^{-1/3}$), or triplets ($X^{5/3} T^{2/3} B^{-1/3}$) or ($T^{2/3} B^{-1/3} Y^{-4/3}$).¹ The vector-like quarks in these models are expected to couple preferentially to third-generation quarks and can have flavour-changing neutral-current decays in addition to the charged-current decays characteristic of chiral quarks [12, 14]. Thus, the up-type T quark can decay into a W boson and a b -quark, and also into a top quark and a Z or Higgs boson. The relative couplings to the massive bosons of the Standard Model are determined by the gauge representation of the vector-like quarks. The relative couplings to the W , Z and Higgs bosons can be expressed in terms of the ξ_W , ξ_Z and ξ_H parameters, respectively [15]. In the asymptotic limit of large VLQ mass, these ξ parameters correspond to the branching ratios of the T quark into their respective decay modes. The asymptotic limit holds to a very good approximation for VLQ masses above 1 TeV. For a T singlet, $\xi_W = 0.5$ and $\xi_Z = \xi_H = 0.25$. For T quarks that are in an ($X T$) doublet, or in a ($T B$) doublet with mixing only to up-type SM singlets [14, 15], $\xi_W = 0$, and $\xi_Z = \xi_H = 0.5$.

At the LHC, vector-like quarks with masses below ~ 1 TeV would be produced mostly in pairs via the strong interaction. For higher masses, however, single production, mediated by the electroweak interaction, may dominate depending on the coupling strength of the interaction between the vector-like quark and the SM quarks [13]. The single-production channel for vector-like quarks provides a unique opportunity to probe the universal coupling strength (κ) in addition to the relative couplings and branching ratios that can be probed in pair production searches. The universal coupling strength controls both the production cross section and the resonance width of the VLQ. For a VLQ with mass m_T , the resonance width Γ_T scales as $\Gamma_T \propto \kappa^2 m_T^3$ [15]. Thus, the relative width (Γ_T/m_T) of the VLQ resonance scales quadratically with both κ and m_T , and is independent of the multiplet representation.

The dominant channel for resonant production of a single T quark is t -channel production mediated by a

¹ The indices in superscript indicate the electric charges of the vector-like quarks. These indices are omitted in the notation for the rest of the paper

gauge boson (Figure 1(a)). The final state is characterised by the presence of multiple (b -tagged) jets from the decay of the produced heavy quarks and bosons, along with the recoiling initial-state quark, which typically manifests as a forward jet. In the four-flavour scheme, and assuming that the T quark couples only to SM quarks of the third generation, this process requires an initial-state gluon to split into a $b\bar{b}$ or $t\bar{t}$ pair. Given the difference in masses between the top and bottom quarks, b -associated (or W -mediated) T -quark production is kinematically favoured over t -associated (or Z -mediated) production. However, in certain gauge representations, such as for a $(T B)$ doublet with mixing only to up-type SM singlets [14, 15], or for an $(X T)$ doublet, the coupling to W bosons vanishes, and the t -associated mode is the only allowed production channel. Therefore, both production modes are theoretically interesting, even though the parameter space in the limit of $\xi_W \rightarrow 0$ is difficult to probe due to small production cross sections. Non-resonant T -quark production (Figure 1(b)) is subdominant compared to resonant production in the b -associated mode. By contrast, in the t -associated mode, both the resonant and non-resonant T -quark production processes have comparable cross sections, as both require the splitting of an initial-state gluon into a $t\bar{t}$ pair. The relative contribution of non-resonant production grows with resonance width, and is therefore larger at higher coupling strengths.

Physical realisations of Composite Higgs models require the presence of additional scalar [16] and vector bosons [17–19] for UV-completeness, thus opening up production and decay channels for the VLQs in addition to the ones discussed above. However, processes involving additional BSM particles are not considered in this paper, and results are interpreted in the context of a minimal extension of the Standard Model including only one VLQ multiplet [15].

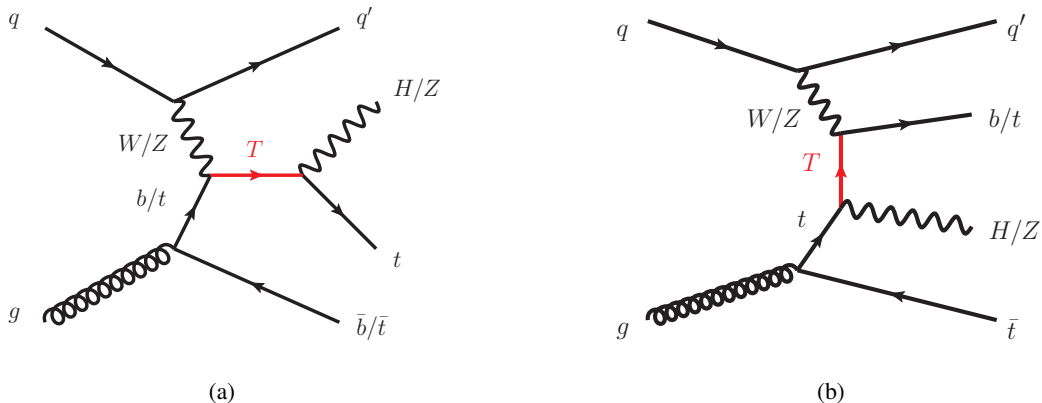


Figure 1: Example of leading-order Feynman diagrams of single vector-like T production in association with a b -quark or t -quark and subsequent decay into either Ht or Zt in the (a) resonant and (b) non-resonant modes.

The ATLAS and CMS collaborations have a broad programme of searches that has largely focused on pair production of vector-like quarks, targeting different decay modes and final states separately. A combination of all ATLAS pair production analyses using the data collected by the ATLAS detector in 2015 and 2016 delivered the most stringent limits to date on pair-produced vector-like quarks [20], with masses observed to be excluded below 1.31 TeV for T and 1.03 TeV for B for any combination of decay modes. The T (B) singlet configuration was excluded for masses up to 1.31 (1.21) TeV, and T (B) quarks in the $(T B)$ doublet configuration were excluded up to masses of 1.37 (1.35) TeV. Searches by both ATLAS [21–24] and CMS [25–30] targeting single vector-like quark production have set limits on the allowed vector-like quark parameter space in terms of model-dependent parameters such as coupling strengths and mixing angles. These searches have mostly focused on the b -associated single production modes for VLQs. A search

by ATLAS for single VLQ production in the $T \rightarrow Wb$ channel has excluded $\sigma \times \mathcal{B}(T \rightarrow Wb)$ above ~ 100 fb for b -associated T production in the mass range of 1.0–1.9 TeV [23]. An ATLAS search [24] in the $T \rightarrow Z(\ell\ell)t$ channel has excluded $\sigma \times \mathcal{B}(T \rightarrow Zt)$ for b -associated T production above ~ 90 fb (~ 40 fb) at a mass of 1.0 TeV (2.0 TeV) in the singlet hypothesis. A CMS search for t -associated T production, also in $T \rightarrow Z(\ell\ell)t$ final states [27], has excluded $\sigma \times \mathcal{B}(T \rightarrow Zt)$ above ~ 100 fb (~ 40 fb) at a mass of 0.8 TeV (1.7 TeV) under the doublet hypothesis. Conversely, the CMS search for T production in the $T \rightarrow Z(\nu\nu)t$ channel [31] excluded $\sigma \times \mathcal{B}(T \rightarrow Zt)$ down to ~ 200 fb (~ 20 fb) at a mass of 0.6 TeV (1.8 TeV) under the singlet hypothesis, for a decay width of 30%. A recently published search by ATLAS in the all-hadronic final state [21] excludes $\sigma \times \mathcal{B}(T \rightarrow Ht)$ for b -associated T production above ~ 30 – 100 fb in the 1.0–2.3 TeV mass range for a wide range of coupling strengths.

These exclusion limits were all derived at 95% CL, assuming that the VLQs couple exclusively to SM quarks in the third generation, and production modes involving other BSM particles were not considered.

This paper presents a search for the single production of the up-type vector-like quark T , with subsequent decays into Ht with $H \rightarrow b\bar{b}$, or into Zt with $Z \rightarrow q\bar{q}$ (Figure 1). Both the b - and t -associated production modes are considered in this search. The search uses 139 fb^{-1} of pp collision data at $\sqrt{s} = 13$ TeV recorded by the ATLAS Collaboration during Run 2 of the Large Hadron Collider (LHC). Data are analysed in the lepton+jets final state, characterised by an isolated electron or muon with high transverse momentum and multiple jets and b -jets. The presence of heavy hadronic boosted objects in the events is used as an important distinguishing characteristic of the signal. In the absence of a significant excess above the SM expectation, the results are used to set upper limits on the single production of T quarks for several scenarios of the mass, the universal coupling strength κ , and the relative couplings to W , Z , and Higgs bosons.

2 ATLAS detector

The ATLAS detector [32] at the LHC covers nearly the entire solid angle around the collision point.² It consists of an inner tracking detector surrounded by a thin superconducting solenoid, electromagnetic and hadron calorimeters, and a muon spectrometer incorporating three large superconducting air-core toroidal magnets.

The inner-detector system is immersed in a 2 T axial magnetic field and provides charged-particle tracking in the range $|\eta| < 2.5$. The high-granularity silicon pixel detector covers the vertex region and typically provides four measurements per track, the first hit normally being in the insertable B-layer installed before Run 2 [33, 34]. It is followed by the silicon microstrip tracker, which usually provides eight measurements per track. These silicon detectors are complemented by the transition radiation tracker (TRT), which enables radially extended track reconstruction up to $|\eta| = 2.0$. The TRT also provides electron identification information based on the fraction of hits (typically 30 in total) above a higher energy-deposit threshold corresponding to transition radiation.

² ATLAS uses a right-handed coordinate system with its origin at the nominal interaction point (IP) in the centre of the detector and the z -axis along the beam pipe. The x -axis points from the IP to the centre of the LHC ring, and the y -axis points upwards. Cylindrical coordinates (r, ϕ) are used in the transverse plane, ϕ being the azimuthal angle around the z -axis. The pseudorapidity is defined in terms of the polar angle θ as $\eta = -\ln \tan(\theta/2)$. Angular distance is measured in units of $\Delta R \equiv \sqrt{(\Delta\eta)^2 + (\Delta\phi)^2}$.

The calorimeter system covers the pseudorapidity range $|\eta| < 4.9$. Within the region $|\eta| < 3.2$, electromagnetic calorimetry is provided by barrel and endcap high-granularity lead/liquid-argon (LAr) calorimeters, with an additional thin LAr presampler covering $|\eta| < 1.8$ to correct for energy loss in material upstream of the calorimeters. Hadron calorimetry is provided by the steel/scintillator-tile calorimeter, segmented into three barrel structures within $|\eta| < 1.7$, and two copper/LAr hadron endcap calorimeters. The solid angle coverage is completed with forward copper/LAr and tungsten/LAr calorimeter modules optimised for electromagnetic and hadronic energy measurements respectively.

The muon spectrometer (MS) comprises separate trigger and high-precision tracking chambers measuring the deflection of muons in a magnetic field generated by the superconducting air-core toroidal magnets. The field integral of the toroids ranges between 2.0 and 6.0 T m across most of the detector. Three layers of precision chambers, each consisting of layers of monitored drift tubes, cover the region $|\eta| < 2.7$, complemented by cathode-strip chambers in the forward region, where the background is highest. The muon trigger system covers the range $|\eta| < 2.4$ with resistive-plate chambers in the barrel, and thin-gap chambers in the endcap regions.

Interesting events are selected by the first-level trigger system implemented in custom hardware, followed by selections made by algorithms implemented in software in the high-level trigger [35]. The first-level trigger accepts events from the 40 MHz bunch crossings at a rate below 100 kHz, which the high-level trigger further reduces in order to record events to disk at about 1 kHz.

An extensive software suite [36] is used in data simulation, in the reconstruction and analysis of real and simulated data, in detector operations, and in the trigger and data acquisition systems of the experiment.

3 Object reconstruction

Interaction vertices from proton–proton collisions are reconstructed from at least two tracks with transverse momentum (p_T) larger than 500 MeV that are consistent with originating from the beam collision region in the x – y plane. If more than one primary vertex candidate is found, the candidate whose associated tracks form the largest sum of squared p_T [37] is selected as the hard-scatter primary vertex.

Electron candidates [38] are reconstructed from energy clusters in the electromagnetic calorimeter associated with reconstructed tracks in the inner detector. They are required to have $p_T > 30$ GeV and $|\eta_{\text{cluster}}| < 2.47$. Candidates in the transition region between the electromagnetic barrel and endcap calorimeters ($1.37 < |\eta_{\text{cluster}}| < 1.52$) are excluded. They are required to satisfy the ‘tight’ likelihood-based identification criteria [38] based on calorimeter, tracking and combined variables that provide separation between electrons and jets. Muon candidates [39] are reconstructed by matching tracks in the MS to those found in the inner detector. The resulting muon candidates are re-fitted using the complete track information from both detector systems. Muon candidates are required to satisfy the ‘medium’ identification criteria [39], and to have $p_T > 30$ GeV and $|\eta| < 2.5$. Electron (muon) candidates are matched to the primary vertex by requiring that the significance of their transverse impact parameter, d_0 , satisfies $|d_0/\sigma(d_0)| < 5(3)$, where $\sigma(d_0)$ is the measured uncertainty in d_0 , and by requiring that their longitudinal impact parameter, z_0 , satisfies $|z_0 \sin \theta| < 0.5$ mm. To further reduce the background from non-prompt leptons, photon conversions and hadrons, the lepton candidates are also required to be isolated in the tracking system and the calorimeter.

Candidate jets are reconstructed with the anti- k_t algorithm [40, 41] with a radius parameter $R = 0.4$ (referred to as ‘small- R jets’). The input constituents for jet reconstruction are built by combining

topological clusters of energy in the calorimeter [42] with measured tracks in the inner detector using the particle-flow algorithm [43]. The reconstructed jets are then calibrated to the particle level by the application of a jet energy scale derived from simulation and *in situ* corrections based on $\sqrt{s} = 13$ TeV data [44]. Calibrated jets are required to have $p_T > 25$ GeV and $|\eta| < 4.5$. Quality criteria are imposed to reject events that contain any jets arising from non-collision sources or detector noise [45]. Jets with $|\eta| < 2.5$ are labelled ‘central’ jets for the purposes of event selection and categorisation, while jets with $2.5 < |\eta| < 4.5$ are called ‘forward’ jets. Requirements based on the jet-vertex tagger (JVT) [46] algorithm are imposed on central jets with $p_T < 60$ GeV and $|\eta| < 2.4$ to suppress contamination from jets that originate from pile-up interactions. Pile-up contamination for jets with $|\eta| > 2.4$ is reduced by requirements on the closely related forward JVT (fJVT) algorithm for jets with $p_T < 120$ GeV [47].

In order to identify b -hadrons in the event, variable- R [48] jets built from reconstructed tracks in the inner detector are used. Track-jets containing b -hadrons are identified (b -tagged) via the multivariate ‘DL1’ algorithm [49], which uses information about the kinematic and topological properties of displaced tracks associated with the jet, and of secondary and tertiary decay vertices reconstructed from these tracks. For each jet, a value of the multivariate b -tagging discriminant is calculated. In this analysis, a jet is considered b -tagged if this value is above the threshold corresponding to an average 77% efficiency to tag a b -quark jet, with a light-jet³ rejection factor of ~ 112 and a charm-jet rejection factor of ~ 5 , as determined for jets with $p_T > 20$ GeV and $|\eta| < 2.5$ in simulated $t\bar{t}$ events.

Overlaps between candidate objects are removed sequentially. Firstly, electron candidates that lie within $\Delta R = 0.01$ of a muon candidate are removed to suppress contributions from muon bremsstrahlung. Overlaps between electron and jet candidates are resolved next, and finally, overlaps between remaining jet candidates and muon candidates are removed. Clusters associated with identified electrons are not excluded during jet reconstruction. In order to avoid double-counting of electrons as jets, the closest jet whose axis is within $\Delta R = 0.2$ of an electron is discarded. If the electron is within $\Delta R = 0.4$ of the axis of any jet after this initial removal, the jet is retained and the electron is removed. The overlap removal procedure applied to the remaining jet candidates and muon candidates is designed to remove those muons that are likely to have arisen in the decay chain of hadrons and to retain the overlapping jet instead. Jets and muons may also appear in close proximity when the jet results from high- p_T muon bremsstrahlung, and in such cases the jet should be removed and the muon retained. Such jets are characterised by having very few matching inner-detector tracks. Selected muons that satisfy $\Delta R(\mu, \text{jet}) < 0.04 + 10 \text{ GeV}/p_T^\mu$ are rejected if the jet has at least three tracks originating from the primary vertex; otherwise the jet is removed and the muon is kept.

The candidate small- R jets surviving the overlap removal procedure discussed above are used as inputs for further jet reclustering [50] using the variable- R jet reconstruction algorithm with $\rho = 550$ GeV. The parameter ρ controls the evolution of the effective size of the reclustered jet as $R = \rho/p_T$. Since the input constituents of these reclustered jets are already calibrated, no further calibration of them is required. Uncertainties in the energy and mass scales and resolutions of the constituent small- R jets are propagated to the kinematics of the reclustered (RC) jets. In order to suppress contributions from pile-up and soft radiation, the RC jets are trimmed [51] by removing all small- R (sub)jets within a RC jet that have p_T below 5% of the p_T of the reclustered jet. Due to the pile-up suppression and $p_T > 25$ GeV requirements imposed on the small- R jets, the average fraction of small- R jets removed by the trimming requirement is less than 1%. The resulting RC jets are required to have $|\eta| < 2.0$ and are used to identify high- p_T hadronically decaying top quark, Higgs boson or W/Z boson candidates by placing requirements on their

³ Light-jet refers to a jet originating from the hadronisation of a light quark (u, d, s) or a gluon.

transverse momentum, mass, and number of constituents. Hadronically decaying top-quark candidates are reconstructed as RC jets with $p_T > 400$ GeV and mass larger than 140 GeV. Top-quark candidates with $p_T < 700$ GeV are required to contain at least two constituent subjets. Higgs boson candidates are reconstructed as RC jets with $p_T > 350$ GeV, a mass between 105 and 140 GeV, and a p_T -dependent requirement on the number of subjets (exactly two for $p_T < 600$ GeV, and one or two for $p_T > 600$ GeV). RC jets are tagged as arising from a W or Z boson if they have $p_T > 350$ GeV, and a mass between 70 and 105 GeV. Furthermore, candidate W/Z (V boson) RC jets are required to have exactly two subjets if they have $p_T < 450$ GeV, while candidates with one or two subjets are allowed at higher p_T . In the following, these are referred to as ‘ t -tagged’, ‘ H -tagged’ and ‘ V -tagged’ jets, respectively, while the term ‘jet’ without further qualifiers is used to refer to central small- R jets.

The missing transverse momentum \vec{p}_T^{miss} (with magnitude E_T^{miss}) is defined as the negative vector sum of the \vec{p}_T of all selected and calibrated objects in the event, including a term to account for energy from soft particles in the event which are not associated with any of the selected objects. This soft term is calculated from inner-detector tracks matched to the selected primary vertex to make it more resilient to contamination from pile-up interactions [52].

To reconstruct boosted leptonic top-quark candidates in the event, the lepton and \vec{p}_T^{miss} in the event are first used to construct a leptonic W -boson candidate. The azimuthal direction and p_T of the neutrino daughter of the W boson are then chosen to be the same as the azimuthal direction and magnitude of the missing transverse momentum, and the neutrino p_z is determined by imposing a W mass constraint on the lepton–neutrino system. This amounts to solving a quadratic equation. If two solutions exist to the quadratic equation, the one with the lowest neutrino p_z is chosen. If no solution exists, the E_T^{miss} value is shifted until the equation has a unique solution. The leptonic W -boson candidate thus constructed is combined with a candidate b -jet in a two-step process. First, the b -tagged track-jet that is closest to the leptonic W -boson candidate in η – ϕ space is identified. Then, the closest small- R jet to this b -tagged jet with $\Delta R < 0.4$ is found and combined with the leptonic W -boson candidate. The b -jet is required to be within $\Delta R = 1.5$ of the leptonic W -boson candidate. Furthermore, in order to avoid double-counting, any b -jet within $\Delta R = 1.0$ of a t -tagged, H -tagged or V -tagged jet is not considered for leptonic top-quark reconstruction. The reconstructed leptonic top-quark candidate is required to have $p_T > 300$ GeV. The average reconstruction efficiency with these requirements in signal events is around 50%.

4 Data sample and event preselection

As described in Section 1, this search is based on a dataset of pp collisions at $\sqrt{s} = 13$ TeV with 25 ns bunch spacing collected by the ATLAS experiment during the 2015–2018 data-taking period, corresponding to an integrated luminosity of 139 fb^{-1} . Only events recorded with a single-electron trigger, a single-muon trigger, or a E_T^{miss} trigger under stable beam conditions and for which all detector subsystems were operational are considered [53].

Single-lepton triggers [54, 55] with low p_T threshold and lepton isolation requirements are combined in a logical OR with higher-threshold triggers without isolation requirements to give maximum efficiency. For muons, triggers with a p_T threshold of 20 (26) GeV in 2015 (2016–2018) and isolation requirements, are combined with triggers with a 50 GeV threshold with no isolation requirement. A trigger with a 60 GeV threshold was added for the 2017–2018 data-taking period. The lowest p_T threshold for electron triggers was 24 (26) GeV in 2015 (2016–2018), while the highest p_T threshold varied from 120 GeV to 300 GeV

Table 1: Summary of preselection requirements.

Preselection requirements
Single-lepton or E_T^{miss} trigger
=1 isolated e OR μ
≥ 3 jets
≥ 1 b -tagged jets
$E_T^{\text{miss}} > 20$ GeV
$E_T^{\text{miss}} + m_T^W > 60$ GeV
$m_{\text{eff}} > 600$ GeV

during the data-taking period. The E_T^{miss} trigger [56] used an E_T^{miss} threshold of 70 GeV in the HLT in 2015 and a run-period-dependent E_T^{miss} threshold varying between 90 GeV and 110 GeV in other years.

Events satisfying the trigger selection are required to have at least one primary vertex candidate, and exactly one selected electron or muon. For events that only pass a single-lepton trigger, the selected lepton is required to match the lepton reconstructed by the trigger within $\Delta R < 0.15$. Events that do not satisfy the single-lepton trigger acceptance or matching conditions are selected only if they pass the E_T^{miss} trigger requirements and the offline reconstructed E_T^{miss} is above 200 GeV. The combination of single-lepton and E_T^{miss} triggers maximises the efficiency of the trigger selection.

In addition to the above, events are required to have at least three small- R jets and at least one b -tagged variable-radius jet. All selected small- R jets are considered for the purpose of event selection and categorisation, including those used to build RC jets.

The background from multijet production is suppressed by placing requirements on E_T^{miss} as well as on the transverse mass of the lepton and E_T^{miss} system (m_T^W):⁴ $E_T^{\text{miss}} > 20$ GeV and $E_T^{\text{miss}} + m_T^W > 60$ GeV.

In order to select events that are kinematically close to those expected from signal, an additional selection is placed on the ‘effective mass’ (m_{eff}) observable, which is defined as the scalar sum of the p_T of all central small- R jets and leptons in the event and the E_T^{miss} . All events considered in the analysis are required to have $m_{\text{eff}} > 600$ GeV.

The above requirements are referred to as the ‘preselection’ and are summarised in Table 1.

5 Signal and background modelling

Signal and background processes were modelled using Monte Carlo (MC) simulations. In the simulation, the masses of the top quark and Higgs boson were set to 172.5 GeV and 125 GeV, respectively. All simulated samples, except those produced with the SHERPA [57] event generator, utilised the EVTGEN program [58] to model the decays of heavy-flavour hadrons. While EVTGEN 1.2.0 was used for $t\bar{t}W$ and $t\bar{t}Z$ samples, EVTGEN 1.6.0 was used for all the other samples. In samples where the parton showering and hadronisation were modelled with PYTHIA 8 [59], a set of tuned parameters called the A14 tune [60] was

⁴ $m_T^W = \sqrt{2p_T^\ell E_T^{\text{miss}}(1 - \cos \Delta\phi)}$, where p_T^ℓ is the transverse momentum (energy) of the muon (electron) and $\Delta\phi$ is the azimuthal angle separation between the lepton and the direction of the missing transverse momentum.

used for underlying-event modelling, and the NNPDF2.3LO parton distribution function (PDF) set [61] was used for the showering and hadronisation processes. The H7UE parameter tune [62] was used instead for samples that employ HERWIG 7 for hadronisation and showering, with the MMHT2014LO PDF set [63].

To model the effects of pile-up, events from minimum-bias interactions were generated using the PYTHIA 8.186 event generator and overlaid on the simulated hard-scatter events according to the luminosity profile of the recorded data. The generated events were processed through a simulation [64] of the ATLAS detector geometry and response using GEANT4 [65]. A faster simulation, where the full GEANT4 simulation of the calorimeter response is replaced by a detailed parameterisation of the shower shapes [66], was adopted for some of the samples used to estimate systematic uncertainties. In these cases, the systematic uncertainties were estimated by comparing these alternative samples with versions of the nominal samples that were also processed through the same fast detector simulation. Simulated events are processed through the same reconstruction software as the data, and corrections are applied so that the object identification efficiencies, energy scales and energy resolutions match those determined from data control samples.

5.1 Signal modelling

Single production of T quarks was simulated with samples produced at leading order in the four-flavour scheme with MADGRAPH5_AMC@NLO 2.3.3 [67], using NNPDF3.0LO [68] PDF sets. The generator was interfaced to PYTHIA 8.212 [69] for the modelling of parton showering and hadronisation. The matrix elements were calculated according to the phenomenological model given in Ref. [15] and all tree-level processes are included. The VLQs are assumed to couple exclusively to SM quarks of the third generation. Separate samples are generated for $T(\rightarrow Ht)qb$, $T(\rightarrow Zt)qb$, $T(\rightarrow Ht)qt$, and $T(\rightarrow Zt)qt$ processes in the 1.0–2.3 TeV mass range at fixed values of mass and κ . Matrix-element-based event weights [70] calculated during the generation are used to reweight the events in each sample to other values of mass and κ , to fill out a grid in the mass– κ plane. Samples at specific values of the relative couplings ξ_W , ξ_Z and ξ_H are obtained by reweighting the samples for the individual production and decay modes according to their corresponding branching fractions and combining them. All signal samples are normalised to cross sections calculated at next-to-leading order (NLO) [71] in quantum chromodynamics (QCD). Since the NLO cross sections were computed in a narrow-width approximation, a correction factor is applied to them to account for finite-width effects [72] and an additional correction is applied to account for non-resonant T -quark production [73]. A change in the dynamic scale in MADGRAPH at the threshold $\Gamma_T/m_T = 0.1$ leads to a discontinuity in the computed cross section [73]. As a result, two different parameterisations of the cross section are available: $\sigma_{\text{low}}(\Gamma_T/m_T)$ for the $\Gamma_T/m_T < 0.1$ regime, and $\sigma_{\text{high}}(\Gamma_T/m_T)$ for $\Gamma_T/m_T > 0.1$. An averaging procedure is used in order to obtain a smooth cross section $\sigma(\Gamma_T/m_T)$ across the mass and coupling grid:

$$\sigma(\Gamma_T/m_T) = \begin{cases} \sigma_{\text{low}}(\Gamma_T/m_T) + \frac{1}{2}(\sigma_{\text{high}}(0.1) - \sigma_{\text{low}}(0.1)), & \text{if } \Gamma_T/m_T < 0.1 \\ \sigma_{\text{high}}(\Gamma_T/m_T) - \frac{1}{2}(\sigma_{\text{high}}(0.1) - \sigma_{\text{low}}(0.1)), & \text{if } \Gamma_T/m_T \geq 0.1 \end{cases}$$

An additional uncertainty of $\frac{1}{2}(\sigma_{\text{high}}(0.1) - \sigma_{\text{low}}(0.1))$ is assigned to the cross section at every point to account for this choice.

5.2 Background modelling

After preselection, the main source of background is the production of $t\bar{t}$. The production of a top quark in association with a W boson (Wt) makes significant contributions in regimes of high transverse momentum. The remaining background contributions originate mostly from W +jets processes.

The production of $t\bar{t}$ and single-top-quark events was modelled using the POWHEG BOX v2 [74–77] generator at NLO with the NNPDF3.0_{NLO} [68] PDF set. The h_{damp} parameter⁵ for $t\bar{t}$ samples was set to $1.5 m_{\text{top}}$ [78]. The events were interfaced to PYTHIA 8.230 [69] to model the parton shower, hadronisation, and underlying event.

Samples to model Wt production were generated using the diagram removal scheme [79], which is designed to remove interference and overlap with $t\bar{t}$ production. The related uncertainty is estimated by comparison with an alternative sample generated using the diagram subtraction scheme [78, 79] and the same generator set-up as the nominal sample. Separate samples were generated to model s -channel and t -channel single top-quark production.

The uncertainty associated with using the chosen parton shower and hadronisation model is evaluated by comparing the sample from the nominal generator set-up with a sample also produced with the POWHEG BOX v2 [74–77] generator using the NNPDF3.0_{NLO} [68] PDF set, but with the events interfaced with HERWIG 7.04 [62, 80] to model the parton shower and hadronisation.

To assess the uncertainty in the matching of NLO matrix elements and parton showers for $t\bar{t}$ samples, the POWHEG BOX sample is compared with a sample of events generated with MADGRAPH5_AMC@NLO 2.6.0 interfaced with PYTHIA 8.230 [69]. The samples used to estimate this uncertainty for single top-quark production were generated with MADGRAPH5_AMC@NLO 2.6.2, also interfaced with PYTHIA 8.230 [69]. For both samples, the NNPDF3.0_{NLO} set of PDFs [68] was used in the matrix-element calculations.

The $t\bar{t}$ samples were generated inclusively, but events are categorised depending on the flavour content of additional particle jets not originating from the decay of the $t\bar{t}$ system (see Ref. [81] for details). Events labelled as either $t\bar{t}+\geq 1b$ or $t\bar{t}+\geq 1c$ are generically referred to in the rest of the paper as $t\bar{t}$ +HF events, where HF stands for ‘heavy flavour’. The remaining events are labelled as $t\bar{t}$ +light-jets events, including those with no additional jets.

The inclusive cross section for $t\bar{t}$ production was corrected to the theory prediction at next-to-next-to-leading order (NNLO) in QCD including the resummation of next-to-next-to-leading logarithmic (NNLL) soft-gluon terms calculated using TOP++ 2.0 [82–88]. For proton–proton collisions at a centre-of-mass energy of $\sqrt{s} = 13$ TeV, this cross section corresponds to $\sigma(t\bar{t})_{\text{NNLO+NNLL}} = 832 \pm 51$ pb using a top-quark mass of $m_{\text{top}} = 172.5$ GeV. The cross-section uncertainties due to the PDF and α_s were calculated using the PDF4LHC15 prescription [89] with the MSTW2008_{NNLO} [90, 91], CT10_{NNLO} [92, 93] and NNPDF2.3_{LO} [61] PDF sets in the five-flavour scheme, and were added in quadrature to the effect of the factorisation and renormalisation scale uncertainties.

The production of $W/Z(V)$ +jets was simulated with the SHERPA 2.2.1 [94] generator using NLO matrix elements for up to two partons, and leading-order (LO) matrix elements for up to four partons, calculated with the Comix [95] and OPENLOOPS 1 [96–98] libraries. They were matched with the SHERPA parton shower [99] using the MEPS@NLO prescription [100–103] and the set of tuned parameters developed by

⁵ The h_{damp} parameter is a resummation damping factor and one of the parameters that controls the matching of POWHEG BOX matrix elements to the parton shower and thus effectively regulates the high- p_T radiation against which the $t\bar{t}$ system recoils.

the SHERPA authors. The NNPDF3.0_{NNLO} set of PDFs [68] was used and the samples are normalised to a NNLO prediction [104].

Samples of diboson final states (VV) were simulated with the SHERPA 2.2.1 or 2.2.2 [94] generator depending on the process, including off-shell effects and Higgs boson contributions, where appropriate. Only processes with at least one lepton in the final state are considered in this search. Fully leptonic final states and semileptonic final states, where one boson decays leptonically and the other hadronically, were generated using matrix elements at NLO accuracy in QCD for up to one additional parton and at LO accuracy for up to three additional parton emissions. Samples for the loop-induced processes $gg \rightarrow VV$ were generated using LO-accurate matrix elements for up to one additional parton emission for both the cases of fully leptonic and semileptonic final states. The matrix-element calculations were matched and merged with the SHERPA parton shower based on Catani–Seymour dipole factorisation [95, 99] using the MEPS@NLO prescription [100–103]. The virtual QCD corrections were provided by the OPENLOOPS 1 library [96–98]. The NNPDF3.0_{NNLO} set of PDFs was used [68], along with the dedicated set of tuned parton-shower parameters developed by the SHERPA authors.

The production of $t\bar{t}W$ and $t\bar{t}Z$ events was modelled using the MADGRAPH5_AMC@NLO 2.3.3 [67] generator at NLO with the NNPDF3.0_{NLO} [68] PDF set. The events were interfaced to PYTHIA 8.210 [69]. The production of $t\bar{t}H$ events was modelled using the POWHEG BOX v2 [74–77, 105] generator at NLO with the NNPDF3.0_{NLO} [68] PDF set. The production of tH events was modelled using the MADGRAPH5_AMC@NLO 2.3.3 [67] generator at NLO with the NNPDF3.0_{NLO} [68] PDF set. Events in both of these samples were interfaced with PYTHIA 8.230 [69] for showering and hadronisation. The production of four-top-quark events in the SM was simulated at LO using MADGRAPH5_AMC@NLO 2.2.2 and the NNPDF2.3_{LO} PDF set, interfaced to PYTHIA 8.186 in combination with the A14 underlying-event tune, and normalised to the NLO theoretical cross section.

Multijet events were generated using PYTHIA 8.230 [69] with leading-order matrix elements for dijet production and interfaced to a p_T -ordered parton shower. Events from this simulation are normalised to data in a multijet-enriched region obtained by inverting the requirements on the E_T^{miss} and m_T^W observables in the preselection, and also requiring the lepton p_T to be below 100 GeV.

6 Analysis strategy

The search described in this paper targets the production of a single T quark that decays to a leptonically decaying top quark and a hadronically decaying Higgs or Z boson. Both b -associated and t -associated single- T production are considered in the search. The four resulting production and decay modes are:

1. $T(\rightarrow Zt)qb$: b -associated T production with $T \rightarrow Zt$ decay
2. $T(\rightarrow Ht)qb$: b -associated T production with $T \rightarrow Ht$ decay
3. $T(\rightarrow Zt)qt$: t -associated T production with $T \rightarrow Zt$ decay
4. $T(\rightarrow Ht)qt$: t -associated T production with $T \rightarrow Ht$ decay

To test for the presence of signal, a likelihood fit is performed on the distribution of the m_{eff} variable (defined in Section 4) across a set of 24 ‘fit regions’ constructed from events in the preselection sample. These regions are summarised in Table 2. The fit regions are designed to be pure in one or more of the four targeted signal modes, or in specific background processes. The combined use of these regions in the fit

allows the search to retain sensitivity to all of the processes that can occur simultaneously in a benchmark model, and the signal-depleted regions serve to improve the description of the expected background. In the following, the strategy and motivation behind the event categorisation model is described.

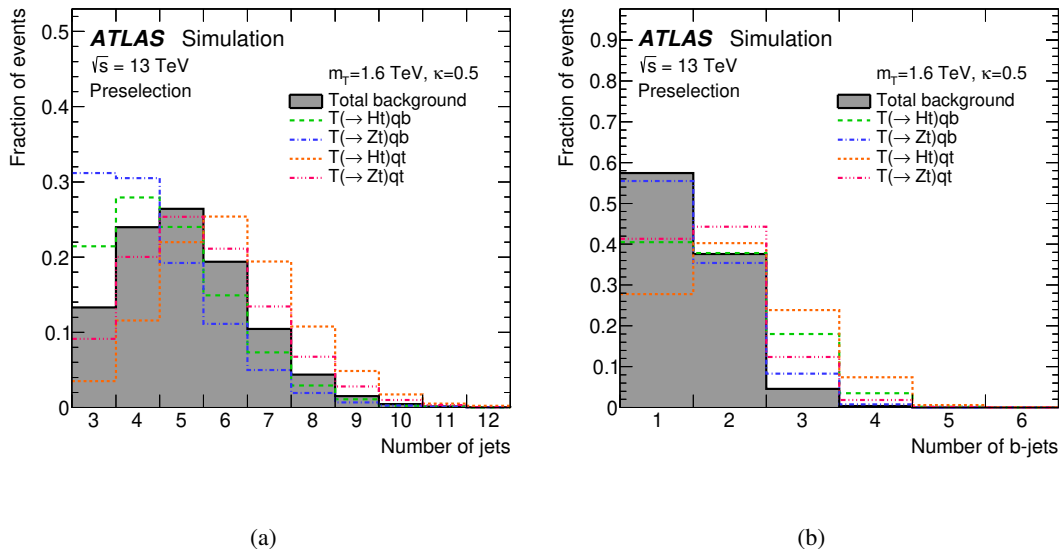


Figure 2: Comparison of the shape of the distribution of (a) the central jet multiplicity, and (b) the b -tagged jet multiplicity in the preselection region, between the total background (filled area) and the signal scenarios considered in this search for T quarks with a mass of 1.6 TeV and $\kappa = 0.5$. The last bin in each distribution contains the overflow.

Different T -quark production modes can be distinguished by the number of jets in the final state, as illustrated in Figure 2(a). For b -associated signal production with a leptonically decaying top quark and hadronically decaying Higgs or Z boson, four central jets are expected in the final state at leading order in the four-flavour scheme. However, some of these jets can merge due to the collimation of the decay daughters from boosted Higgs or Z bosons. Furthermore, the initial b -quark from gluon splitting can sometimes be produced at high pseudorapidity and therefore not be reconstructed in the central region. Conversely, since exactly one lepton is required to be present in the final state, one of the top quarks in events with t -associated production can be expected to decay hadronically, producing extra jets. Based on these arguments, the basic category of regions targeting b -associated production modes (henceforth labelled as LJ, standing for ‘Low Jet multiplicity’) are required to have 3–5 jets, while regions targeting t -associated production modes (henceforth labelled as HJ, standing for ‘High Jet multiplicity’) are required to have ≥ 6 jets.

The different T -quark decay modes are characterised by differences in the multiplicity of b -tagged jets (Figure 2(b)). Events with $T \rightarrow Zt$ decays typically contain fewer b -jets than events with $T \rightarrow Ht$ decays, due to the dominant Higgs boson decay to bottom-quark pairs. Accordingly, regions targeting $T \rightarrow Zt$ decays are required to have exactly 1 or 2 b -tagged jets, while events with exactly 3 or ≥ 4 b -tagged jets are used to target $T \rightarrow Ht$ decays.

Since the top quark, Z boson or Higgs boson daughters of the heavy T quark are often produced at high- p_T in boosted states, signal events are characterised by high multiplicities of tagged boosted objects. The distribution of the multiplicities of H -tagged (H) jets, leptonic top-quark (t_l) candidates, t -tagged (t_h) jets, and V -tagged (V) jets in the preselection region are shown in Figures 3(a)–3(d). The specific requirements

on the multiplicities of these boosted objects that are applied in each fit region are tailored to the signal or background process targeted by that particular region. For example, regions in the $\geq 3b$ categories are designed to be sensitive to $T \rightarrow Ht$ signals, and therefore at least one H -tagged jet is required in these regions. Conversely, at least one V -tagged jet is required in all regions of the 1–2b category, since these regions target $T \rightarrow Zt$ decays. Signal events with t -associated T -quark production contain an additional top quark that can decay hadronically. Therefore, the presence of a hadronic top-tagged jet is required in some signal regions. Events can also have V -tagged jets arising from semi-boosted hadronic top quarks, in cases where the decay products of the top quark are not collimated enough to produce a t -tagged jet. Finally, an LJ region and HJ region are used in the fit to constrain the normalisation of $t\bar{t}+\geq 1b$ and $t\bar{t}+\geq 1c$ backgrounds, requiring $\geq 4b$ and no boosted hadronic objects.

As discussed in Section 1, the initial quark recoiling from the gauge boson in single- T production often emerges at high pseudorapidity, resulting in the presence of jets in the forward region (Figure 3(e)). Thus, at least one forward jet (fj) is required in the signal-enriched fit regions to increase the signal purity. On the other hand, a 0fj requirement is applied in the regions used to control the $t\bar{t}+\geq 1b$ and $t\bar{t}+\geq 1c$ background normalisations, in order to deplete the signal fraction in those regions.

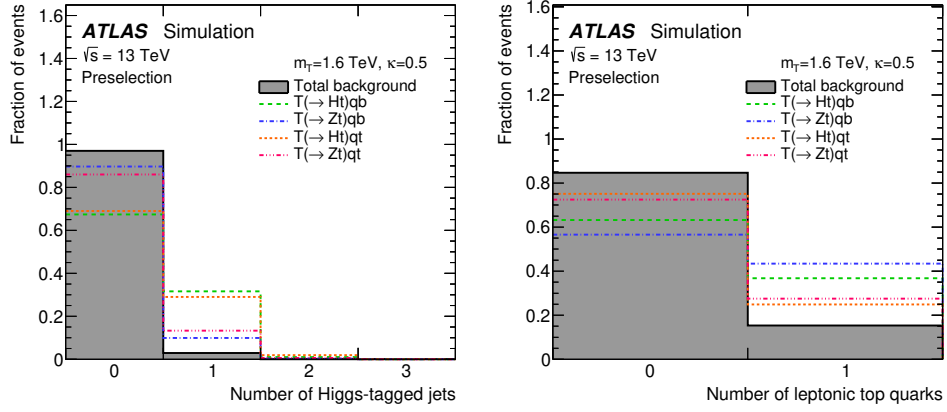
Background predictions in the fit regions are validated in a set of 20 validation regions, designed to be statistically independent of the fit regions and yet kinematically similar to them (Table 3). These regions are created by adopting a combination of inverted tagged boosted-object multiplicity requirements, or specifically vetoing forward jets. The maximum allowed signal contamination in the overall yield in each validation region is required to be $< 10\%$, assuming a signal cross section of 100 fb. This value was chosen as an upper bound on the allowed cross section in the considered mass range, corresponding to the observed exclusion limits from previous searches.

The choice of m_{eff} as the final fitted observable is driven by the strong signal discrimination power of this observable, as can be seen in Figure 3(f). Due to the presence of highly energetic jets and leptons from the decay of the T quark, the average m_{eff} in signal events is much larger than in background events. The shape of the m_{eff} distribution depends on the assumed mass m_T of the T quark, as well as on the T -quark production and decay modes. In particular, an extra factor of m_T^2/s leads to an enhancement of the partonic cross section at low centre-of-mass energies for the $T(\rightarrow Ht)qb$ and $T(\rightarrow Ht)qt$ processes [106], and consequently the m_{eff} distribution shifts to lower values.⁶ Nevertheless, the discrimination power of this observable is relatively independent of the signal model parameters, and the search is therefore sensitive across a wide range of parameter space.

⁶ Again, m_T refers to the mass of the T quark, and s is the usual Mandelstam variable.

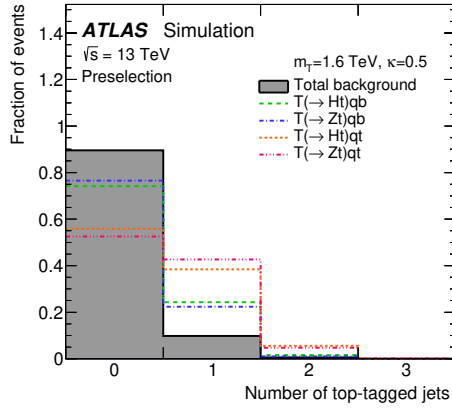
Table 2: Definition of the 24 regions (referred to as ‘fit regions’) that enter the likelihood fit. Events are categorised in terms of jet (j), b -tagged jet (b), forward jet (fj), V -tagged jet (V), Higgs-tagged jet (H), hadronic top-tagged jet (t_h), and leptonic top-quark candidate (t_l) multiplicities.

Fit regions				
Jet mult.	b -tag mult.	Region	Targeted signal / bkg	
3–5	1	LJ, 1b, ≥ 1 fj, 0(t_h+t_l), 0H, ≥ 1 V	$T(\rightarrow Zt)qb$	
		LJ, 1b, ≥ 1 fj, 0 t_h , ≥ 1 t_l , 0H, ≥ 1 V		
	2	LJ, 2b, ≥ 1 fj, 0(t_h+t_l), 0H, ≥ 1 V		
		LJ, 2b, ≥ 1 fj, 0 t_h , ≥ 1 t_l , 0H, ≥ 1 V		
	3	LJ, 3b, ≥ 1 fj, 0(t_h+t_l), ≥ 1 H, 0V		$T(\rightarrow Ht)qb$
		LJ, 3b, ≥ 1 fj, 0 t_h , ≥ 1 t_l , ≥ 1 H, 0V		
		LJ, 3b, ≥ 1 fj, ≥ 1 t_h , 0 t_l , ≥ 1 H, 0V		
		LJ, ≥ 4 b, ≥ 1 fj, 0(t_h+t_l), ≥ 1 H, 0V		
	≥ 4	LJ, ≥ 4 b, ≥ 1 fj, 0 t_h , ≥ 1 t_l , ≥ 1 H, 0V		
		LJ, ≥ 4 b, ≥ 1 fj, ≥ 1 t_h , 0 t_l , ≥ 1 H, 0V		
		LJ, ≥ 4 b, 0fj, ≥ 1 t_l , 0H, 0(V+ t_h)	$t\bar{t}+\geq 1b, t\bar{t}+\geq 1c$	
≥ 6	1	HJ, 1b, ≥ 1 fj, 0 t_h , 1 t_l , 0H, ≥ 1 V	$T(\rightarrow Zt)qt$	
		HJ, 1b, ≥ 1 fj, 1 t_h , 0 t_l , 0H, ≥ 1 V		
		HJ, 1b, ≥ 1 fj, ≥ 2 (t_h+t_l), 0H, ≥ 1 V		
	2	HJ, 2b, ≥ 1 fj, 0 t_h , 1 t_l , 0H, ≥ 1 V		
		HJ, 2b, ≥ 1 fj, 1 t_h , 0 t_l , 0H, ≥ 1 V		
		HJ, 2b, ≥ 1 fj, ≥ 2 (t_h+t_l), 0H, ≥ 1 V		
	3	HJ, 3b, ≥ 1 fj, 1 t_l , ≥ 1 H, 0(V+ t_h)		$T(\rightarrow Ht)qt$
		HJ, 3b, ≥ 1 fj, 0 t_l , ≥ 1 H, 1(V+ t_h)		
		HJ, 3b, ≥ 1 fj, ≥ 1 H, ≥ 2 (V+ t_l+t_h)		
		HJ, ≥ 4 b, ≥ 1 fj, 1 t_l , ≥ 1 H, 0(V+ t_h)		
≥ 4	HJ, ≥ 4 b, ≥ 1 fj, 0 t_l , ≥ 1 H, 1(V+ t_h)			
	HJ, ≥ 4 b, ≥ 1 fj, ≥ 1 H, ≥ 2 (V+ t_l+t_h)			
	HJ, ≥ 4 b, 0fj, ≥ 1 t_l , 0H, 0(V+ t_h)	$t\bar{t}+\geq 1b, t\bar{t}+\geq 1c$		

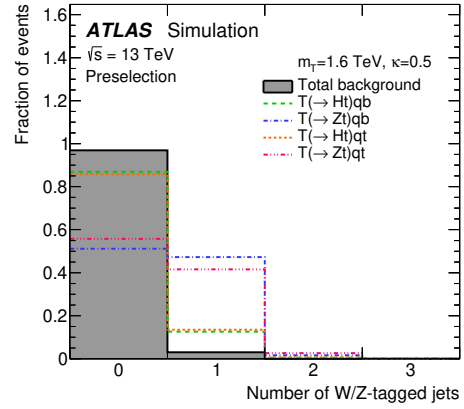


(a)

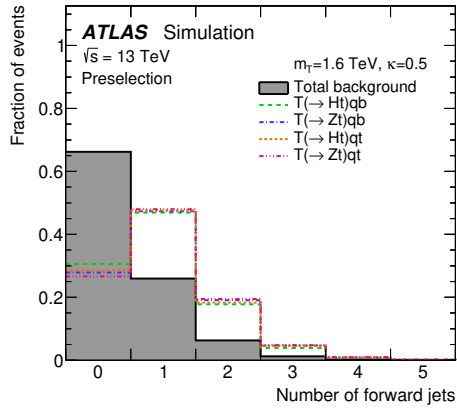
(b)



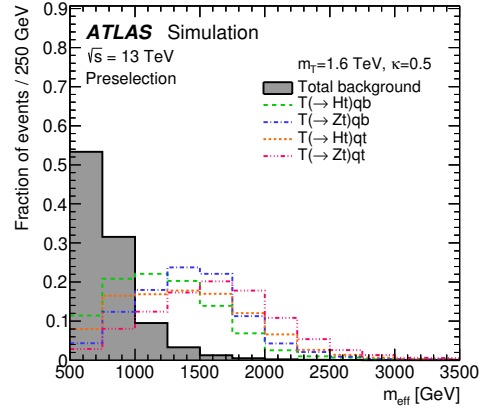
(c)



(d)



(e)



(f)

Figure 3: Comparison of the shape of the distribution of (a) Higgs-tagged jet multiplicity, (b) leptonic top-quark candidate multiplicity, (c) hadronic top-tagged jet multiplicity, (d) W/Z -tagged jet multiplicity, (e) the forward jet multiplicity, and (f) the effective mass m_{eff} , between the total background (filled area) and the signal scenarios considered in this search for a T with a mass of 1.6 TeV and $\kappa = 0.5$, in the preselection region. The last bin in each distribution contains the overflow.

Table 3: Event categorisation into validation regions in terms of jet (j), b -tagged jet (b), forward jet (fj), V -tagged jet (V), Higgs-tagged jet (H), hadronic top-tagged jet (t_h), and leptonic top-quark candidate (t_l) multiplicities. The selection follows the same principle as the fit region categorisation defined in Table 2, but maintains orthogonality by inverting either the forward jet cut or the cuts on tagged boosted objects.

Validation regions		
Jet mult.	b -tag mult.	Region
3–5	1	LJ, 1b, 0fj, 0 t_h , 0 t_l , 0H, $\geq 1V$
		LJ, 1b, 0fj, 0 t_h , $\geq 1t_l$, 0H, $\geq 1V$
		LJ, 1b, $\geq 1fj$, $\geq 1(t_h+t_l)$, 0H, 0V
		LJ, 1b, $\geq 1fj$, $\geq 1t_h$, 0 t_l , 0H, $\geq 1V$
	2	LJ, 2b, 0fj, 0 t_h , 0 t_l , 0H, $\geq 1V$
		LJ, 2b, 0fj, 0 t_h , $\geq 1t_l$, 0H, $\geq 1V$
		LJ, 2b, $\geq 1fj$, $\geq 1(t_h+t_l)$, 0H, 0V
		LJ, 2b, $\geq 1fj$, $\geq 1t_h$, 0 t_l , 0H, $\geq 1V$
	≥ 3	LJ, $\geq 3b$, 0fj, 0(t_h+t_l), $\geq 1H$, 0V
LJ, $\geq 3b$, $\geq 1fj$, 0H, $\geq 1(V+t_l+t_h)$		
≥ 6	1	HJ, 1b, 0fj, 1(t_h+t_l), 0H, $\geq 1V$
		HJ, 1b, 0fj, $\geq 2(t_h+t_l)$, 0H, $\geq 1V$
		HJ, 1b, $\geq 1fj$, 0 t_h , 0 t_l , $\geq 1H$, $\geq 1V$
		HJ, 1b, $\geq 1fj$, $\geq 2(t_h+t_l)$, $\geq 1H$, 0V
	2	HJ, 2b, 0fj, 1(t_h+t_l), 0H, $\geq 1V$
		HJ, 2b, 0fj, $\geq 2(t_h+t_l)$, 0H, $\geq 1V$
		HJ, 2b, $\geq 1fj$, 0 t_h , 0 t_l , $\geq 1H$, $\geq 1V$
		HJ, 2b, $\geq 1fj$, $\geq 2(t_h+t_l)$, $\geq 1H$, 0V
	≥ 3	HJ, $\geq 3b$, 0fj, $\geq 1H$, $\geq 1(V+t_l+t_h)$
HJ, $\geq 3b$, $\geq 1fj$, 0H, $\geq 1(V+t_l+t_h)$		

7 Kinematic reweighting of background

Recent measurements of differential cross sections have demonstrated that the current simulations of $t\bar{t}$ processes overestimate the upper tail of the top-quark p_T spectrum [107, 108]. Conversely, the cross section for this process is underestimated at high jet multiplicities [107]. There are similar issues of accuracy in the modelling of W +jets processes [109] in the regime of high jet multiplicities and/or high- H_T (where H_T is defined as the scalar sum of the p_T of central jets in the event). This leads to discrepancies in the shapes of the m_{eff} and N_{jets} spectra between the data and expected background in the kinematic regimes relevant for this search. Data-driven reweighting factors are therefore used to correct the observed discrepancies in these processes. These corrections are derived using the following iterative procedure.

For a given group of background processes, a ‘reweighting source region’ (RSR) is first identified, which is enriched in events from that process group, and depleted in signal events. Then, the reweighting factor $R_a(x)$ for any observable x , for the process group a , can be calculated as

$$R_a(x) = \frac{\text{Data}(x) - \text{MC}^{\text{non-}a}(x)}{\text{MC}^a(x)}.$$

For each group of processes, reweighting factors are first derived from the jet multiplicity distribution. After correcting the N_{jets} distribution of the process with this initial reweighting, a second set of reweighting factors is derived as a function of a reduced m_{eff} variable, which is defined as $m_{\text{eff}}^{\text{red}} = m_{\text{eff}} - (N_{\text{jets}} - 3) \times 50$ GeV. The constant value of 50 GeV approximately corresponds to the average p_T of each additional jet expected in $t\bar{t}$ events. Thus, this definition makes the shape of the reweighting functions in the $m_{\text{eff}}^{\text{red}}$ variable more consistent across N_{jets} . The residual dependence on N_{jets} is addressed by deriving the reweighting in exclusive N_{jets} bins. The $m_{\text{eff}}^{\text{red}}$ reweighting factors are parameterised by sigmoid functions to mitigate statistical fluctuations.

The subdominant $W(\ell\nu)$ +jets background process is corrected first. However, since it is difficult to isolate $W(\ell\nu)$ +jets events in the preselection sample with $\geq 1b$ selection, the correction factors for this process are extrapolated from a sample enriched in $Z(\ell\ell)$ +jets instead. This sample is obtained by selecting events containing exactly two leptons with the same flavour and opposite electric charges, and requiring the invariant mass of the lepton pair ($m_{\ell\ell}$) to be consistent with the Z boson mass (m_Z). To match the kinematic regime of the preselection more closely, events in this sample must also contain at least three small- R jets, at least one of which is b -tagged. Contamination from $t\bar{t}$ processes is suppressed by requiring $E_T^{\text{miss}} < 100$ GeV. The corrections derived from this sample are applied to both the W +jets and Z +jets events in the preselection sample, before correction factors for the $t\bar{t}$ background are derived.

Since $t\bar{t}$ events share the same final state as tW production, these two processes are grouped together for the purposes of deriving the reweighting factors. A sample enriched in $t\bar{t}$ +light-jets and tW production, selected by requiring exactly one lepton, at least three small- R jets and exactly two b -jets, is used to derive combined correction factors for both processes. The same correction factors are also applied to the $t\bar{t}+\geq 1b$ and $t\bar{t}+\geq 1c$ processes in the analysis.

The selection requirements for the RSRs are summarised in Table 4.

The m_{eff} distribution in the preselection region, before and after the application of the full reweighting, is shown in Figure 4. Since the preselection region is kinematically very close to the RSRs, almost perfect agreement can be seen between the data and the expected background after reweighting. As explained later in Section 8, dedicated reweighting factors are derived for the alternative simulations that

Table 4: Reweighting source regions from which the reweighting functions for $t\bar{t}$ and tW production and W/Z +jets production are derived.

Reweighting source regions				
Lepton multiplicity	Jet multiplicity	b -tag multiplicity	Other requirements	Targeted background
1	≥ 3	2	–	$t\bar{t} + tW$
2	≥ 3	1	$ m_{\ell\ell} - m_Z \leq 10 \text{ GeV},$ $E_T^{\text{miss}} < 100 \text{ GeV}$	Z +jets

are used to estimate the modelling uncertainties for $t\bar{t}$, Wt and W/Z +jets backgrounds. As a result, the modelling uncertainties of these background processes vanish in the RSRs, and are small in regions that are kinematically close to them. This is reflected in the small uncertainty bands seen in Figure 4. The reweighted modelling uncertainties in the fit and validation regions are substantially larger, since they are kinematically further away from the RSRs.

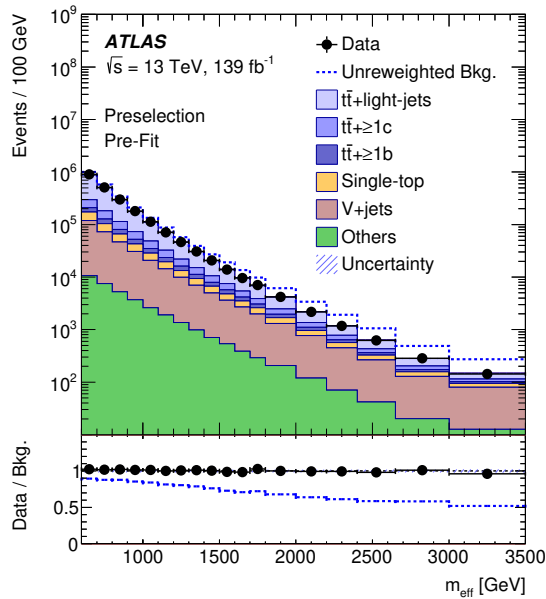


Figure 4: Comparison of the m_{eff} distribution between the data and unweighted (blue dashed line) and reweighted (stacked histograms) background predictions in the preselection region before the likelihood fit. The ‘others’ background includes the $t\bar{t} V/H$, VH , tZ , $t\bar{t}t\bar{t}$, diboson, and multijet backgrounds. The last bin in the distribution contains the overflow. The bottom panel displays the ratios of data to the total background predictions.

8 Systematic uncertainties

The impact of several sources of systematic uncertainty on the normalisation of signal and background and/or the shape of the m_{eff} distributions is considered. Each systematic uncertainty is considered to be

correlated across processes, channels, and bins of the signal discriminant, unless explicitly stated otherwise. Uncertainties from different sources are considered to be uncorrelated with each other.

The leading sources of uncertainty in this search arise from the modelling of the $t\bar{t}$ and single-top Wt backgrounds, the flavour-tagging efficiencies (b , c and light), and the jet mass resolution. The relative contributions of these uncertainties vary depending on the analysis region, and therefore their relative impact on the search sensitivity depends on the signal process being considered. The following sections describe each of the systematic uncertainties considered in this analysis. An overview of the combined impact of the different groups of systematic uncertainties is furthermore given in Table 7.

8.1 Experimental uncertainties

Uncertainties associated with leptons arise from the efficiencies of the trigger selection, reconstruction, identification, and isolation criteria, as well as the lepton momentum scale and resolution. These are measured in data using $Z \rightarrow \ell^+\ell^-$, $W \rightarrow \ell\nu$ and $J/\psi \rightarrow \ell^+\ell^-$ events [39, 110]. The combined effect of all these uncertainties results in an overall normalisation uncertainty in signal and background of approximately 1%.

Uncertainties associated with jets arise from the jet energy scale (JES) and resolution (JER), the jet mass scale (JMS) and resolution (JMR), and the efficiency of the JVT requirements imposed to reject jets from pile-up. The JES and JER uncertainties are estimated by combining information from collision data, test-beam data and simulation [44, 111]. The JES (JER) uncertainties are split into 30 (8) uncorrelated components, corresponding to different physical sources. The uncertainty in the JMS is estimated by comparing each nominal sample with two corresponding alternative event samples, in which the mass of each jet is either raised or lowered by 10%, respectively. The uncertainty in the JMR is estimated by comparing each nominal sample with an alternative event sample in which the mass of each jet is smeared by a Gaussian function whose width is shifted by 20% relative to the nominal JMR. As previously mentioned, the above uncertainties associated with jets are propagated to the RC jets from which the hadronic tagged boosted objects are constructed.

The flavour-tagging efficiencies for b -, c -, and light-jets in simulation are corrected to match efficiencies measured in data control samples. Uncertainties in these efficiencies are also estimated in these auxiliary measurements, following the methods described in Refs. [112–114]. A set of nine independent uncertainty sources are considered for b -jets, while five sources are considered for c -jets, and six components are considered for light-flavour jets. These components are taken to be uncorrelated among b -jets, c -jets, and light-jets. An additional extrapolation uncertainty component is considered for high- p_T jets that are outside the kinematic reach of the calibration data sample; it is taken to be correlated amongst the jet flavours. Finally, an uncertainty related to the application of the c -jet scale factors to τ -jets is considered, but has a negligible impact in this analysis.

8.2 Background modelling uncertainties

An uncertainty of +5.5/−6.1% is assigned to the inclusive $t\bar{t}$ production cross section [88], including contributions from varying the factorisation and renormalisation scales, and from uncertainties in the PDF, α_s , and the top-quark mass, all added in quadrature. Normalisation uncertainties of 50% each are assigned to the normalisation of $t\bar{t}+\geq 1b$ and $t\bar{t}+\geq 1c$ processes. These uncertainties are motivated by the observed level of agreement between data and simulation in dedicated measurements of the cross section of the

$t\bar{t}+\geq 1b$ process [115]. For single-top processes, a $\pm 5\%$ uncertainty in the total cross section, estimated as a weighted average of the theoretical uncertainties in t -, Wt - and s -channel production [116–118], is included.

A number of sources of systematic uncertainty affecting the modelling of $t\bar{t}$ +jets and single-top production are considered. Uncertainties due to the choice of the NLO generator are estimated by comparing the nominal POWHEG+PYTHIA 8 samples with alternative samples generated by MADGRAPH5_AMC@NLO and showered by PYTHIA 8. The nominal samples are compared with POWHEG+HERWIG 7 samples to estimate the uncertainties in the modelling of the parton showering and hadronisation processes. The alternative samples used to evaluate modelling uncertainties are described in detail in Section 5.2. The uncertainty due to initial-state radiation (ISR) is estimated by simultaneously varying the h_{damp} parameter and the renormalisation and factorisation scales, and choosing the Var3c up/down variants of the A14 tune as described in Ref. [119]. The impact of final-state radiation (FSR) is evaluated by doubling or halving the renormalisation scale for emissions from the parton shower. The NNPDF3.0LO replicas are used to evaluate the PDF uncertainties for the nominal PDF. These uncertainties are all considered to be uncorrelated among $t\bar{t}$ +light-jets, $t\bar{t}+\geq 1c$, $t\bar{t}+\geq 1b$ and single-top samples, but correlated across the subcategories of the single-top background (s -channel, t -channel or tW). Furthermore, these uncertainties are treated as uncorrelated amongst LJ and HJ analysis regions and regions with 0, 1 or ≥ 2 tagged boosted objects. The impact of this correlation scheme on the search sensitivity was studied and compared with a scheme where the modelling uncertainties are correlated across all fit regions. The expected cross-section limits are around 10% higher with the current correlation scheme for low VLQ masses, whereas the impact is negligible for high mass signals.

An additional systematic uncertainty in Wt -channel production, concerning the separation between $t\bar{t}$ and Wt at NLO [79], is assessed by comparing the nominal sample, which uses the so-called ‘diagram removal’ scheme, with an alternative sample using the ‘diagram subtraction’ scheme.

The uncertainties in the modelling of the W/Z +jets backgrounds are estimated by varying the values of the internal renormalisation and factorisation scale parameters in SHERPA. An additional $\pm 30\%$ normalisation uncertainty for the W/Z +jets background is considered for events in analysis regions with different b -tag multiplicity (1, 2, 3, ≥ 4), uncorrelated among b -tag multiplicities. This uncertainty is based on variations of the factorisation and renormalisation scales and SHERPA matching parameters [120]. Since a dedicated reweighting of the jet multiplicity spectrum is applied to V +jets events, these uncertainties are considered to be correlated between LJ and HJ regions. Each of these uncertainties is also considered to be correlated between W +jets and Z +jets processes.

The kinematic reweighting of the main background processes (described in Section 7) is also derived for each of the modelling uncertainties described above, so that each alternative background model matches the data (and the nominal background prediction) in the reweighting source regions. Thus, the role of the modelling uncertainties after this reweighting is to account for extrapolations in kinematics and background composition between the reweighting source region and the fit and validation regions.

Uncertainties in the reweighting procedure itself arise mainly from the statistical uncertainties in the reweighting source regions and the choice of the functional form for parameterisation. These uncertainties are evaluated by shifting the fitted function to $\pm 2\sigma$ from its nominal value using the uncertainties of the fitted parameters and taking their internal correlations into account. These shifts represent possible variations in both the scale and the shape of the reweighting function, although the functional form of the parameterisation is not altered.

Since the diboson, $t\bar{t}W/Z$ and $t\bar{t}H$ processes contribute a small fraction of the events in the fit regions, their shape uncertainties have a negligible impact on the results, and only cross-section uncertainties are considered. The assigned uncertainties, due to the PDF and scale uncertainties in the NLO calculation, are $\pm 15\%$ for $t\bar{t}W/Z$ (treated as uncorrelated between LJ and HJ regions), and $+9/-12\%$ for $t\bar{t}H$. Uncertainties in the diboson background include a 5% uncertainty in the inclusive cross section calculated at NLO [121]. An additional uncorrelated 24% uncertainty in the production cross section is considered for each additional jet in the event, based on a comparison among different algorithms for merging LO matrix elements and parton showers [122]. The uncertainty estimate is based on the average jet multiplicity in each fit region, which is approximately three in the LJ regions (i.e. one additional jet from radiation) and six in the HJ regions (i.e. four additional jets from radiation). A $\pm 30\%$ normalisation uncertainty is considered for the production of additional heavy-flavour jets. Since the leading two b -tagged jets in diboson events are expected to arise from $W \rightarrow cs$ or $Z \rightarrow bb$ decays, this uncertainty is only applied to fit regions with ≥ 3 b -jets. All of these uncertainties are added in quadrature in each region, and the resulting uncertainty is treated as uncorrelated between LJ and HJ regions, as well as between low- b ($1-2b$) and high- b ($\geq 3b$) regions. The total normalisation uncertainty for diboson processes in LJ regions is 24% and 38% in low- and high- b regions, respectively; in HJ regions it is 48% and 56% in low- and high- b regions, respectively.

9 Statistical analysis

For each benchmark scenario considered in this search, the m_{eff} distributions across all search regions are jointly analysed to test for the presence of the predicted signal. A binned likelihood function $\mathcal{L}(\mu, \theta)$ is constructed as a product of Poisson probability terms over all m_{eff} bins considered in the search.

The likelihood function depends on the signal-strength parameter μ , which multiplies the predicted production cross section for signal, and θ , a set of nuisance parameters that encode the effect of systematic uncertainties in the signal and background expectations. Therefore, the expected total number of events in a given bin depends on μ and θ .

Nuisance parameters corresponding to all systematic uncertainties are implemented in the likelihood function with Gaussian constraints. In each bin of the m_{eff} distributions, uncertainties due to the limited size of the simulated samples are also taken into account by dedicated parameters in the fit that are independent across bins. These parameters are implemented with Poisson constraints.

For a given value of μ , variations in the nuisance parameters θ allow the expectations for signal and background to change according to the corresponding systematic uncertainties. The fitted values of θ correspond to deviations from the nominal expectations that globally provide the best fit to the data. This procedure reduces the impact of systematic uncertainties on the search sensitivity and improves the background prediction by taking advantage of the highly populated background-dominated regions included in the likelihood fit.

The improvement in the background prediction is verified by performing fits under the background-only hypothesis and checking how well the data agrees with the post-fit background in validation regions that are disjoint from the regions used in the fit.

The test statistic q_μ , as implemented in a framework based on RooStats [123, 124] and HistFitter [125], is defined as the profile likelihood ratio: $q_\mu = -2 \ln(\mathcal{L}(\mu, \hat{\theta}_\mu) / \mathcal{L}(\hat{\mu}, \hat{\theta}))$. Here, $\hat{\mu}$ and $\hat{\theta}$ are the values of the parameters μ and θ that simultaneously maximise the likelihood function $\mathcal{L}(\mu, \theta)$ (subject to the constraint

$0 \leq \hat{\mu} \leq \mu$), whereas $\hat{\theta}_\mu$ are the values of the nuisance parameters that maximise the likelihood function for a given value of μ . The statistic used for the discovery test, to test the compatibility of the observed data with the background-only hypothesis, is obtained by setting $\mu = 0$ in the profile likelihood ratio and leaving $\hat{\mu}$ unconstrained: $q_0 = -2 \ln(\mathcal{L}(0, \hat{\theta}_0) / \mathcal{L}(\hat{\mu}, \hat{\theta}))$. The p -value of the discovery test is given by the integral of the probability distribution of q_0 above the observed q_0 value when assuming the background-only hypothesis, and it is computed using the asymptotic approximation detailed in Refs. [126, 127]. For each signal scenario considered, the upper limit on the signal production cross section is computed using q_μ in the CL_s method [128, 129], also in the asymptotic approximation. For a given signal scenario, values of the production cross section (parameterised by μ) yielding $\text{CL}_s < 0.05$ are excluded at $\geq 95\%$ CL. The exclusion limits obtained using the asymptotic approximation are then compared with limits calculated using pseudoexperiments for 2 TeV benchmark signal points close to the obtained constraints. The central values of the limits computed using the two methods agree within 5%, while the uncertainty bands agree within 10%–15%.

10 Results

10.1 Likelihood fits to data

A likelihood fit, as described in Section 9, is performed under the background-only hypothesis. A comparison between the overall observed and expected yields in each fit region is shown, before and after the fit to data, in Figure 5. As can be seen, the combined impact of the systematic uncertainties has been constrained as a result of the fit, using information from the large number of events in signal-depleted regions with different background contributions. Consequently, an improved background prediction is obtained with reduced uncertainty across regions, including those with significant fractions of expected signal events. The data and pre- and post-fit background yields in four of the most sensitive search regions are given in Table 5 and Table 6, respectively.

The pre- and post-fit m_{eff} distributions in these four regions are furthermore shown in Figure 6 and Figure 7. The post-fit agreement between the data and prediction in the fit regions is good overall. A comparison of the observed and expected yields in all validation regions, pre- and post-fit, is shown in Figure 8. The pre- and post-fit m_{eff} distributions in the validation regions closest to the four selected fit regions are shown in Figure 9 and Figure 10. The expected background in these regions agrees with the data within uncertainties, both before and after the fit. The general post-fit improvement in the estimated background in the validation regions, which are not included in the fit, gives confidence in the background estimation procedure.

The impact of the different sources of uncertainty on the signal-strength parameter μ is reported in Table 7 for a T singlet and T doublet signal near the expected sensitivity of the search. As can be seen, the results are dominated by systematic uncertainties. The largest overall impact is related to the modelling of background processes, in particular $t\bar{t} + \geq 1b$ production. The systematic uncertainty associated with jets also has a significant impact. The relative size of impacts from different sources of uncertainty differs between T singlet and T doublet signals due to their kinematic differences. Uncertainties related to $t\bar{t} + \geq 1b$ modelling and b -tagging contribute significantly more in the T doublet scenario, whereas single-top modelling has a larger impact in the T singlet scenario.

The data-driven kinematic reweighting procedure described in Section 7 provides better agreement between the data and the nominal pre-fit background, and, as described in Section 8, modelling uncertainties

affecting the dominant background processes are also reweighted. This procedure improves the stability of the likelihood fit. However, the fit is robust against these changes to the pre-fit background model, and the post-fit values of the modelling uncertainties are not significantly impacted by the reweighting procedure.

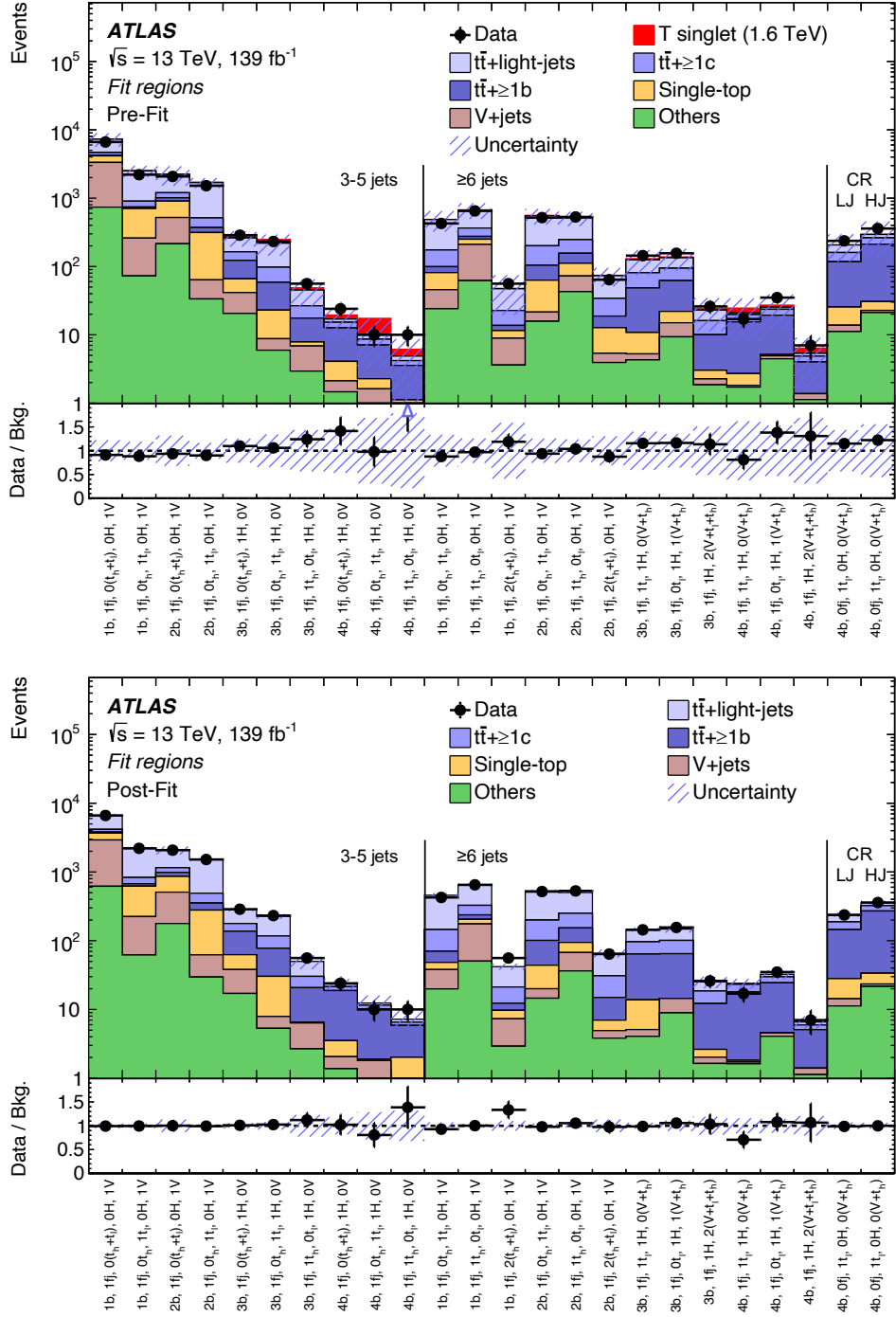


Figure 5: Comparison between the data and background prediction for the yields in each of the fit regions considered (top) pre-fit and (bottom) post-fit, performed under the background-only hypothesis. The two rightmost regions shown in the plot are the 3–5j (LJ) and $\geq 6j$ (HJ) control regions, respectively. The ‘others’ background includes the $t\bar{t} V/H, VH, tZ, t\bar{t}t\bar{t}$, diboson, and multijet backgrounds. The expected T singlet signal (solid red) for $m_T = 1.6$ TeV and $\kappa = 0.5$ is included in the pre-fit figure. The bottom panels display the ratios of data to the total background prediction. The hashed area represents the total uncertainty in the background.

Table 5: Predicted and observed yields in four of the most sensitive search regions (depending on the signal scenario) considered. The background prediction is shown before the fit to data. The ‘rare backgrounds’ category includes the VH , tZ and $t\bar{t}\bar{t}$ backgrounds. Also shown are the signal predictions for different benchmark scenarios considered. The individual systematic uncertainties for the different background processes can be correlated, and do not necessarily add in quadrature to equal the systematic uncertainty in the total background yield. The quoted uncertainties are the sum in quadrature of statistical and systematic uncertainties in the yields.

	LJ, 2b, $\geq 1fj$, 0 t_h , $\geq 1t_l$, 0H, $\geq 1V$	LJ, $\geq 4b$, $\geq 1fj$, 0 t_h , $\geq 1t_l$, $\geq 1H$, 0V	HJ, 2b, $\geq 1fj$, $\geq 2(t_h+t_l)$, 0H, $\geq 1V$	HJ, $\geq 4b$, $\geq 1fj$, $\geq 1H$, $\geq 2(V+t_l+t_h)$
T singlet ($m_T = 1.6$ TeV, $\kappa = 0.5$)	31.8 ± 4.9	7.2 ± 3.5	1.3 ± 0.4	1.0 ± 0.5
T doublet ($m_T = 1.6$ TeV, $\kappa = 0.5$)	21.8 ± 2.4	8.5 ± 5.6	7.3 ± 2.1	7.1 ± 4.5
$t\bar{t}$ +light-jets	1170 ± 210	1.6 ± 2	39.1 ± 9.5	0.49 ± 0.29
$t\bar{t} + \geq 1c$	143 ± 80	1.5 ± 1.3	15.3 ± 9.9	0.86 ± 0.58
$t\bar{t} + \geq 1b$	57 ± 32	4.8 ± 3.9	6.1 ± 4.3	2.6 ± 2
Single-top	250 ± 50	0.66 ± 0.87	7.3 ± 7.5	<0.001
$t\bar{t}W/Z$	13.2 ± 3.1	0.33 ± 0.19	2.5 ± 1.1	0.22 ± 0.82
$t\bar{t}H$	1.5 ± 0.2	0.51 ± 0.15	0.34 ± 0.14	0.42 ± 0.12
W +jets	25.7 ± 9.4	0.70 ± 1.3	1.2 ± 1.1	0.24 ± 0.15
Z +jets	4.4 ± 1.7	<0.001	0.25 ± 0.10	0.007 ± 0.007
Dibosons	3.8 ± 1.4	0.02 ± 0.03	0.21 ± 0.15	<0.001
Multijet	12.9 ± 7.3	0.025 ± 0.017	0.61 ± 0.46	0.16 ± 0.14
Rare backgrounds	2.0 ± 0.3	0.03 ± 0.04	0.25 ± 0.14	0.33 ± 0.06
Total background	1690 ± 280	10.2 ± 4.8	73 ± 20	5.4 ± 2.5
Data	1519	10	64	7

Table 6: Predicted and observed yields in four of the most sensitive search regions (depending on the signal scenario) considered. The background prediction is shown after the fit to data under the background-only hypothesis. The “rare backgrounds” category includes the VH , tZ and $t\bar{t}t\bar{t}$ backgrounds. The individual systematic uncertainties for the different background processes can be correlated, and do not necessarily add in quadrature to equal the systematic uncertainty in the total background yield. The quoted uncertainties are computed after taking into account correlations among nuisance parameters and among processes. The statistical uncertainty is added in quadrature to the systematic uncertainties.

	LJ, $2b, \geq 1fj, 0t_h,$ $\geq 1t_l, 0H, \geq 1V$	LJ, $\geq 4b, \geq 1fj, 0t_h,$ $\geq 1t_l, \geq 1H, 0V$	HJ, $2b, \geq 1fj,$ $\geq 2(t_h+t_l), 0H, \geq 1V$	HJ, $\geq 4b, \geq 1fj, \geq 1H,$ $\geq 2(V+t_l+t_h)$
$t\bar{t}$ +light-jets	1033 ± 72	0.6 ± 0.8	33.6 ± 4.5	0.57 ± 0.24
$t\bar{t}+\geq 1c$	144 ± 54	1.5 ± 1.0	15.6 ± 5.5	0.82 ± 0.32
$t\bar{t}+\geq 1b$	75 ± 22	8 ± 3	8.2 ± 2.3	3.8 ± 1.1
Single-top	223 ± 55	0.09 ± 0.55	2.3 ± 4.5	<0.001
$t\bar{t}W/Z$	12.1 ± 2.3	0.36 ± 0.18	2.3 ± 0.8	0.62 ± 0.76
$t\bar{t}H$	1.46 ± 0.21	0.51 ± 0.11	0.29 ± 0.08	0.40 ± 0.09
W +jets	26.6 ± 7.1	0.6 ± 1.0	0.8 ± 0.5	0.22 ± 0.13
Z +jets	4.5 ± 1.2	<0.001	0.27 ± 0.08	0.005 ± 0.006
Dibosons	3.4 ± 1.2	0.017 ± 0.029	0.17 ± 0.13	<0.001
Multijet	9.5 ± 5.7	0.018 ± 0.015	0.45 ± 0.41	0.12 ± 0.12
Rare backgrounds	2.0 ± 0.2	0.03 ± 0.03	0.22 ± 0.08	0.31 ± 0.05
Total background	1534 ± 56	12.1 ± 3.5	64 ± 8	6.8 ± 1.5
Data	1519	10	64	7

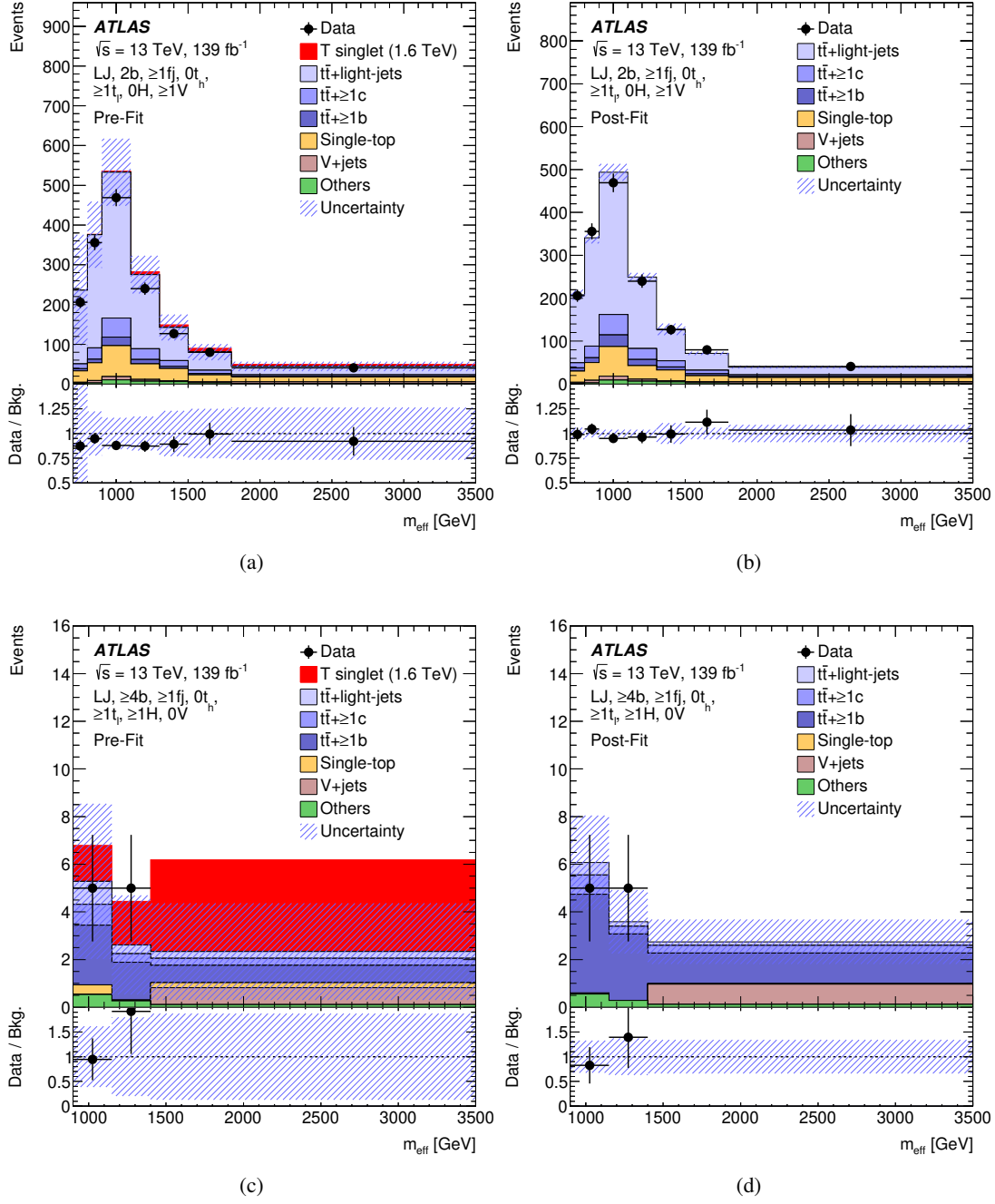


Figure 6: Comparison between the data and prediction for the m_{eff} distribution under the background-only hypothesis, in the (LJ, 2b, $\geq 1f_j$, $0t_h$, $\geq 1t_l$, 0H, $\geq 1V$) region (a) pre-fit and (b) post-fit, and the (LJ, $\geq 4b$, $\geq 1f_j$, $0t_h$, $\geq 1t_l$, $\geq 1H$, 0V) region (c) pre-fit and (d) post-fit. The expected T singlet signal (solid red) for $m_T = 1.6$ TeV and $\kappa = 0.5$ is included in the pre-fit figures. The ‘others’ background includes the $t\bar{t} V/H$, VH , tZ , $t\bar{t}t\bar{t}$, diboson, and multijet backgrounds. The bottom panels display the ratios of data to the total background prediction. The hashed area represents the total uncertainty in the background. The last bin in each distribution contains the overflow.

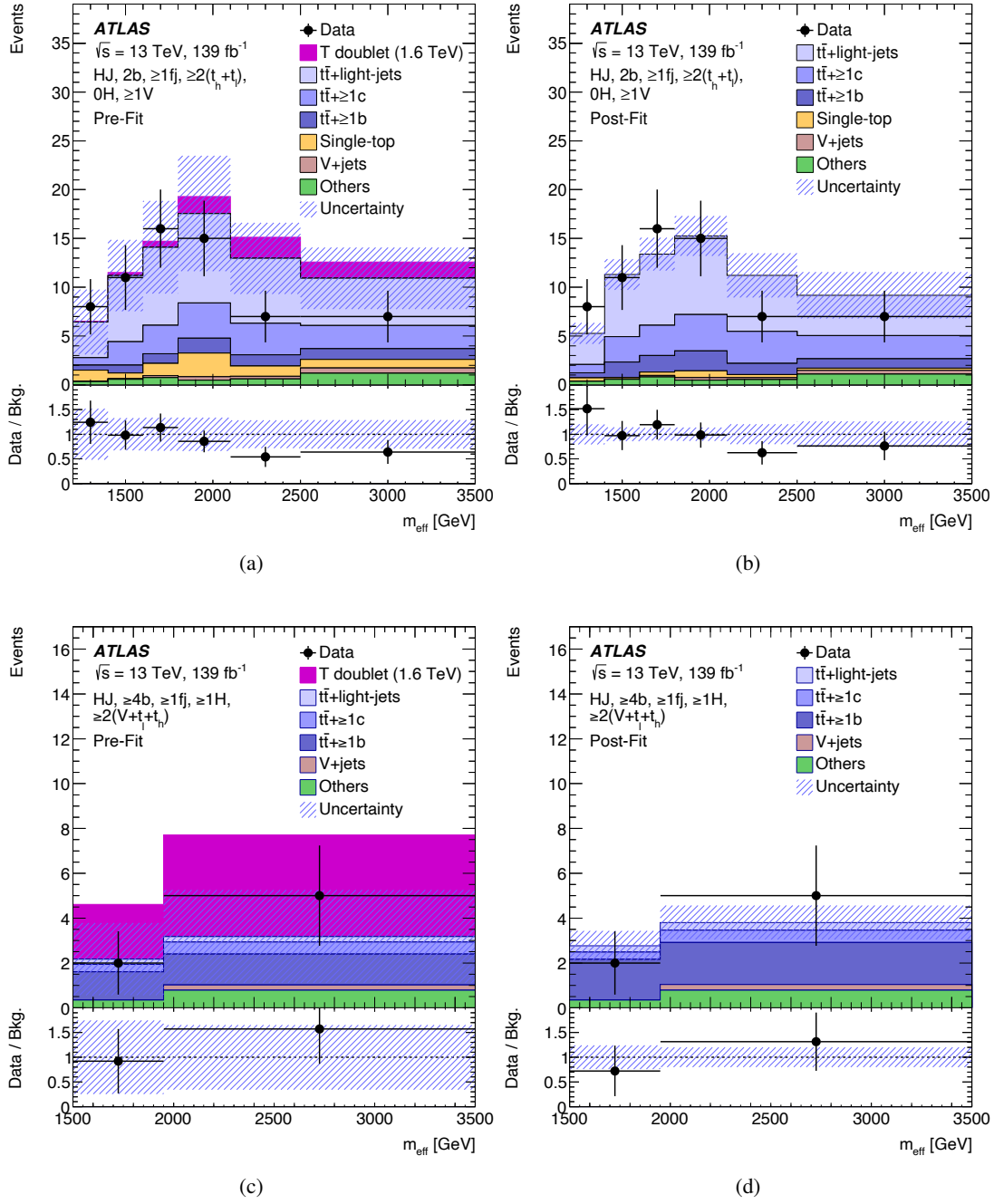


Figure 7: Comparison between the data and prediction for the m_{eff} distribution under the background-only hypothesis, in the (HJ, 2b, $\geq 1f_j$, $\geq 2(t_h+t_l)$, 0H, $\geq 1V$) region (a) pre-fit and (b) post-fit, and the (HJ, $\geq 4b$, $\geq 1f_j$, $\geq 1H$, $\geq 2(V+t_h+t_l)$) region (c) pre-fit and (d) post-fit. The expected T doublet signal (solid purple) for $m_T = 1.6$ TeV and $\kappa = 0.5$ is included in the pre-fit figures. The ‘others’ background includes the $t\bar{t} V/H$, VH , tZ , $t\bar{t}t\bar{t}$, diboson, and multijet backgrounds. The bottom panels display the ratios of data to the total background prediction. The hashed area represents the total uncertainty in the background. The last bin in each distribution contains the overflow.

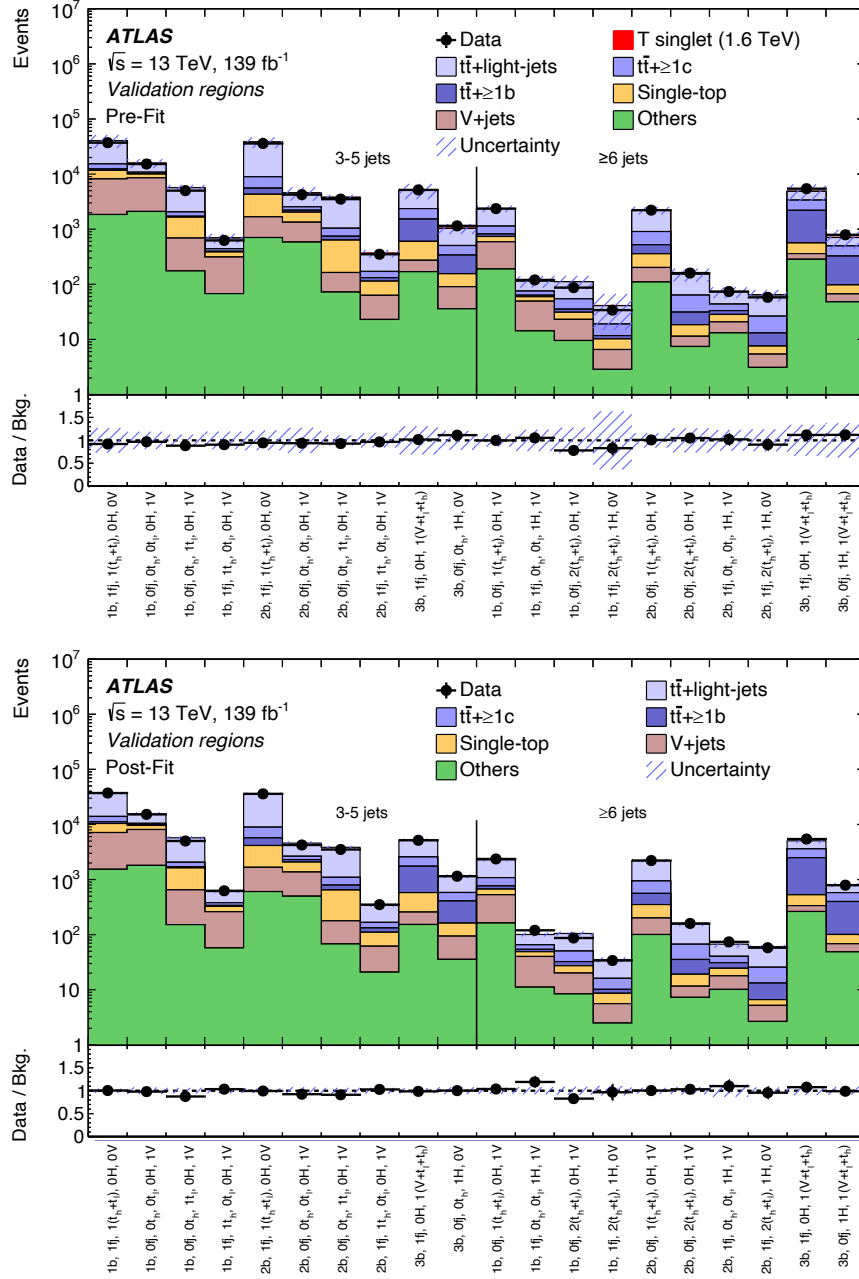


Figure 8: Comparison between the data and background prediction for the yields in each of the VRs considered (top) pre-fit and (bottom) post-fit, performed under the background-only hypothesis considering only the fit regions. The ‘others’ background includes the $t\bar{t} V/H$, VH , tZ , $t\bar{t}t\bar{t}$, diboson, and multijet backgrounds. The expected T singlet signal (solid red) for $m_T = 1.6 \text{ TeV}$ and $\kappa = 0.5$ is included in the pre-fit figure. The bottom panels display the ratios of data to the total background prediction. The hashed area represents the total uncertainty in the background.

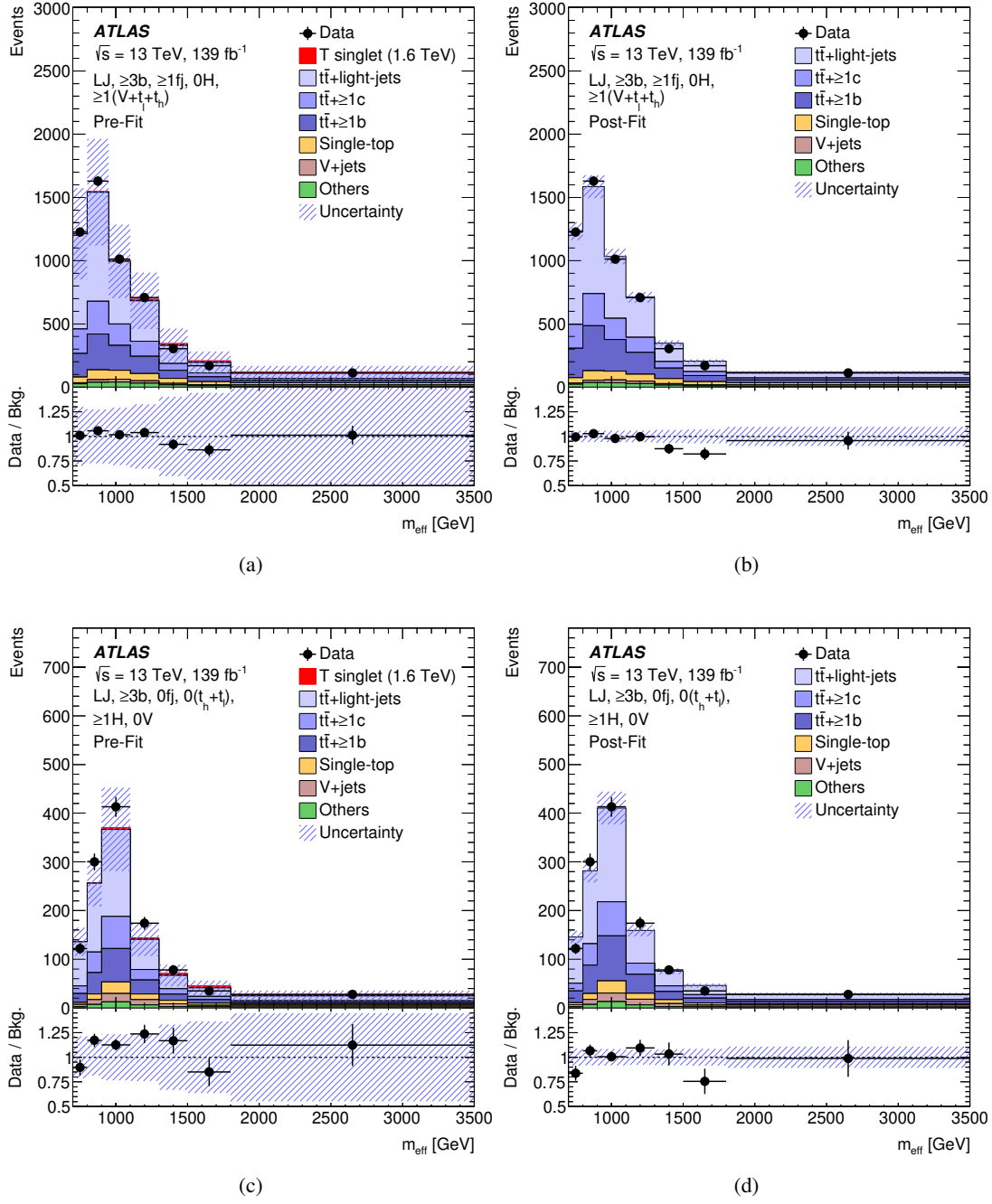


Figure 9: Comparison between the data and prediction for the m_{eff} distribution under the background-only hypothesis, in the $(LJ, \geq 3b, \geq 1fj, 0H, \geq 1(V+t_l+t_h))$ validation region (a) pre-fit and (b) post-fit, and the $(LJ, \geq 3b, 0fj, 0(t_h+t_l), \geq 1H, 0V)$ validation region (c) pre-fit and (d) post-fit. The expected T singlet signal (solid red) for $m_T = 1.6$ TeV and $\kappa = 0.5$ is included in the pre-fit figures. The ‘others’ background includes the $t\bar{t} V/H, VH, tZ, t\bar{t}t\bar{t}$, diboson, and multijet backgrounds. The bottom panels display the ratios of data to the total background prediction. The hashed area represents the total uncertainty in the background. The last bin in each distribution contains the overflow.

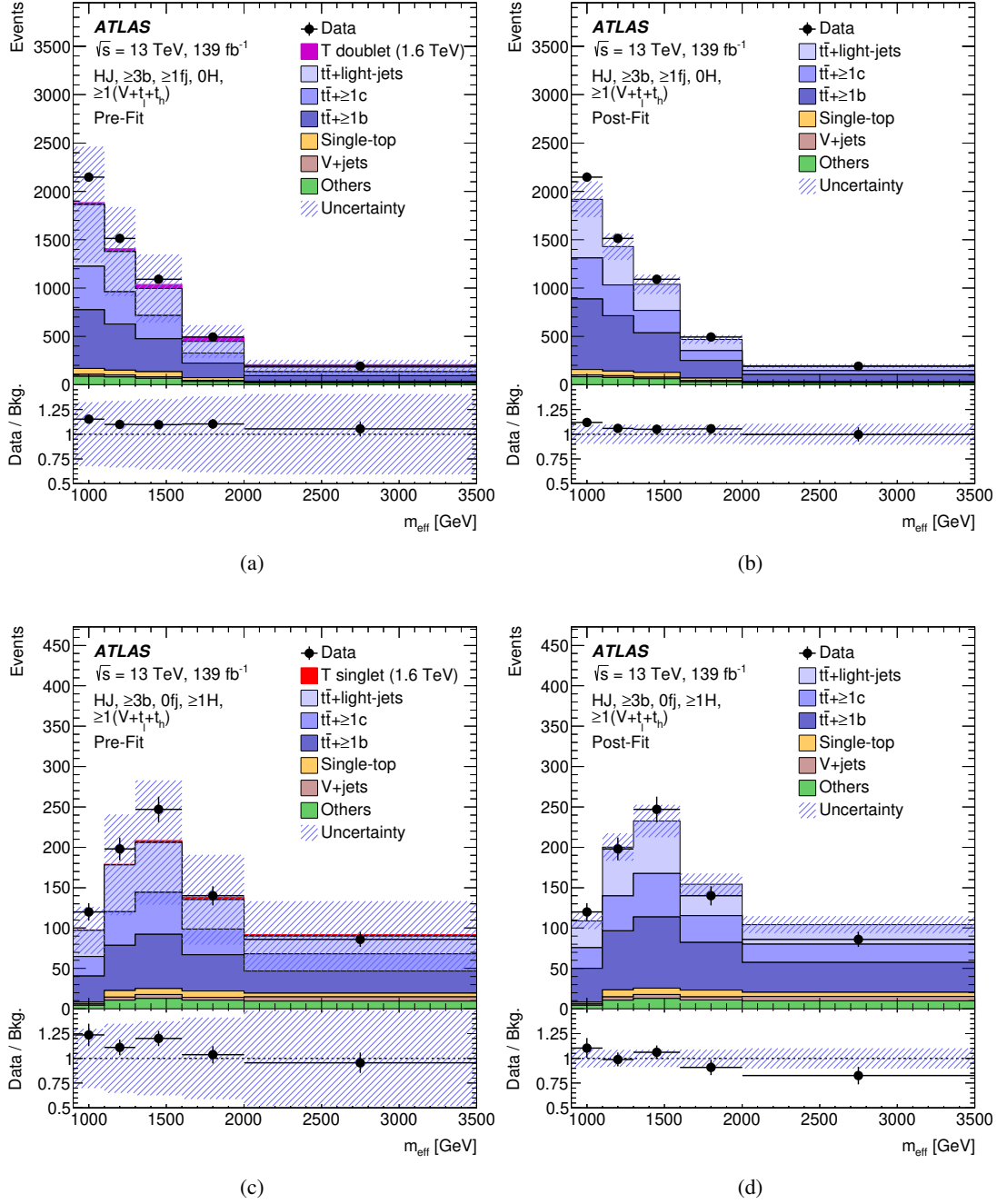


Figure 10: Comparison between the data and prediction for the m_{eff} distribution under the background-only hypothesis, in the $(HJ, \geq 3b, \geq 1fj, 0H, \geq 1(V+t_l+t_h))$ validation region (a) pre-fit and (b) post-fit, and the $(HJ, \geq 3b, 0fj, \geq 1H, \geq 1(V+t_l+t_h))$ validation region (c) pre-fit and (d) post-fit. The expected T doublet signal (solid purple) for $m_T = 1.6$ TeV and $\kappa = 0.5$ is included in the pre-fit figures. The ‘others’ background includes the $t\bar{t} V/H, VH, tZ, t\bar{t}\bar{t}$, diboson, and multijet backgrounds. The bottom panels display the ratios of data to the total background prediction. The hashed area represents the total uncertainty in the background. The last bin in each distribution contains the overflow.

Table 7: Breakdown of the contributions to the uncertainties in μ , shown for the singlet T signal with $\kappa = 0.4$ and the doublet T signal with $\kappa = 0.7$, both with $m_T = 1.5$ TeV. The contributions from the different sources of uncertainty are evaluated after the fit. The $\Delta\mu$ values are obtained by repeating the fit after having fixed a certain set of nuisance parameters corresponding to a group of systematic uncertainties, and then evaluating $(\Delta\mu)^2$ by subtracting the resulting squared uncertainty of μ from its squared uncertainty found in the full fit.

Uncertainty source	T singlet	T doublet
	$m_T = 1.5$ TeV, $\kappa = 0.4$	$m_T = 1.5$ TeV, $\kappa = 0.7$
	$\Delta\mu$	$\Delta\mu$
Process modelling uncertainties		
$t\bar{t}$ +light-jets	± 0.05	± 0.11
$t\bar{t} + \geq 1c$	± 0.03	± 0.08
$t\bar{t} + \geq 1b$	± 0.09	± 0.27
Single-top	± 0.12	± 0.07
W/Z +jets	± 0.03	± 0.09
Object uncertainties		
Jets	± 0.07	± 0.13
b -tagging	± 0.03	± 0.11
Other sources	± 0.02	± 0.04
Background reweighting	± 0.04	± 0.11
Total systematic uncertainty	± 0.23	± 0.33
Total statistical uncertainty	± 0.09	± 0.17

10.2 Limits on single vector-like quark production

No significant excess above the SM prediction is found in any of the considered regions in the background-only fit. Unconditional fits with a floating signal-strength parameter μ were also consistent with the background-only hypothesis. Upper limits at 95% CL on the single- T production cross section are derived in both the singlet (T) and doublet ($T B$) scenarios.

The observed cross-section limits at each point in the parameter space are compared with the NLO theoretical prediction to set exclusion limits on model parameters. Since the theory cross-section calculations with finite-width effects and non-resonant contributions are only reliable for relative T -quark widths (Γ_T/m_T) up to $\sim 50\%$ [106], results are presented only in this restricted regime.

The obtained limits corresponding to the singlet and doublet scenarios are shown in Figure 11 and Figure 12, respectively, for a set of three values of the common coupling parameter κ , chosen to approximately span the sensitivity range of the search in each scenario. The corresponding limits are also derived in the mass versus coupling plane, where exclusion contours indicate the interpolated intersection between the planes of excluded and theoretically predicted cross sections, shown in Figure 13 for both the singlet and doublet scenarios. Additionally, upper limits on the production cross section of both the singlet and doublet scenarios are derived as a function of mass and coupling, as shown in Figures 14 and 15. As expected, the exclusion limits on the T -quark mass are generally stronger in the singlet scenario than in the doublet scenario. All T -quark masses below 2.1 TeV (expected 1.9 TeV) are excluded for singlet T quarks at couplings $\kappa \geq 0.6$. At a mass of 1.6 TeV, κ values above 0.3 (expected 0.41) are all excluded. By comparison, the previous ATLAS search in the all-hadronic $T \rightarrow Ht$ channel has excluded κ values above ~ 0.5 (expected ~ 0.65) at a mass of 1.6 TeV [21]. In the doublet scenario, the limits on the considered mass range extend down to coupling values of $\kappa = 0.55$, corresponding to a T -quark mass limit of 1.0 TeV. Masses up to 1.68 TeV are excluded at $\kappa = 0.75$, at a relative T -quark width threshold of 50%.

The expected limits on the cross section get progressively stronger at larger masses in both scenarios, as the decay products of the T quark become more boosted, and the fraction of signal in the highest m_{eff} bins increases. The limits deteriorate at larger values of κ , since this regime corresponds to large resonance width and a larger fraction of the signal resides in the low mass regime away from the peak of the resonance. As can be seen, the observed limits exceed the expected limits in both benchmark scenarios in a few cases. These deviations are larger for the singlet scenario, reaching almost 2σ at high masses. These findings can be ascribed to downward statistical fluctuations in a few of the most signal-sensitive bins, most notably in the last bin of the (LJ, $\geq 4b$, $\geq 1f_j$, $0t_h$, $\geq 1t_l$, $\geq 1H$, $0V$) region, which has no data events, and the last few bins of the (HJ, $\geq 4b$, $\geq 1f_j$, $0t_h$, $1t_l$, $\geq 1H$, $0V$) region. The origin of these discrepancies was investigated, and no evidence of any systematic bias was found. Notably, the pre- and post-fit m_{eff} distributions in the corresponding validation regions, shown in Figure 9 and Figure 10, respectively, exhibit good agreement between the data and expectations. Several other fit regions with kinematic features and background compositions similar to those in the two regions mentioned above show good agreement between data and predictions. The observed discrepancies were therefore deemed to be consistent with statistical fluctuations.

Finally, the results are interpreted in a more generalised representation of the parameter space, displaying the largest excluded mass as a function of Γ_T/m_T and the relative coupling parameter ξ_W (Figure 16). As discussed in Section 1, the T -quark width is determined by the T -quark mass m_T and the universal coupling constant κ and is independent of the multiplet representation. The relative coupling parameter ξ_W controls the branching fraction $\mathcal{B}(T \rightarrow Wb)$. For ease of representation, the limits are shown for the

assumption $\xi_Z = \xi_H$, which is valid for all VLQ multiplet scenarios in the phenomenological model discussed in Section 1. Since the relative coupling constants $\xi_{W,Z,H}$ must sum to unity, the assumption of equal ξ_Z and ξ_H fully determines the values of these parameters for any given value of ξ_W .

In all of the benchmarks considered in this search, only the contributions from T -quark production were taken into account. In particular, limits presented in the doublet ($T B$) scenario neglect contributions from B -quark production. The most relevant signature of B -quark production for this analysis would occur in the $B \rightarrow Wt$ decay channel, when the top quark decays leptonically and the W boson decays hadronically. This process has a signature almost identical to the $T \rightarrow Zt$ decay signatures considered in the search, and would therefore make very similar contributions to the fit regions. By the same argument, contributions from B -quark production in the RSRs and the background control regions are expected to be negligible. Thus, the limits presented for the doublet scenario in this paper can be considered to be conservative.

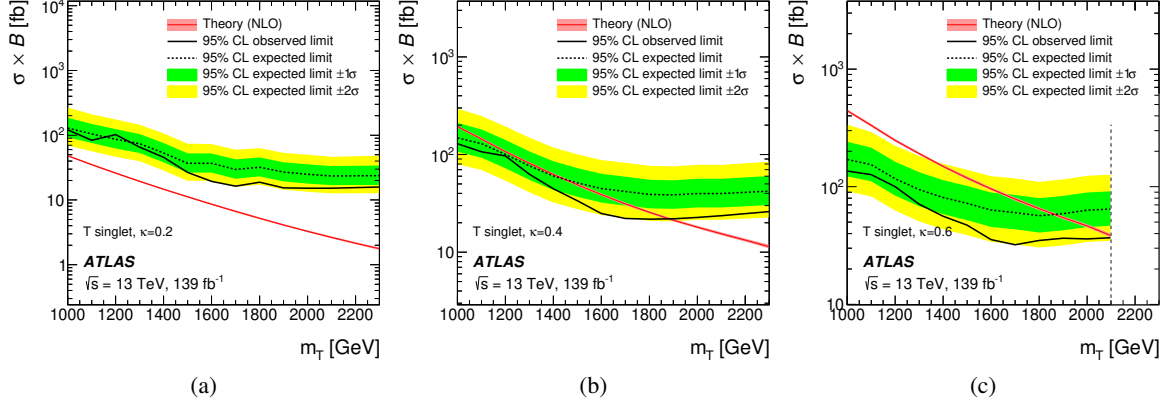


Figure 11: Observed (solid black line) and expected (dashed black line) 95% CL upper limits on the single- T production cross section as a function of the T -quark mass in the singlet scenario with the common coupling parameter (a) $\kappa = 0.2$, (b) $\kappa = 0.4$, and (c) $\kappa = 0.6$. The surrounding shaded bands correspond to ± 1 and ± 2 standard deviations around the expected limit. The red line shows the NLO theoretical cross-section prediction, with the surrounding shaded band representing the corresponding uncertainty. Limits are only presented in the regime $\Gamma_T/m_T \leq 50\%$, where the theory calculations are known to be valid, as indicated by the vertical grey dashed line.

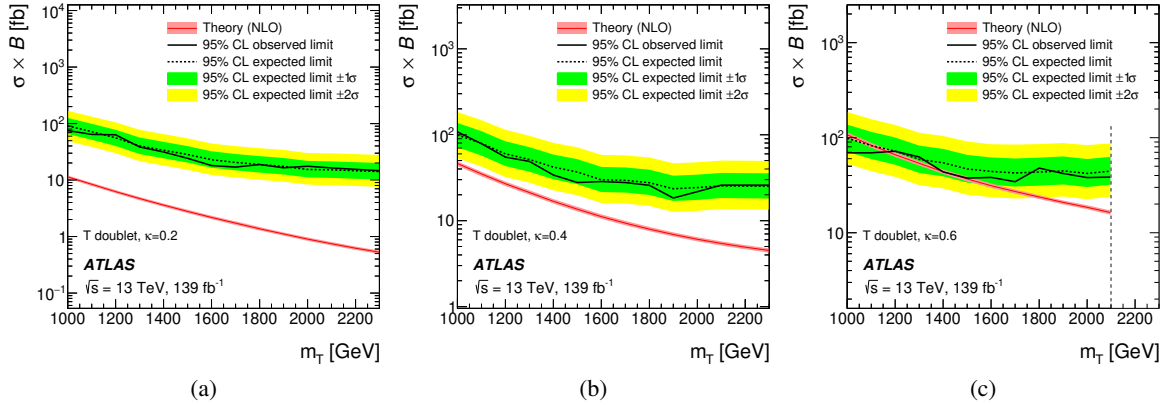


Figure 12: Observed (solid black line) and expected (dashed black line) 95% CL upper limits on the single- T production cross section as a function of the T -quark mass in the doublet scenario with the common coupling parameter (a) $\kappa = 0.2$, (b) $\kappa = 0.4$, and (c) $\kappa = 0.6$. The surrounding shaded bands correspond to ± 1 and ± 2 standard deviations around the expected limit. The red line shows the NLO theoretical cross-section prediction, with the surrounding shaded band representing the corresponding uncertainty. Limits are only presented in the regime $\Gamma_T/m_T \leq 50\%$, where the theory calculations are known to be valid, as indicated by the vertical grey dashed line.

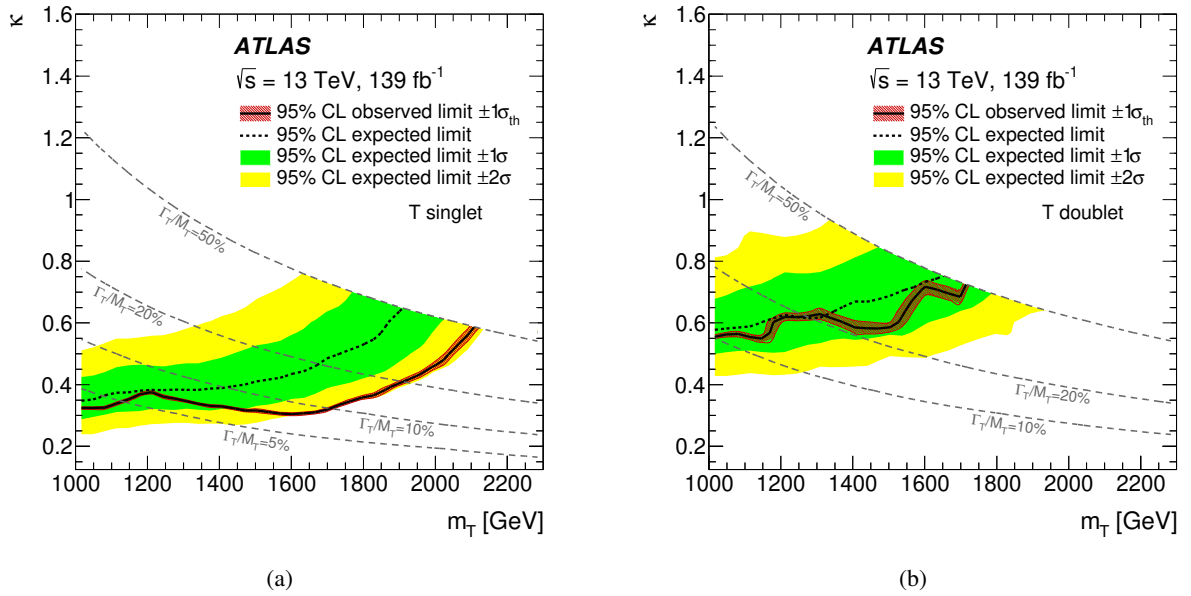


Figure 13: Observed (solid black line) and expected (dashed black line) 95% CL exclusion limits on the universal coupling constant κ as a function of the T -quark mass in the (a) SU(2) singlet and (b) SU(2) doublet scenarios. All values of κ above the black contour lines are excluded at each mass point. The shaded bands correspond to ± 1 and ± 2 standard deviations around the expected limit. The red hashed area around the observed limit corresponds to the theoretical uncertainty of the NLO cross-section prediction. The grey dashed lines represent configurations of (m_T, κ) resulting in equal values of the relative resonance width Γ_T/m_T . Limits are only presented in the regime $\Gamma_T/m_T \leq 50\%$, where the theory calculations are known to be valid.

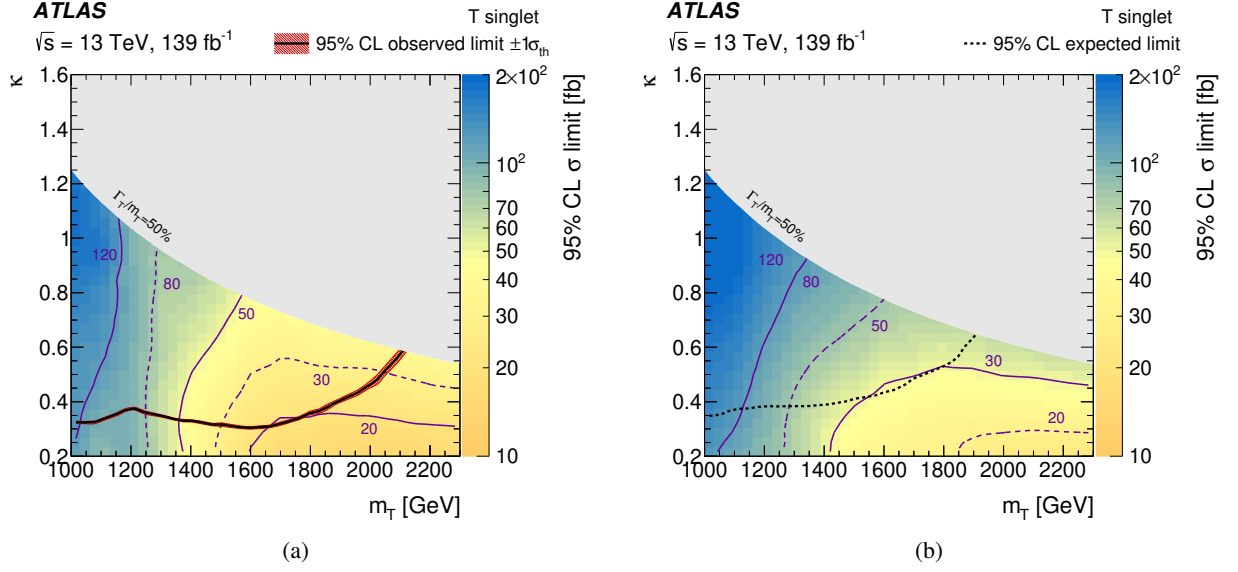


Figure 14: (a) Observed and (b) expected 95% CL exclusion limits on the cross section times branching ratio of single T -quark production as a function of the universal coupling constant κ and the T -quark mass in the SU(2) singlet scenario. The red hashed area around the observed limit corresponds to the theoretical uncertainty of the NLO cross-section prediction. All values of κ above the black contour line are excluded at each mass point. The purple contour lines denote exclusion limits of equal cross section times branching ratio in units of fb. Limits are only presented in the regime $\Gamma_T/m_T \leq 50\%$, where the theory calculations are known to be valid.

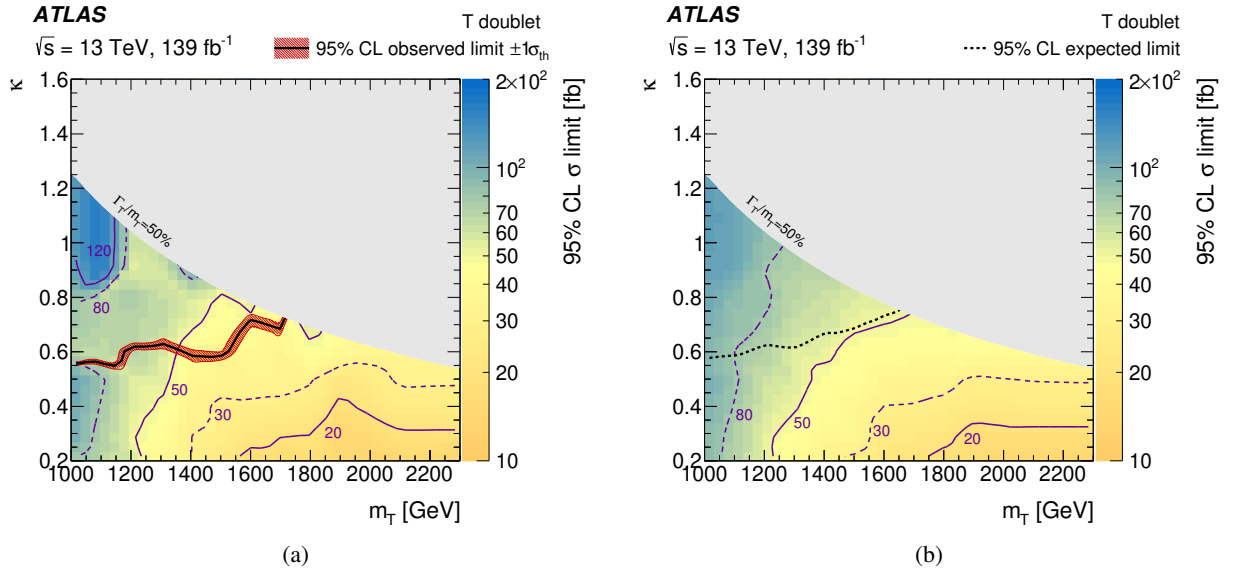
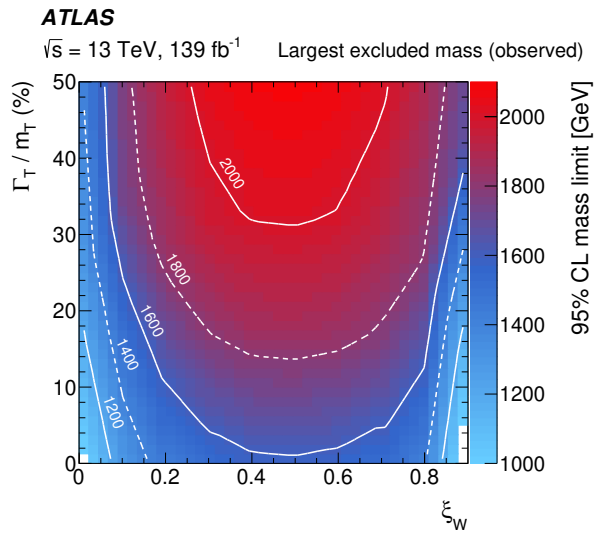
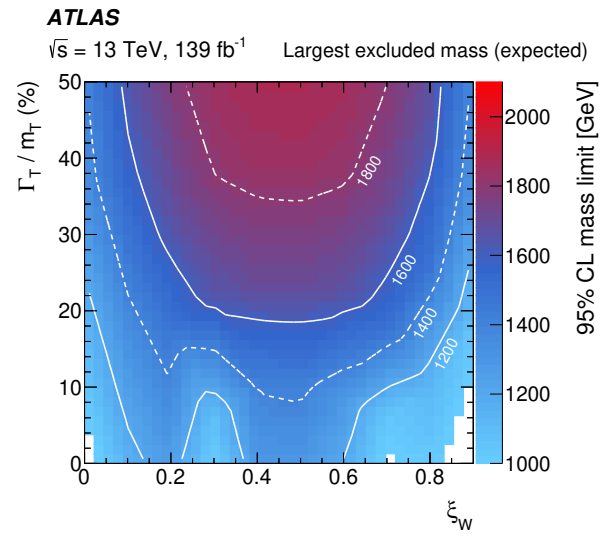


Figure 15: (a) Observed and (b) expected 95% CL exclusion limits on the cross section times branching ratio of single T -quark production as a function of the universal coupling constant κ and the T -quark mass in the SU(2) doublet scenario. The red hashed area around the observed limit corresponds to the theoretical uncertainty of the NLO cross-section prediction. All values of κ above the black contour line are excluded at each mass point. The purple contour lines denote exclusion limits of equal cross section times branching ratio in units of fb. Limits are only presented in the regime $\Gamma_T/m_T \leq 50\%$, where the theory calculations are known to be valid.



(a)



(b)

Figure 16: (a) Observed and (b) expected upper limits at 95% CL on the T -quark mass as a function of the relative resonance width (Γ_T/m_T) and the relative coupling parameter ξ_W , for the assumption $\mathcal{B}(T \rightarrow Ht) = \mathcal{B}(T \rightarrow Zt)$. The white contour lines denote exclusion limits of equal mass in units of GeV. The white regions represent points in parameter space that are not excluded for any mass in the considered range.

11 Conclusion

A search for the single production of up-type vector-like quarks (T), with subsequent decays $T \rightarrow Ht$ with $H \rightarrow b\bar{b}$ or $T \rightarrow Zt$ with $Z \rightarrow q\bar{q}$, is presented. The search uses pp collision data at $\sqrt{s} = 13$ TeV, collected by the ATLAS detector at the LHC during the 2015–2018 Run 2 data-taking period. The recorded dataset corresponds to an integrated luminosity of 139 fb^{-1} . Events are analysed in the lepton+jets final state, characterised by the presence of a single lepton and multiple jets and b -jets in the event. The search exploits the presence of boosted, hadronically decaying Higgs and vector bosons, and hadronically or leptonically decaying top quarks in signal events.

No significant excess above Standard Model expectations is observed, and 95% CL upper limits are set on the production cross section of single T quarks. The results are interpreted in benchmark scenarios to set limits on the mass and universal coupling strength (κ) of the vector-like quark. For singlet T quarks, all masses below 2.1 TeV are excluded at couplings $\kappa \geq 0.6$, while the limits extend down to $\kappa = 0.3$ for a T -quark mass of 1.6 TeV. For T quarks in the doublet scenario, where the production cross section is much lower, coupling values as low as $\kappa = 0.55$ are excluded at a T -quark mass of 1.0 TeV. The limits extend up to 1.68 TeV and $\kappa = 0.75$, at a threshold of 50% relative T -quark width.

Acknowledgements

We thank CERN for the very successful operation of the LHC, as well as the support staff from our institutions without whom ATLAS could not be operated efficiently.

We acknowledge the support of ANPCyT, Argentina; YerPhI, Armenia; ARC, Australia; BMWFW and FWF, Austria; ANAS, Azerbaijan; CNPq and FAPESP, Brazil; NSERC, NRC and CFI, Canada; CERN; ANID, Chile; CAS, MOST and NSFC, China; Minciencias, Colombia; MEYS CR, Czech Republic; DNRF and DNSRC, Denmark; IN2P3-CNRS and CEA-DRF/IRFU, France; SRNSFG, Georgia; BMBF, HGF and MPG, Germany; GSRI, Greece; RGC and Hong Kong SAR, China; ISF and Benoziyo Center, Israel; INFN, Italy; MEXT and JSPS, Japan; CNRST, Morocco; NWO, Netherlands; RCN, Norway; MEiN, Poland; FCT, Portugal; MNE/IFA, Romania; MESTD, Serbia; MSSR, Slovakia; ARRS and MIZŠ, Slovenia; DSI/NRF, South Africa; MICINN, Spain; SRC and Wallenberg Foundation, Sweden; SERI, SNSF and Cantons of Bern and Geneva, Switzerland; MOST, Taiwan; TENMAK, Türkiye; STFC, United Kingdom; DOE and NSF, United States of America. In addition, individual groups and members have received support from BCKDF, CANARIE, Compute Canada and CRC, Canada; PRIMUS 21/SCI/017 and UNCE SCI/013, Czech Republic; COST, ERC, ERDF, Horizon 2020 and Marie Skłodowska-Curie Actions, European Union; Investissements d’Avenir Labex, Investissements d’Avenir IDEX and ANR, France; DFG and AvH Foundation, Germany; Herakleitos, Thales and Aristeia programmes co-financed by EU-ESF and the Greek NSRF, Greece; BSF-NSF and MINERVA, Israel; Norwegian Financial Mechanism 2014-2021, Norway; NCN and NAWA, Poland; La Caixa Banking Foundation, CERCA Programme Generalitat de Catalunya and PROMETEO and GenT Programmes Generalitat Valenciana, Spain; Göran Gustafssons Stiftelse, Sweden; The Royal Society and Leverhulme Trust, United Kingdom.

The crucial computing support from all WLCG partners is acknowledged gratefully, in particular from CERN, the ATLAS Tier-1 facilities at TRIUMF (Canada), NDGF (Denmark, Norway, Sweden), CC-IN2P3 (France), KIT/GridKA (Germany), INFN-CNAF (Italy), NL-T1 (Netherlands), PIC (Spain), ASGC

(Taiwan), RAL (UK) and BNL (USA), the Tier-2 facilities worldwide and large non-WLCG resource providers. Major contributors of computing resources are listed in Ref. [[130](#)].

References

- [1] ATLAS Collaboration, *Observation of a new particle in the search for the Standard Model Higgs boson with the ATLAS detector at the LHC*, *Phys. Lett. B* **716** (2012) 1, arXiv: [1207.7214 \[hep-ex\]](#).
- [2] CMS Collaboration, *Observation of a new boson at a mass of 125 GeV with the CMS experiment at the LHC*, *Phys. Lett. B* **716** (2012) 30, arXiv: [1207.7235 \[hep-ex\]](#).
- [3] L. Susskind, *Dynamics of Spontaneous Symmetry Breaking in the Weinberg-Salam Theory*, *Phys. Rev. D* **20** (1979) 2619.
- [4] C. T. Hill and E. H. Simmons, *Strong dynamics and electroweak symmetry breaking*, *Phys. Rept.* **381** (2003) 235, arXiv: [hep-ph/0203079](#).
- [5] S. Dimopoulos and J. Preskill, *Massless Composites With Massive Constituents*, *Nucl. Phys. B* **199** (1982) 206.
- [6] D. B. Kaplan and H. Georgi, *$SU(2) \times U(1)$ Breaking by Vacuum Misalignment*, *Phys. Lett. B* **136** (1984) 183.
- [7] D. B. Kaplan, H. Georgi and S. Dimopoulos, *Composite Higgs Scalars*, *Phys. Lett. B* **136** (1984) 187.
- [8] M. Schmaltz and D. Tucker-Smith, *Little Higgs review*, *Ann. Rev. Nucl. Part. Sci.* **55** (2005) 229, arXiv: [hep-ph/0502182](#).
- [9] M. Perelstein, M. E. Peskin and A. Pierce, *Top quarks and electroweak symmetry breaking in little Higgs models*, *Phys. Rev. D* **69** (2004) 075002, arXiv: [hep-ph/0310039](#).
- [10] T. Gherghetta and A. Pomarol, *Bulk fields and supersymmetry in a slice of AdS*, *Nucl. Phys. B* **586** (2000) 141, arXiv: [hep-ph/0003129](#).
- [11] S. P. Martin, *Extra vector-like matter and the lightest Higgs scalar boson mass in low-energy supersymmetry*, *Phys. Rev. D* **81** (2010) 035004, arXiv: [0910.2732 \[hep-ph\]](#).
- [12] F. del Aguila and M. J. Bowick, *The Possibility of New Fermions With $\Delta I = 0$ Mass*, *Nucl. Phys. B* **224** (1983) 107.
- [13] J. A. Aguilar-Saavedra, *Mixing with vector-like quarks: constraints and expectations*, *EPJ Web Conf.* **60** (2013) 16012, arXiv: [1306.4432 \[hep-ph\]](#).
- [14] J. A. Aguilar-Saavedra, *Identifying top partners at LHC*, *JHEP* **11** (2009) 030, arXiv: [0907.3155 \[hep-ph\]](#).
- [15] M. Buchkremer, G. Cacciapaglia, A. Deandrea and L. Panizzi, *Model Independent Framework for Searches of Top Partners*, *Nucl. Phys. B* **876** (2013) 376, arXiv: [1305.4172 \[hep-ph\]](#).
- [16] M. Chala, *Direct bounds on heavy toplike quarks with standard and exotic decays*, *Phys. Rev. D* **96** (2017) 015028, arXiv: [1705.03013 \[hep-ph\]](#).
- [17] J. C. Criado and M. Perez-Victoria, *Vector-like quarks with non-renormalizable interactions*, *JHEP* **01** (2020) 057, arXiv: [1908.08964 \[hep-ph\]](#).

- [18] M. Chala, J. Juknevich, G. Perez and J. Santiago, *The Elusive Gluon*, **JHEP** **01** (2015) 092, arXiv: [1411.1771 \[hep-ph\]](#).
- [19] J. P. Araque, N. F. Castro and J. Santiago, *Interpretation of Vector-like Quark Searches: Heavy Gluons in Composite Higgs Models*, **JHEP** **11** (2015) 120, arXiv: [1507.05628 \[hep-ph\]](#).
- [20] ATLAS Collaboration, *Combination of the searches for pair-produced vector-like partners of the third-generation quarks at $\sqrt{s} = 13$ TeV with the ATLAS detector*, **Phys. Rev. Lett.** **121** (2018) 211801, arXiv: [1808.02343 \[hep-ex\]](#).
- [21] ATLAS Collaboration, *Search for single production of a vector-like T quark decaying into a Higgs boson and top quark with fully hadronic final states using the ATLAS detector*, **Phys. Rev. D** **105** (2022) 092012, arXiv: [2201.07045 \[hep-ex\]](#).
- [22] ATLAS Collaboration, *Search for large missing transverse momentum in association with one top-quark in proton-proton collisions at $\sqrt{s} = 13$ TeV with the ATLAS detector*, **JHEP** **05** (2019) 041, arXiv: [1812.09743 \[hep-ex\]](#).
- [23] ATLAS Collaboration, *Search for single production of vector-like quarks decaying into Wb in pp collisions at $\sqrt{s} = 13$ TeV with the ATLAS detector*, **JHEP** **05** (2019) 164, arXiv: [1812.07343 \[hep-ex\]](#).
- [24] ATLAS Collaboration, *Search for pair- and single-production of vector-like quarks in final states with at least one Z boson decaying into a pair of electrons or muons in pp collision data collected with the ATLAS detector at $\sqrt{s} = 13$ TeV*, **Phys. Rev. D** **98** (2018) 112010, arXiv: [1806.10555 \[hep-ex\]](#).
- [25] CMS Collaboration, *Search for single production of vector-like quarks decaying into a b quark and a W boson in proton-proton collisions at $\sqrt{s} = 13$ TeV*, **Phys. Lett. B** **772** (2017) 634, arXiv: [1701.08328 \[hep-ex\]](#).
- [26] CMS Collaboration, *Search for single production of a heavy vector-like T quark decaying to a Higgs boson and a top quark with a lepton and jets in the final state*, **Phys. Lett. B** **771** (2017) 80, arXiv: [1612.00999 \[hep-ex\]](#).
- [27] CMS Collaboration, *Search for single production of a vector-like T quark decaying to a Z boson and a top quark in proton-proton collisions at $\sqrt{s} = 13$ TeV*, **Phys. Lett. B** **781** (2018) 574, arXiv: [1708.01062 \[hep-ex\]](#).
- [28] CMS Collaboration, *Search for single production of vector-like quarks decaying to a top quark and a W boson in proton-proton collisions at $\sqrt{s} = 13$ TeV*, **Eur. Phys. J. C** **79** (2019) 90, arXiv: [1809.08597 \[hep-ex\]](#).
- [29] CMS Collaboration, *Search for electroweak production of a vector-like quark decaying to a top quark and a Higgs boson using boosted topologies in fully hadronic final states*, **JHEP** **04** (2017) 136, arXiv: [1612.05336 \[hep-ex\]](#).
- [30] CMS Collaboration, *Search for electroweak production of a vector-like T quark using fully hadronic final states*, **JHEP** **01** (2020) 036, arXiv: [1909.04721 \[hep-ex\]](#).
- [31] CMS Collaboration, *Search for single production of a vector-like T quark decaying to a top quark and a Z boson in the final state with jets and missing transverse momentum at $\sqrt{s} = 13$ TeV*, **JHEP** **05** (2022) 093, arXiv: [2201.02227 \[hep-ex\]](#).

- [32] ATLAS Collaboration, *The ATLAS Experiment at the CERN Large Hadron Collider*, **JINST** **3** (2008) S08003.
- [33] ATLAS Collaboration, *ATLAS Insertable B-Layer: Technical Design Report*, ATLAS-TDR-19; CERN-LHCC-2010-013, 2010, URL: <https://cds.cern.ch/record/1291633>, Addendum: ATLAS-TDR-19-ADD-1; CERN-LHCC-2012-009, 2012, URL: <https://cds.cern.ch/record/1451888>.
- [34] B. Abbott et al., *Production and integration of the ATLAS Insertable B-Layer*, **JINST** **13** (2018) T05008, arXiv: [1803.00844](https://arxiv.org/abs/1803.00844) [[physics.ins-det](#)].
- [35] ATLAS Collaboration, *Performance of the ATLAS trigger system in 2015*, **Eur. Phys. J. C** **77** (2017) 317, arXiv: [1611.09661](https://arxiv.org/abs/1611.09661) [[hep-ex](#)].
- [36] ATLAS Collaboration, *The ATLAS Collaboration Software and Firmware*, ATL-SOFT-PUB-2021-001, 2021, URL: <https://cds.cern.ch/record/2767187>.
- [37] ATLAS Collaboration, *Vertex Reconstruction Performance of the ATLAS Detector at $\sqrt{s} = 13$ TeV*, ATL-PHYS-PUB-2015-026, 2015, URL: <https://cds.cern.ch/record/2037717>.
- [38] ATLAS Collaboration, *Electron reconstruction and identification in the ATLAS experiment using the 2015 and 2016 LHC proton–proton collision data at $\sqrt{s} = 13$ TeV*, **Eur. Phys. J. C** **79** (2019) 639, arXiv: [1902.04655](https://arxiv.org/abs/1902.04655) [[hep-ex](#)].
- [39] ATLAS Collaboration, *Muon reconstruction and identification efficiency in ATLAS using the full Run 2 pp collision data set at $\sqrt{s} = 13$ TeV*, **Eur. Phys. J. C** **81** (2021) 578, arXiv: [2012.00578](https://arxiv.org/abs/2012.00578) [[hep-ex](#)].
- [40] M. Cacciari, G. P. Salam and G. Soyez, *The anti- k_t jet clustering algorithm*, **JHEP** **04** (2008) 063, arXiv: [0802.1189](https://arxiv.org/abs/0802.1189) [[hep-ph](#)].
- [41] M. Cacciari, G. P. Salam and G. Soyez, *FastJet user manual*, **Eur. Phys. J. C** **72** (2012) 1896, arXiv: [1111.6097](https://arxiv.org/abs/1111.6097) [[hep-ph](#)].
- [42] ATLAS Collaboration, *Topological cell clustering in the ATLAS calorimeters and its performance in LHC Run 1*, **Eur. Phys. J. C** **77** (2017) 490, arXiv: [1603.02934](https://arxiv.org/abs/1603.02934) [[hep-ex](#)].
- [43] ATLAS Collaboration, *Jet reconstruction and performance using particle flow with the ATLAS Detector*, **Eur. Phys. J. C** **77** (2017) 466, arXiv: [1703.10485](https://arxiv.org/abs/1703.10485) [[hep-ex](#)].
- [44] ATLAS Collaboration, *Jet energy scale and resolution measured in proton–proton collisions at $\sqrt{s} = 13$ TeV with the ATLAS detector*, **Eur. Phys. J. C** **81** (2021) 689, arXiv: [2007.02645](https://arxiv.org/abs/2007.02645) [[hep-ex](#)].
- [45] ATLAS Collaboration, *Selection of jets produced in 13 TeV proton–proton collisions with the ATLAS detector*, ATLAS-CONF-2015-029, 2015, URL: <https://cds.cern.ch/record/2037702>.
- [46] ATLAS Collaboration, *Performance of pile-up mitigation techniques for jets in pp collisions at $\sqrt{s} = 8$ TeV using the ATLAS detector*, **Eur. Phys. J. C** **76** (2016) 581, arXiv: [1510.03823](https://arxiv.org/abs/1510.03823) [[hep-ex](#)].
- [47] ATLAS Collaboration, *Identification and rejection of pile-up jets at high pseudorapidity with the ATLAS detector*, **Eur. Phys. J. C** **77** (2017) 580, arXiv: [1705.02211](https://arxiv.org/abs/1705.02211) [[hep-ex](#)], Erratum: **Eur. Phys. J. C** **77** (2017) 712.

- [48] D. Krohn, J. Thaler and L.-T. Wang, *Jets with Variable R*, **JHEP** **06** (2009) 059, arXiv: [0903.0392 \[hep-ph\]](#).
- [49] ATLAS Collaboration, *ATLAS flavour-tagging algorithms for the LHC Run 2 pp collision dataset*, (2022), arXiv: [2211.16345 \[physics.data-an\]](#).
- [50] B. Nachman, P. Nef, A. Schwartzman, M. Swiatlowski and C. Wanotayaroj, *Jets from Jets: Re-clustering as a tool for large radius jet reconstruction and grooming at the LHC*, **JHEP** **02** (2015) 075, arXiv: [1407.2922 \[hep-ph\]](#).
- [51] D. Krohn, J. Thaler and L.-T. Wang, *Jet Trimming*, **JHEP** **02** (2010) 084, arXiv: [0912.1342 \[hep-ph\]](#).
- [52] ATLAS Collaboration, *Performance of missing transverse momentum reconstruction with the ATLAS detector using proton-proton collisions at $\sqrt{s} = 13$ TeV*, **Eur. Phys. J. C** **78** (2018) 903, arXiv: [1802.08168 \[hep-ex\]](#).
- [53] ATLAS Collaboration, *Performance of the ATLAS Trigger System in 2015*, **Eur. Phys. J. C** **77** (2017) 317, arXiv: [1611.09661 \[hep-ex\]](#).
- [54] ATLAS Collaboration, *Performance of the ATLAS muon triggers in Run 2*, **JINST** **15** (2020) P09015, arXiv: [2004.13447 \[hep-ex\]](#).
- [55] ATLAS Collaboration, *Performance of electron and photon triggers in ATLAS during LHC Run 2*, **Eur. Phys. J. C** **80** (2020) 47, arXiv: [1909.00761 \[hep-ex\]](#).
- [56] ATLAS Collaboration, *Performance of the missing transverse momentum triggers for the ATLAS detector during Run-2 data taking*, **JHEP** **08** (2020) 080, arXiv: [2005.09554 \[hep-ex\]](#).
- [57] T. Gleisberg et al., *Event generation with SHERPA 1.1*, **JHEP** **02** (2009) 007, arXiv: [0811.4622 \[hep-ph\]](#).
- [58] D. J. Lange, *The EvtGen particle decay simulation package*, **Nucl. Instrum. Meth. A** **462** (2001) 152.
- [59] T. Sjöstrand, S. Mrenna and P. Skands, *A brief introduction to PYTHIA 8.1*, **Comput. Phys. Commun.** **178** (2008) 852, arXiv: [0710.3820 \[hep-ph\]](#).
- [60] ATLAS Collaboration, *ATLAS Pythia 8 tunes to 7 TeV data*, ATL-PHYS-PUB-2014-021, 2014, URL: <https://cds.cern.ch/record/1966419>.
- [61] NNPDF Collaboration, R. D. Ball et al., *Parton distributions with LHC data*, **Nucl. Phys. B** **867** (2013) 244, arXiv: [1207.1303 \[hep-ph\]](#).
- [62] J. Bellm et al., *Herwig 7.0/Herwig++ 3.0 release note*, **Eur. Phys. J. C** **76** (2016) 196, arXiv: [1512.01178 \[hep-ph\]](#).
- [63] L. A. Harland-Lang, A. D. Martin, P. Motylinski and R. S. Thorne, *Parton distributions in the LHC era: MMHT 2014 PDFs*, **Eur. Phys. J. C** **75** (2015) 204, arXiv: [1412.3989 \[hep-ph\]](#).
- [64] ATLAS Collaboration, *The ATLAS Simulation Infrastructure*, **Eur. Phys. J. C** **70** (2010) 823, arXiv: [1005.4568 \[physics.ins-det\]](#).
- [65] S. Agostinelli et al., *GEANT4 – a simulation toolkit*, **Nucl. Instrum. Meth. A** **506** (2003) 250.
- [66] ATLAS Collaboration, *The simulation principle and performance of the ATLAS fast calorimeter simulation FastCaloSim*, ATL-PHYS-PUB-2010-013 (2010), <https://cds.cern.ch/record/1300517>.

- [67] J. Alwall et al., *The automated computation of tree-level and next-to-leading order differential cross sections, and their matching to parton shower simulations*, **JHEP** **07** (2014) 079, arXiv: [1405.0301 \[hep-ph\]](#).
- [68] The NNPDF Collaboration, R. D. Ball et al., *Parton distributions for the LHC run II*, **JHEP** **04** (2015) 040, arXiv: [1410.8849 \[hep-ph\]](#).
- [69] T. Sjöstrand et al., *An introduction to PYTHIA 8.2*, **Comput. Phys. Commun.** **191** (2015) 159, arXiv: [1410.3012 \[hep-ph\]](#).
- [70] O. Mattelaer, *On the maximal use of Monte Carlo samples: re-weighting events at NLO accuracy*, **Eur. Phys. J. C** **76** (2016) 674, arXiv: [1607.00763 \[hep-ph\]](#).
- [71] G. Cacciapaglia et al., *Next-to-leading-order predictions for single vector-like quark production at the LHC*, **Phys. Lett. B** **793** (2019) 206, arXiv: [1811.05055 \[hep-ph\]](#).
- [72] A. Roy, N. Nikiforou, N. Castro and T. Andeen, *Novel interpretation strategy for searches of singly produced vectorlike quarks at the LHC*, **Phys. Rev. D** **101** (2020) 115027, arXiv: [2003.00640 \[hep-ph\]](#).
- [73] A. Roy and T. Andeen, *Non-resonant diagrams for single production of top and bottom partners*, **Phys. Lett. B** **833** (2022) 137330, arXiv: [2202.02640 \[hep-ph\]](#).
- [74] S. Frixione, G. Ridolfi and P. Nason, *A positive-weight next-to-leading-order Monte Carlo for heavy flavour hadroproduction*, **JHEP** **09** (2007) 126, arXiv: [0707.3088 \[hep-ph\]](#).
- [75] P. Nason, *A new method for combining NLO QCD with shower Monte Carlo algorithms*, **JHEP** **11** (2004) 040, arXiv: [hep-ph/0409146](#).
- [76] S. Frixione, P. Nason and C. Oleari, *Matching NLO QCD computations with parton shower simulations: the POWHEG method*, **JHEP** **11** (2007) 070, arXiv: [0709.2092 \[hep-ph\]](#).
- [77] S. Alioli, P. Nason, C. Oleari and E. Re, *A general framework for implementing NLO calculations in shower Monte Carlo programs: the POWHEG BOX*, **JHEP** **06** (2010) 043, arXiv: [1002.2581 \[hep-ph\]](#).
- [78] ATLAS Collaboration, *Studies on top-quark Monte Carlo modelling for Top2016*, ATL-PHYS-PUB-2016-020, 2016, URL: <https://cds.cern.ch/record/2216168>.
- [79] S. Frixione, E. Laenen, P. Motylinski, C. White and B. R. Webber, *Single-top hadroproduction in association with a W boson*, **JHEP** **07** (2008) 029, arXiv: [0805.3067 \[hep-ph\]](#).
- [80] M. Bähr et al., *Herwig++ physics and manual*, **Eur. Phys. J. C** **58** (2008) 639, arXiv: [0803.0883 \[hep-ph\]](#).
- [81] ATLAS Collaboration, *Search for the Standard Model Higgs boson produced in association with top quarks and decaying into $b\bar{b}$ in pp collisions at $\sqrt{s}=8$ TeV with the ATLAS detector*, **Eur. Phys. J. C** **75** (2015) 349, arXiv: [1503.05066 \[hep-ex\]](#).
- [82] M. Beneke, P. Falgari, S. Klein and C. Schwinn, *Hadronic top-quark pair production with NNLL threshold resummation*, **Nucl. Phys. B** **855** (2012) 695, arXiv: [1109.1536 \[hep-ph\]](#).

- [83] M. Cacciari, M. Czakon, M. Mangano, A. Mitov and P. Nason, *Top-pair production at hadron colliders with next-to-next-to-leading logarithmic soft-gluon resummation*, [Phys. Lett. B **710** \(2012\) 612](#), arXiv: [1111.5869 \[hep-ph\]](#).
- [84] P. Bärnreuther, M. Czakon and A. Mitov, *Percent-Level-Precision Physics at the Tevatron: Next-to-Next-to-Leading Order QCD Corrections to $q\bar{q} \rightarrow t\bar{t} + X$* , [Phys. Rev. Lett. **109** \(2012\) 132001](#), arXiv: [1204.5201 \[hep-ph\]](#).
- [85] M. Czakon and A. Mitov, *NNLO corrections to top-pair production at hadron colliders: the all-fermionic scattering channels*, [JHEP **12** \(2012\) 054](#), arXiv: [1207.0236 \[hep-ph\]](#).
- [86] M. Czakon and A. Mitov, *NNLO corrections to top pair production at hadron colliders: the quark-gluon reaction*, [JHEP **01** \(2013\) 080](#), arXiv: [1210.6832 \[hep-ph\]](#).
- [87] M. Czakon, P. Fiedler and A. Mitov, *Total Top-Quark Pair-Production Cross Section at Hadron Colliders Through $O(\alpha_S^4)$* , [Phys. Rev. Lett. **110** \(2013\) 252004](#), arXiv: [1303.6254 \[hep-ph\]](#).
- [88] M. Czakon and A. Mitov, *Top++: A program for the calculation of the top-pair cross-section at hadron colliders*, [Comput. Phys. Commun. **185** \(2014\) 2930](#), arXiv: [1112.5675 \[hep-ph\]](#).
- [89] J. Butterworth et al., *PDF4LHC recommendations for LHC Run II*, [J. Phys. G **43** \(2016\) 023001](#), arXiv: [1510.03865 \[hep-ph\]](#).
- [90] A. D. Martin, W. J. Stirling, R. S. Thorne and G. Watt, *Parton distributions for the LHC*, [Eur. Phys. J. C **63** \(2009\) 189](#), arXiv: [0901.0002 \[hep-ph\]](#).
- [91] A. D. Martin, W. J. Stirling, R. S. Thorne and G. Watt, *Uncertainties on α_S in global PDF analyses and implications for predicted hadronic cross sections*, [Eur. Phys. J. C **64** \(2009\) 653](#), arXiv: [0905.3531 \[hep-ph\]](#).
- [92] H.-L. Lai et al., *New parton distributions for collider physics*, [Phys. Rev. D **82** \(2010\) 074024](#), arXiv: [1007.2241 \[hep-ph\]](#).
- [93] J. Gao et al., *CT10 next-to-next-to-leading order global analysis of QCD*, [Phys. Rev. D **89** \(2014\) 033009](#), arXiv: [1302.6246 \[hep-ph\]](#).
- [94] E. Bothmann et al., *Event generation with Sherpa 2.2*, [SciPost Phys. **7** \(2019\) 034](#), arXiv: [1905.09127 \[hep-ph\]](#).
- [95] T. Gleisberg and S. Höche, *Comix, a new matrix element generator*, [JHEP **12** \(2008\) 039](#), arXiv: [0808.3674 \[hep-ph\]](#).
- [96] F. Buccioni et al., *OpenLoops 2*, [Eur. Phys. J. C **79** \(2019\) 866](#), arXiv: [1907.13071 \[hep-ph\]](#).
- [97] F. Cascioli, P. Maierhöfer and S. Pozzorini, *Scattering Amplitudes with Open Loops*, [Phys. Rev. Lett. **108** \(2012\) 111601](#), arXiv: [1111.5206 \[hep-ph\]](#).
- [98] A. Denner, S. Dittmaier and L. Hofer, *COLLIER: A fortran-based complex one-loop library in extended regularizations*, [Comput. Phys. Commun. **212** \(2017\) 220](#), arXiv: [1604.06792 \[hep-ph\]](#).
- [99] S. Schumann and F. Krauss, *A parton shower algorithm based on Catani–Seymour dipole factorisation*, [JHEP **03** \(2008\) 038](#), arXiv: [0709.1027 \[hep-ph\]](#).

- [100] S. Höche, F. Krauss, M. Schönherr and F. Siegert, *A critical appraisal of NLO+PS matching methods*, **JHEP** **09** (2012) 049, arXiv: [1111.1220 \[hep-ph\]](#).
- [101] S. Höche, F. Krauss, M. Schönherr and F. Siegert, *QCD matrix elements + parton showers. The NLO case*, **JHEP** **04** (2013) 027, arXiv: [1207.5030 \[hep-ph\]](#).
- [102] S. Catani, F. Krauss, B. R. Webber and R. Kuhn, *QCD Matrix Elements + Parton Showers*, **JHEP** **11** (2001) 063, arXiv: [hep-ph/0109231](#).
- [103] S. Höche, F. Krauss, S. Schumann and F. Siegert, *QCD matrix elements and truncated showers*, **JHEP** **05** (2009) 053, arXiv: [0903.1219 \[hep-ph\]](#).
- [104] C. Anastasiou, L. Dixon, K. Melnikov and F. Petriello, *High-precision QCD at hadron colliders: Electroweak gauge boson rapidity distributions at next-to-next-to leading order*, **Phys. Rev. D** **69** (2004) 094008, arXiv: [hep-ph/0312266](#).
- [105] H. B. Hartanto, B. Jäger, L. Reina and D. Wackerth, *Higgs boson production in association with top quarks in the POWHEG BOX*, **Phys. Rev. D** **91** (2015) 094003, arXiv: [1501.04498 \[hep-ph\]](#).
- [106] A. Deandrea, T. Flacke, B. Fuks, L. Panizzi and H.-S. Shao, *Single production of vector-like quarks: the effects of large width, interference and NLO corrections*, **JHEP** **08** (2021) 107, arXiv: [2105.08745 \[hep-ph\]](#).
- [107] ATLAS Collaboration, *Measurements of top-quark pair differential and double-differential cross-sections in the ℓ +jets channel with pp collisions at $\sqrt{s} = 13$ TeV using the ATLAS detector*, **Eur. Phys. J. C** **79** (2019) 1028, arXiv: [1908.07305 \[hep-ex\]](#), Erratum: **Eur. Phys. J. C** **80** (2020) 1092.
- [108] ATLAS Collaboration, *Measurement of the $t\bar{t}$ production cross-section and lepton differential distributions in $e\mu$ dilepton events from pp collisions at $\sqrt{s} = 13$ TeV with the ATLAS detector*, **Eur. Phys. J. C** **80** (2020) 528, arXiv: [1910.08819 \[hep-ex\]](#).
- [109] ATLAS Collaboration, *ATLAS simulation of boson plus jets processes in Run 2*, ATL-PHYS-PUB-2017-006, 2017, URL: <https://cds.cern.ch/record/2261937>.
- [110] ATLAS Collaboration, *Electron and photon performance measurements with the ATLAS detector using the 2015–2017 LHC proton–proton collision data*, **JINST** **14** (2019) P12006, arXiv: [1908.00005 \[hep-ex\]](#).
- [111] ATLAS Collaboration, *Jet energy scale and resolution measured in proton–proton collisions at $\sqrt{s} = 13$ TeV with the ATLAS detector*, **Eur. Phys. J. C** **81** (2020) 689, arXiv: [2007.02645 \[hep-ex\]](#).
- [112] ATLAS Collaboration, *ATLAS b-jet identification performance and efficiency measurement with $t\bar{t}$ events in pp collisions at $\sqrt{s} = 13$ TeV*, **Eur. Phys. J. C** **79** (2019) 970, arXiv: [1907.05120 \[hep-ex\]](#).
- [113] ATLAS Collaboration, *Measurement of the c-jet mistagging efficiency in $t\bar{t}$ events using pp collision data at $\sqrt{s} = 13$ TeV collected with the ATLAS detector*, **Eur. Phys. J. C** **82** (2022) 95, arXiv: [2109.10627 \[hep-ex\]](#).

- [114] ATLAS Collaboration, *Calibration of the light-flavour jet mistagging efficiency of the b -tagging algorithms with Z +jets events using 139 fb^{-1} of ATLAS proton-proton collision data at $\sqrt{s} = 13 \text{ TeV}$, (2023), arXiv: [2301.06319 \[hep-ex\]](#).*
- [115] ATLAS Collaboration, *Measurements of inclusive and differential fiducial cross-sections of $t\bar{t}$ production with additional heavy-flavour jets in proton-proton collisions at $\sqrt{s} = 13 \text{ TeV}$ with the ATLAS detector*, *JHEP* **04** (2019) 046, arXiv: [1811.12113 \[hep-ex\]](#).
- [116] N. Kidonakis, *Next-to-next-to-leading-order collinear and soft gluon corrections for t -channel single top quark production*, *Phys. Rev. D* **83** (2011) 091503, arXiv: [1103.2792 \[hep-ph\]](#).
- [117] N. Kidonakis, *Two-loop soft anomalous dimensions for single top quark associated production with a W^- or H^-* , *Phys. Rev. D* **82** (2010) 054018, arXiv: [1005.4451 \[hep-ph\]](#).
- [118] N. Kidonakis, *NNLL resummation for s -channel single top quark production*, *Phys. Rev. D* **81** (2010) 054028, arXiv: [1001.5034 \[hep-ph\]](#).
- [119] ATLAS Collaboration, *Studies on top-quark Monte Carlo modelling with Sherpa and MG5_aMC@NLO*, ATL-PHYS-PUB-2017-007, 2017, URL: <https://cds.cern.ch/record/2261938>.
- [120] ATLAS Collaboration, *Measurement of Higgs boson decay into b -quarks in associated production with a top-quark pair in pp collisions at $\sqrt{s} = 13 \text{ TeV}$ with the ATLAS detector*, *JHEP* **06** (2022) 097, arXiv: [2111.06712 \[hep-ex\]](#).
- [121] J. M. Campbell and R. K. Ellis, *Update on vector boson pair production at hadron colliders*, *Phys. Rev. D* **60** (1999) 113006, arXiv: [hep-ph/9905386](#).
- [122] J. Alwall et al., *Comparative study of various algorithms for the merging of parton showers and matrix elements in hadronic collisions*, *Eur. Phys. J. C* **53** (2008) 473, arXiv: [0706.2569 \[hep-ph\]](#).
- [123] W. Verkerke and D. P. Kirkby, *The RooFit toolkit for data modeling*, eConf **C0303241** (2003) MOLT007, ed. by L. Lyons and M. Karagoz, arXiv: [physics/0306116](#).
- [124] L. Moneta et al., *The RooStats Project*, *PoS ACAT2010* (2010) 057, ed. by T. Speer et al., arXiv: [1009.1003 \[physics.data-an\]](#).
- [125] M. Baak et al., *HistFitter software framework for statistical data analysis*, *Eur. Phys. J. C* **75** (2015) 153, arXiv: [1410.1280 \[hep-ex\]](#).
- [126] G. Cowan, K. Cranmer, E. Gross and O. Vitells, *Asymptotic formulae for likelihood-based tests of new physics*, *Eur. Phys. J. C* **71** (2011) 1554, arXiv: [1007.1727 \[physics.data-an\]](#).
- [127] G. Cowan, K. Cranmer, E. Gross and O. Vitells, *Erratum to: Asymptotic formulae for likelihood-based tests of new physics*, *Eur. Phys. J. C* **73** (2013).
- [128] T. Junk, *Confidence level computation for combining searches with small statistics*, *Nucl. Instrum. Meth. A* **434** (1999) 435, arXiv: [hep-ex/9902006](#).
- [129] A. L. Read, *Presentation of search results: The CL_S technique*, *J. Phys. G* **28** (2002) 2693.

- [130] *ATLAS Computing Acknowledgements*, tech. rep., CERN, 2021,
URL: <https://cds.cern.ch/record/2776662>.

The ATLAS Collaboration

G. Aad ¹⁰², B. Abbott ¹²⁰, K. Abeling ⁵⁵, S.H. Abidi ²⁹, A. Abouhorma ^{35e},
H. Abramowicz ¹⁵¹, H. Abreu ¹⁵⁰, Y. Abulaiti ¹¹⁷, A.C. Abusleme Hoffman ^{137a},
B.S. Acharya ^{69a,69b,p}, C. Adam Bourdarios ⁴, L. Adamczyk ^{85a}, L. Adamek ¹⁵⁵,
S.V. Addepalli ²⁶, M.J. Addison ¹⁰¹, J. Adelman ¹¹⁵, A. Adiguzel ^{21c}, S. Adorni ⁵⁶, T. Adye ¹³⁴,
A.A. Affolder ¹³⁶, Y. Afik ³⁶, M.N. Agaras ¹³, J. Agarwala ^{73a,73b}, A. Aggarwal ¹⁰⁰,
C. Agheorghiesei ^{27c}, A. Ahmad ³⁶, F. Ahmadov ^{38,ab}, W.S. Ahmed ¹⁰⁴, S. Ahuja ⁹⁵, X. Ai ^{62a},
G. Aielli ^{76a,76b}, M. Ait Tamlihat ^{35e}, B. Aitbenkikh ^{35a}, I. Aizenberg ¹⁶⁹, M. Akbiyik ¹⁰⁰,
T.P.A. Åkesson ⁹⁸, A.V. Akimov ³⁷, D. Akiyama ¹⁶⁸, N.N. Akolkar ²⁴, K. Al Khoury ⁴¹,
G.L. Alberghi ^{23b}, J. Albert ¹⁶⁵, P. Albicocco ⁵³, S. Alderweireldt ⁵², M. Aleksa ³⁶,
I.N. Aleksandrov ³⁸, C. Alexa ^{27b}, T. Alexopoulos ¹⁰, A. Alfonsi ¹¹⁴, F. Alfonsi ^{23b},
M. Alhroob ¹²⁰, B. Ali ¹³², S. Ali ¹⁴⁸, M. Aliev ³⁷, G. Alimonti ^{71a}, W. Alkakhki ⁵⁵,
C. Allaire ⁶⁶, B.M.M. Allbrooke ¹⁴⁶, C.A. Allendes Flores ^{137f}, P.P. Allport ²⁰, A. Aloisio ^{72a,72b},
F. Alonso ⁹⁰, C. Alpigiani ¹³⁸, M. Alvarez Estevez ⁹⁹, A. Alvarez Fernandez ¹⁰⁰,
M.G. Alvigi ^{72a,72b}, M. Aly ¹⁰¹, Y. Amaral Coutinho ^{82b}, A. Ambler ¹⁰⁴, C. Amelung ³⁶,
M. Amerl ¹⁰¹, C.G. Ames ¹⁰⁹, D. Amidei ¹⁰⁶, S.P. Amor Dos Santos ^{130a}, K.R. Amos ¹⁶³,
V. Ananiev ¹²⁵, C. Anastopoulos ¹³⁹, T. Andeen ¹¹, J.K. Anders ³⁶, S.Y. Andrean ^{47a,47b},
A. Andreazza ^{71a,71b}, S. Angelidakis ⁹, A. Angerami ^{41,ae}, A.V. Anisenkov ³⁷, A. Annovi ^{74a},
C. Antel ⁵⁶, M.T. Anthony ¹³⁹, E. Antipov ¹⁴⁵, M. Antonelli ⁵³, D.J.A. Antrim ^{17a}, F. Anulli ^{75a},
M. Aoki ⁸³, T. Aoki ¹⁵³, J.A. Aparisi Pozo ¹⁶³, M.A. Aparo ¹⁴⁶, L. Aperio Bella ⁴⁸,
C. Appelt ¹⁸, N. Aranzabal ³⁶, V. Araujo Ferraz ^{82a}, C. Arcangeletti ⁵³, A.T.H. Arce ⁵¹,
E. Arena ⁹², J-F. Arguin ¹⁰⁸, S. Argyropoulos ⁵⁴, J.-H. Arling ⁴⁸, A.J. Armbruster ³⁶,
O. Arnaez ⁴, H. Arnold ¹¹⁴, Z.P. Arrubarrena Tame ¹⁰⁹, G. Artoni ^{75a,75b}, H. Asada ¹¹¹,
K. Asai ¹¹⁸, S. Asai ¹⁵³, N.A. Asbah ⁶¹, J. Assahsah ^{35d}, K. Assamagan ²⁹, R. Astalos ^{28a},
R.J. Atkin ^{33a}, M. Atkinson ¹⁶², N.B. Atlay ¹⁸, H. Atmani ^{62b}, P.A. Atlasiddha ¹⁰⁶, K. Augsten ¹³²,
S. Auricchio ^{72a,72b}, A.D. Auriol ²⁰, V.A. Austrup ¹⁷¹, G. Avolio ³⁶, K. Axiotis ⁵⁶,
G. Azuelos ^{108,ai}, D. Babal ^{28b}, H. Bachacou ¹³⁵, K. Bachas ^{152,s}, A. Bachiu ³⁴,
F. Backman ^{47a,47b}, A. Badea ⁶¹, P. Bagnaia ^{75a,75b}, M. Bahmani ¹⁸, A.J. Bailey ¹⁶³,
V.R. Bailey ¹⁶², J.T. Baines ¹³⁴, C. Bakalis ¹⁰, O.K. Baker ¹⁷², E. Bakos ¹⁵, D. Bakshi Gupta ⁸,
R. Balasubramanian ¹¹⁴, E.M. Baldin ³⁷, P. Balek ^{85a}, E. Ballabene ^{71a,71b}, F. Balli ¹³⁵,
L.M. Baltes ^{63a}, W.K. Balunas ³², J. Balz ¹⁰⁰, E. Banas ⁸⁶, M. Bandieramonte ¹²⁹,
A. Bandyopadhyay ²⁴, S. Bansal ²⁴, L. Barak ¹⁵¹, E.L. Barberio ¹⁰⁵, D. Barberis ^{57b,57a},
M. Barbero ¹⁰², G. Barbour ⁹⁶, K.N. Barends ^{33a}, T. Barillari ¹¹⁰, M-S. Barisits ³⁶, T. Barklow ¹⁴³,
P. Baron ¹²², D.A. Baron Moreno ¹⁰¹, A. Baroncelli ^{62a}, G. Barone ²⁹, A.J. Barr ¹²⁶,
J.D. Barr ⁹⁶, L. Barranco Navarro ^{47a,47b}, F. Barreiro ⁹⁹, J. Barreiro Guimarães da Costa ^{14a},
U. Barron ¹⁵¹, M.G. Barros Teixeira ^{130a}, S. Barsov ³⁷, F. Bartels ^{63a}, R. Bartoldus ¹⁴³,
A.E. Barton ⁹¹, P. Bartos ^{28a}, A. Basan ¹⁰⁰, M. Baselga ⁴⁹, A. Bassalat ^{66,b}, M.J. Basso ¹⁵⁵,
C.R. Basson ¹⁰¹, R.L. Bates ⁵⁹, S. Batlamous ^{35e}, J.R. Batley ³², B. Batool ¹⁴¹, M. Battaglia ¹³⁶,
D. Battulga ¹⁸, M. Bauge ^{75a,75b}, M. Bauer ³⁶, P. Bauer ²⁴, J.B. Beacham ⁵¹, T. Beau ¹²⁷,
P.H. Beauchemin ¹⁵⁸, F. Becherer ⁵⁴, P. Bechtel ²⁴, H.P. Beck ^{19,r}, K. Becker ¹⁶⁷,
A.J. Beddall ^{21d}, V.A. Bednyakov ³⁸, C.P. Bee ¹⁴⁵, L.J. Beemster ¹⁵, T.A. Beermann ³⁶,
M. Begalli ^{82d}, M. Begel ²⁹, A. Behera ¹⁴⁵, J.K. Behr ⁴⁸, J.F. Beirer ⁵⁵, F. Beisiegel ²⁴,
M. Belfkir ¹⁵⁹, G. Bella ¹⁵¹, L. Bellagamba ^{23b}, A. Bellerive ³⁴, P. Bellos ²⁰,
K. Beloborodov ³⁷, N.L. Belyaev ³⁷, D. Benckekroun ^{35a}, F. Bendebba ^{35a}, Y. Benhammou ¹⁵¹,
M. Benoit ²⁹, J.R. Bensinger ²⁶, S. Bentvelsen ¹¹⁴, L. Beresford ⁴⁸, M. Beretta ⁵³,

E. Bergeaas Kuutmann [id](#)¹⁶¹, N. Berger [id](#)⁴, B. Bergmann [id](#)¹³², J. Beringer [id](#)^{17a}, S. Berlendis [id](#)⁷,
 G. Bernardi [id](#)⁵, C. Bernius [id](#)¹⁴³, F.U. Bernlochner [id](#)²⁴, F. Bernon [id](#)^{36,102}, T. Berry [id](#)⁹⁵, P. Berta [id](#)¹³³,
 A. Berthold [id](#)⁵⁰, I.A. Bertram [id](#)⁹¹, S. Bethke [id](#)¹¹⁰, A. Betti [id](#)^{75a,75b}, A.J. Bevan [id](#)⁹⁴, M. Bhamjee [id](#)^{33c},
 S. Bhatta [id](#)¹⁴⁵, D.S. Bhattacharya [id](#)¹⁶⁶, P. Bhattarai [id](#)²⁶, V.S. Bhopatkar [id](#)¹²¹, R. Bi [id](#)^{29,ak},
 R.M. Bianchi [id](#)¹²⁹, G. Bianco [id](#)^{23b,23a}, O. Biebel [id](#)¹⁰⁹, R. Bielski [id](#)¹²³, M. Biglietti [id](#)^{77a},
 T.R.V. Billoud [id](#)¹³², M. Bindi [id](#)⁵⁵, A. Bingul [id](#)^{21b}, C. Bini [id](#)^{75a,75b}, A. Biondini [id](#)⁹²,
 C.J. Birch-sykes [id](#)¹⁰¹, G.A. Bird [id](#)^{20,134}, M. Birman [id](#)¹⁶⁹, M. Biros [id](#)¹³³, T. Bisanz [id](#)⁴⁹,
 E. Bisceglie [id](#)^{43b,43a}, D. Biswas [id](#)¹⁷⁰, A. Bitadze [id](#)¹⁰¹, K. Bjørke [id](#)¹²⁵, I. Bloch [id](#)⁴⁸, C. Blocker [id](#)²⁶,
 A. Blue [id](#)⁵⁹, U. Blumenschein [id](#)⁹⁴, J. Blumenthal [id](#)¹⁰⁰, G.J. Bobbink [id](#)¹¹⁴, V.S. Bobrovnikov [id](#)³⁷,
 M. Boehler [id](#)⁵⁴, B. Boehm [id](#)¹⁶⁶, D. Bogavac [id](#)³⁶, A.G. Bogdanchikov [id](#)³⁷, C. Bohm [id](#)^{47a},
 V. Boisvert [id](#)⁹⁵, P. Bokan [id](#)⁴⁸, T. Bold [id](#)^{85a}, M. Bomben [id](#)⁵, M. Bona [id](#)⁹⁴, M. Boonekamp [id](#)¹³⁵,
 C.D. Booth [id](#)⁹⁵, A.G. Borbély [id](#)⁵⁹, I.S. Bordulev [id](#)³⁷, H.M. Borecka-Bielska [id](#)¹⁰⁸, L.S. Borgna [id](#)⁹⁶,
 G. Borissov [id](#)⁹¹, D. Bortoletto [id](#)¹²⁶, D. Boscherini [id](#)^{23b}, M. Bosman [id](#)¹³, J.D. Bossio Sola [id](#)³⁶,
 K. Bouaouda [id](#)^{35a}, N. Bouchhar [id](#)¹⁶³, J. Boudreau [id](#)¹²⁹, E.V. Bouhova-Thacker [id](#)⁹¹, D. Boumediene [id](#)⁴⁰,
 R. Bouquet [id](#)⁵, A. Boveia [id](#)¹¹⁹, J. Boyd [id](#)³⁶, D. Boye [id](#)²⁹, I.R. Boyko [id](#)³⁸, J. Bracinik [id](#)²⁰,
 N. Brahimy [id](#)^{62d}, G. Brandt [id](#)¹⁷¹, O. Brandt [id](#)³², F. Braren [id](#)⁴⁸, B. Brau [id](#)¹⁰³, J.E. Brau [id](#)¹²³,
 R. Brenner [id](#)¹⁶⁹, L. Brenner [id](#)¹¹⁴, R. Brenner [id](#)¹⁶¹, S. Bressler [id](#)¹⁶⁹, D. Britton [id](#)⁵⁹, D. Britzger [id](#)¹¹⁰,
 I. Brock [id](#)²⁴, G. Brooijmans [id](#)⁴¹, W.K. Brooks [id](#)^{137f}, E. Brost [id](#)²⁹, L.M. Brown [id](#)¹⁶⁵,
 T.L. Bruckler [id](#)¹²⁶, P.A. Bruckman de Renstrom [id](#)⁸⁶, B. Brüers [id](#)⁴⁸, D. Bruncko [id](#)^{28b,*}, A. Bruni [id](#)^{23b},
 G. Bruni [id](#)^{23b}, M. Bruschi [id](#)^{23b}, N. Bruscano [id](#)^{75a,75b}, T. Buanes [id](#)¹⁶, Q. Buat [id](#)¹³⁸, D. Buchin [id](#)¹¹⁰,
 A.G. Buckley [id](#)⁵⁹, I.A. Budagov [id](#)^{38,*}, M.K. Bugge [id](#)¹²⁵, O. Bulekov [id](#)³⁷, B.A. Bullard [id](#)¹⁴³,
 S. Burdin [id](#)⁹², C.D. Burgard [id](#)⁴⁹, A.M. Burger [id](#)⁴⁰, B. Burghgrave [id](#)⁸, O. Burlayenko [id](#)⁵⁴,
 J.T.P. Burr [id](#)³², C.D. Burton [id](#)¹¹, J.C. Burzynski [id](#)¹⁴², E.L. Busch [id](#)⁴¹, V. Büscher [id](#)¹⁰⁰, P.J. Bussey [id](#)⁵⁹,
 J.M. Butler [id](#)²⁵, C.M. Buttar [id](#)⁵⁹, J.M. Butterworth [id](#)⁹⁶, W. Buttinger [id](#)¹³⁴, C.J. Buxo Vazquez [id](#)¹⁰⁷,
 A.R. Buzykaev [id](#)³⁷, G. Cabras [id](#)^{23b}, S. Cabrera Urbán [id](#)¹⁶³, D. Caforio [id](#)⁵⁸, H. Cai [id](#)¹²⁹, Y. Cai [id](#)^{14a,14e},
 V.M.M. Cairo [id](#)³⁶, O. Cakir [id](#)^{3a}, N. Calace [id](#)³⁶, P. Calafiura [id](#)^{17a}, G. Calderini [id](#)¹²⁷, P. Calfayan [id](#)⁶⁸,
 G. Callea [id](#)⁵⁹, L.P. Caloba [id](#)^{82b}, D. Calvet [id](#)⁴⁰, S. Calvet [id](#)⁴⁰, T.P. Calvet [id](#)¹⁰², M. Calvetti [id](#)^{74a,74b},
 R. Camacho Toro [id](#)¹²⁷, S. Camarda [id](#)³⁶, D. Camarero Munoz [id](#)²⁶, P. Camarri [id](#)^{76a,76b},
 M.T. Camerlingo [id](#)^{72a,72b}, D. Cameron [id](#)¹²⁵, C. Camincher [id](#)¹⁶⁵, M. Campanelli [id](#)⁹⁶, A. Camplani [id](#)⁴²,
 V. Canale [id](#)^{72a,72b}, A. Canesse [id](#)¹⁰⁴, M. Cano Bret [id](#)⁸⁰, J. Cantero [id](#)¹⁶³, Y. Cao [id](#)¹⁶², F. Capocasa [id](#)²⁶,
 M. Capua [id](#)^{43b,43a}, A. Carbone [id](#)^{71a,71b}, R. Cardarelli [id](#)^{76a}, J.C.J. Cardenas [id](#)⁸, F. Cardillo [id](#)¹⁶³,
 T. Carli [id](#)³⁶, G. Carlino [id](#)^{72a}, J.I. Carlotto [id](#)¹³, B.T. Carlson [id](#)^{129,t}, E.M. Carlson [id](#)^{165,156a},
 L. Carminati [id](#)^{71a,71b}, M. Carnesale [id](#)^{75a,75b}, S. Caron [id](#)¹¹³, E. Carquin [id](#)^{137f}, S. Carrá [id](#)^{71a,71b},
 G. Carratta [id](#)^{23b,23a}, F. Carrio Argos [id](#)^{33g}, J.W.S. Carter [id](#)¹⁵⁵, T.M. Carter [id](#)⁵², M.P. Casado [id](#)^{13j},
 A.F. Casha [id](#)¹⁵⁵, M. Caspar [id](#)⁴⁸, E.G. Castiglia [id](#)¹⁷², F.L. Castillo [id](#)^{63a}, L. Castillo Garcia [id](#)¹³,
 V. Castillo Gimenez [id](#)¹⁶³, N.F. Castro [id](#)^{130a,130e}, A. Catinaccio [id](#)³⁶, J.R. Catmore [id](#)¹²⁵, V. Cavaliere [id](#)²⁹,
 N. Cavalli [id](#)^{23b,23a}, V. Cavalanni [id](#)^{74a,74b}, Y.C. Cekmecelioglu [id](#)⁴⁸, E. Celebi [id](#)^{21a}, F. Celli [id](#)¹²⁶,
 M.S. Centonze [id](#)^{70a,70b}, K. Cerny [id](#)¹²², A.S. Cerqueira [id](#)^{82a}, A. Cerri [id](#)¹⁴⁶, L. Cerrito [id](#)^{76a,76b},
 F. Cerutti [id](#)^{17a}, B. Cervato [id](#)¹⁴¹, A. Cervelli [id](#)^{23b}, G. Cesarini [id](#)⁵³, S.A. Cetin [id](#)^{21d}, Z. Chadi [id](#)^{35a},
 D. Chakraborty [id](#)¹¹⁵, M. Chala [id](#)^{130f}, J. Chan [id](#)¹⁷⁰, W.Y. Chan [id](#)¹⁵³, J.D. Chapman [id](#)³²,
 E. Chapon [id](#)¹³⁵, B. Chargeishvili [id](#)^{149b}, D.G. Charlton [id](#)²⁰, T.P. Charman [id](#)⁹⁴, M. Chatterjee [id](#)¹⁹,
 C. Chauhan [id](#)¹³³, S. Chekanov [id](#)⁶, S.V. Chekulaev [id](#)^{156a}, G.A. Chelkov [id](#)^{38,a}, A. Chen [id](#)¹⁰⁶,
 B. Chen [id](#)¹⁵¹, B. Chen [id](#)¹⁶⁵, H. Chen [id](#)^{14c}, H. Chen [id](#)²⁹, J. Chen [id](#)^{62c}, J. Chen [id](#)¹⁴², M. Chen [id](#)¹²⁶,
 S. Chen [id](#)¹⁵³, S.J. Chen [id](#)^{14c}, X. Chen [id](#)^{62c}, X. Chen [id](#)^{14b,ah}, Y. Chen [id](#)^{62a}, C.L. Cheng [id](#)¹⁷⁰,
 H.C. Cheng [id](#)^{64a}, S. Cheong [id](#)¹⁴³, A. Cheplakov [id](#)³⁸, E. Cheremushkina [id](#)⁴⁸, E. Cherepanova [id](#)¹¹⁴,
 R. Cherkaoui El Moursli [id](#)^{35e}, E. Cheu [id](#)⁷, K. Cheung [id](#)⁶⁵, L. Chevalier [id](#)¹³⁵, V. Chiarella [id](#)⁵³,
 G. Chiarelli [id](#)^{74a}, N. Chiedde [id](#)¹⁰², G. Chiodini [id](#)^{70a}, A.S. Chisholm [id](#)²⁰, A. Chitan [id](#)^{27b},

M. Chitishvili ¹⁶³, M.V. Chizhov ³⁸, K. Choi ¹¹, A.R. Chomont ^{75a,75b}, Y. Chou ¹⁰³,
E.Y.S. Chow ¹¹⁴, T. Chowdhury ^{33g}, L.D. Christopher ^{33g}, K.L. Chu ¹⁶⁹, M.C. Chu ^{64a},
X. Chu ^{14a,14e}, J. Chudoba ¹³¹, J.J. Chwastowski ⁸⁶, D. Cieri ¹¹⁰, K.M. Ciesla ^{85a}, V. Cindro ⁹³,
A. Ciocio ^{17a}, F. Cirotto ^{72a,72b}, Z.H. Citron ^{169,m}, M. Citterio ^{71a}, D.A. Ciubotaru ^{27b},
B.M. Ciungu ¹⁵⁵, A. Clark ⁵⁶, P.J. Clark ⁵², J.M. Clavijo Columbie ⁴⁸, S.E. Clawson ⁴⁸,
C. Clement ^{47a,47b}, J. Clercx ⁴⁸, L. Clissa ^{23b,23a}, Y. Coadou ¹⁰², M. Cobal ^{69a,69c},
A. Coccaro ^{57b}, R.F. Coelho Barrue ^{130a}, R. Coelho Lopes De Sa ¹⁰³, S. Coelli ^{71a}, H. Cohen ¹⁵¹,
A.E.C. Coimbra ^{71a,71b}, B. Cole ⁴¹, J. Collot ⁶⁰, P. Conde Muiño ^{130a,130g}, M.P. Connell ^{33c},
S.H. Connell ^{33c}, I.A. Connelly ⁵⁹, E.I. Conroy ¹²⁶, F. Conventi ^{72a,aj}, H.G. Cooke ²⁰,
A.M. Cooper-Sarkar ¹²⁶, A. Cordeiro Oudot Choi ¹²⁷, F. Cormier ¹⁶⁴, L.D. Corpe ⁴⁰,
M. Corradi ^{75a,75b}, F. Corriveau ^{104,z}, A. Cortes-Gonzalez ¹⁸, M.J. Costa ¹⁶³, F. Costanza ⁴,
D. Costanzo ¹³⁹, B.M. Cote ¹¹⁹, G. Cowan ⁹⁵, K. Cranmer ¹¹⁷, D. Cremonini ^{23b,23a},
S. Crépe-Renaudin ⁶⁰, F. Crescioli ¹²⁷, M. Cristinziani ¹⁴¹, M. Cristoforetti ^{78a,78b,d}, V. Croft ¹¹⁴,
J.E. Crosby ¹²¹, G. Crosetti ^{43b,43a}, A. Cueto ³⁶, T. Cuhadar Donszelmann ¹⁶⁰, H. Cui ^{14a,14e},
Z. Cui ⁷, W.R. Cunningham ⁵⁹, F. Curcio ^{43b,43a}, P. Czodrowski ³⁶, M.M. Czurylo ^{63b},
M.J. Da Cunha Sargedas De Sousa ^{62a}, J.V. Da Fonseca Pinto ^{82b}, C. Da Via ¹⁰¹, W. Dabrowski ^{85a},
T. Dado ⁴⁹, S. Dahbi ^{33g}, T. Dai ¹⁰⁶, C. Dallapiccola ¹⁰³, M. Dam ⁴², G. D'amen ²⁹,
V. D'Amico ¹⁰⁹, J. Damp ¹⁰⁰, J.R. Dandoy ¹²⁸, M.F. Daneri ³⁰, M. Danninger ¹⁴², V. Dao ³⁶,
G. Darbo ^{57b}, S. Darmora ⁶, S.J. Das ^{29,ak}, S. D'Auria ^{71a,71b}, C. David ^{156b}, T. Davidek ¹³³,
B. Davis-Purcell ³⁴, I. Dawson ⁹⁴, H.A. Day-hall ¹³², K. De ⁸, R. De Asmundis ^{72a},
N. De Biase ⁴⁸, S. De Castro ^{23b,23a}, N. De Groot ¹¹³, P. de Jong ¹¹⁴, H. De la Torre ¹⁰⁷,
A. De Maria ^{14c}, A. De Salvo ^{75a}, U. De Sanctis ^{76a,76b}, A. De Santo ¹⁴⁶,
J.B. De Vivie De Regie ⁶⁰, D.V. Dedovich ³⁸, J. Degens ¹¹⁴, A.M. Deiana ⁴⁴, F. Del Corso ^{23b,23a},
J. Del Peso ⁹⁹, F. Del Rio ^{63a}, F. Deliot ¹³⁵, C.M. Delitzsch ⁴⁹, M. Della Pietra ^{72a,72b},
D. Della Volpe ⁵⁶, A. Dell'Acqua ³⁶, L. Dell'Asta ^{71a,71b}, M. Delmastro ⁴, P.A. Delsart ⁶⁰,
S. Demers ¹⁷², M. Demichev ³⁸, S.P. Denisov ³⁷, L. D'Eramo ⁴⁰, D. Derendarz ⁸⁶, F. Derue ¹²⁷,
P. Dervan ⁹², K. Desch ²⁴, K. Dette ¹⁵⁵, C. Deutsch ²⁴, F.A. Di Bello ^{57b,57a},
A. Di Ciaccio ^{76a,76b}, L. Di Ciaccio ⁴, A. Di Domenico ^{75a,75b}, C. Di Donato ^{72a,72b},
A. Di Girolamo ³⁶, G. Di Gregorio ⁵, A. Di Luca ^{78a,78b}, B. Di Micco ^{77a,77b}, R. Di Nardo ^{77a,77b},
C. Diaconu ¹⁰², F.A. Dias ¹¹⁴, T. Dias Do Vale ¹⁴², M.A. Diaz ^{137a,137b}, F.G. Diaz Capriles ²⁴,
M. Didenko ¹⁶³, E.B. Diehl ¹⁰⁶, L. Diehl ⁵⁴, S. Díez Cornell ⁴⁸, C. Diez Pardos ¹⁴¹,
C. Dimitriadi ^{24,161}, A. Dimitrievska ^{17a}, J. Dingfelder ²⁴, I-M. Dinu ^{27b}, S.J. Dittmeier ^{63b},
F. Dittus ³⁶, F. Djama ¹⁰², T. Djobava ^{149b}, J.I. Djuvsland ¹⁶, C. Doglioni ^{101,98}, J. Dolejsi ¹³³,
Z. Dolezal ¹³³, M. Donadelli ^{82c}, B. Dong ¹⁰⁷, J. Donini ⁴⁰, A. D'Onofrio ^{77a,77b},
M. D'Onofrio ⁹², J. Dopke ¹³⁴, A. Doria ^{72a}, M.T. Dova ⁹⁰, A.T. Doyle ⁵⁹, M.A. Draguet ¹²⁶,
E. Drechsler ¹⁴², E. Dreyer ¹⁶⁹, I. Drivas-koulouris ¹⁰, A.S. Drobac ¹⁵⁸, M. Drozdova ⁵⁶,
D. Du ^{62a}, T.A. du Pree ¹¹⁴, F. Dubinin ³⁷, M. Dubovsky ^{28a}, E. Duchovni ¹⁶⁹, G. Duckeck ¹⁰⁹,
O.A. Ducu ^{27b}, D. Duda ⁵², A. Dudarev ³⁶, E.R. Duden ²⁶, M. D'uffizi ¹⁰¹, L. Duflot ⁶⁶,
M. Dührssen ³⁶, C. Dülsen ¹⁷¹, A.E. Dumitriu ^{27b}, M. Dunford ^{63a}, S. Dungs ⁴⁹,
K. Dunne ^{47a,47b}, A. Duperrin ¹⁰², H. Duran Yildiz ^{3a}, M. Düren ⁵⁸, A. Durglishvili ^{149b},
B.L. Dwyer ¹¹⁵, G.I. Dyckes ^{17a}, M. Dyndal ^{85a}, S. Dysch ¹⁰¹, B.S. Dziedzic ⁸⁶,
Z.O. Earnshaw ¹⁴⁶, G.H. Eberwein ¹²⁶, B. Eckerova ^{28a}, S. Eggebrecht ⁵⁵, M.G. Eggleston ⁵¹,
E. Egidio Purcino De Souza ¹²⁷, L.F. Ehrke ⁵⁶, G. Eigen ¹⁶, K. Einsweiler ^{17a}, T. Ekelof ¹⁶¹,
P.A. Ekman ⁹⁸, Y. El Ghazali ^{35b}, H. El Jarrari ^{35e,148}, A. El Moussaouy ^{35a}, V. Ellajosyula ¹⁶¹,
M. Ellert ¹⁶¹, F. Ellinghaus ¹⁷¹, A.A. Elliot ⁹⁴, N. Ellis ³⁶, J. Elmsheuser ²⁹, M. Elsing ³⁶,
D. Emelianov ¹³⁴, Y. Enari ¹⁵³, I. Ene ^{17a}, S. Epari ¹³, J. Erdmann ⁴⁹, P.A. Erland ⁸⁶,
M. Errenst ¹⁷¹, M. Escalier ⁶⁶, C. Escobar ¹⁶³, E. Etzion ¹⁵¹, G. Evans ^{130a}, H. Evans ⁶⁸,

L.S. Evans ⁹⁵, M.O. Evans ¹⁴⁶, A. Ezhilov ³⁷, S. Ezzarqtouni ^{35a}, F. Fabbri ⁵⁹, L. Fabbri ^{23b,23a},
 G. Facini ⁹⁶, V. Fadeyev ¹³⁶, R.M. Fakhrtudinov ³⁷, S. Falciano ^{75a}, L.F. Falda Ulhoa Coelho ³⁶,
 P.J. Falke ²⁴, J. Faltova ¹³³, C. Fan ¹⁶², Y. Fan ^{14a}, Y. Fang ^{14a,14e}, M. Fanti ^{71a,71b},
 M. Faraj ^{69a,69b}, Z. Farazpay ⁹⁷, A. Farbin ⁸, A. Farilla ^{77a}, T. Farooque ¹⁰⁷, S.M. Farrington ⁵²,
 F. Fassi ^{35e}, D. Fassouliotis ⁹, M. Fauci Giannelli ^{76a,76b}, W.J. Fawcett ³², L. Fayard ⁶⁶,
 P. Federic ¹³³, P. Federicova ¹³¹, O.L. Fedin ^{37,a}, G. Fedotov ³⁷, M. Feickert ¹⁷⁰,
 L. Feligioni ¹⁰², A. Fell ¹³⁹, D.E. Fellers ¹²³, C. Feng ^{62b}, M. Feng ^{14b}, Z. Feng ¹¹⁴,
 M.J. Fenton ¹⁶⁰, A.B. Fenyuk ³⁷, L. Ferencz ⁴⁸, R.A.M. Ferguson ⁹¹, S.I. Fernandez Luengo ^{137f},
 M.J.V. Fernoux ¹⁰², J. Ferrando ⁴⁸, A. Ferrari ¹⁶¹, P. Ferrari ^{114,113}, R. Ferrari ^{73a}, D. Ferrere ⁵⁶,
 C. Ferretti ¹⁰⁶, F. Fiedler ¹⁰⁰, A. Filipčić ⁹³, E.K. Filmer ¹, F. Filthaut ¹¹³,
 M.C.N. Fiolhais ^{130a,130c,c}, L. Fiorini ¹⁶³, W.C. Fisher ¹⁰⁷, T. Fitschen ¹⁰¹, P.M. Fitzhugh ¹³⁵,
 I. Fleck ¹⁴¹, P. Fleischmann ¹⁰⁶, T. Flick ¹⁷¹, L. Flores ¹²⁸, M. Flores ^{33d,af},
 L.R. Flores Castillo ^{64a}, F.M. Follega ^{78a,78b}, N. Fomin ¹⁶, J.H. Foo ¹⁵⁵, B.C. Forland ⁶⁸,
 A. Formica ¹³⁵, A.C. Forti ¹⁰¹, E. Fortin ³⁶, A.W. Fortman ⁶¹, M.G. Foti ^{17a}, L. Fountas ^{9,k},
 D. Fournier ⁶⁶, H. Fox ⁹¹, P. Francavilla ^{74a,74b}, S. Francescato ⁶¹, S. Franchellucci ⁵⁶,
 M. Franchini ^{23b,23a}, S. Franchino ^{63a}, D. Francis ³⁶, L. Franco ¹¹³, L. Franconi ⁴⁸, M. Franklin ⁶¹,
 G. Frattari ²⁶, A.C. Freegard ⁹⁴, W.S. Freund ^{82b}, Y.Y. Frid ¹⁵¹, N. Fritzsche ⁵⁰, A. Froch ⁵⁴,
 D. Froidevaux ³⁶, J.A. Frost ¹²⁶, Y. Fu ^{62a}, M. Fujimoto ¹¹⁸, E. Fullana Torregrosa ^{163,*},
 E. Furtado De Simas Filho ^{82b}, M. Furukawa ¹⁵³, J. Fuster ¹⁶³, A. Gabrielli ^{23b,23a},
 A. Gabrielli ¹⁵⁵, P. Gadow ⁴⁸, G. Gagliardi ^{57b,57a}, L.G. Gagnon ^{17a}, E.J. Gallas ¹²⁶,
 B.J. Gallop ¹³⁴, K.K. Gan ¹¹⁹, S. Ganguly ¹⁵³, J. Gao ^{62a}, Y. Gao ⁵², F.M. Garay Walls ^{137a,137b},
 B. Garcia ^{29,ak}, C. García ¹⁶³, A. Garcia Alonso ¹¹⁴, A.G. Garcia Caffaro ¹⁷²,
 J.E. García Navarro ¹⁶³, M. Garcia-Sciveres ^{17a}, G.L. Gardner ¹²⁸, R.W. Gardner ³⁹,
 N. Garelli ¹⁵⁸, D. Garg ⁸⁰, R.B. Garg ^{143,q}, J.M. Gargan ⁵², C.A. Garner ¹⁵⁵, S.J. Gasiorowski ¹³⁸,
 P. Gaspar ^{82b}, G. Gaudio ^{73a}, V. Gautam ¹³, P. Gauzzi ^{75a,75b}, I.L. Gavrilenko ³⁷, A. Gavriyuk ³⁷,
 C. Gay ¹⁶⁴, G. Gaycken ⁴⁸, E.N. Gazis ¹⁰, A.A. Geanta ^{27b,27e}, C.M. Gee ¹³⁶, C. Gemme ^{57b},
 M.H. Genest ⁶⁰, S. Gentile ^{75a,75b}, S. George ⁹⁵, W.F. George ²⁰, T. Geralis ⁴⁶, L.O. Gerlach ⁵⁵,
 P. Gessinger-Befurt ³⁶, M.E. Geyik ¹⁷¹, M. Ghneimat ¹⁴¹, K. Ghorbanian ⁹⁴, A. Ghosal ¹⁴¹,
 A. Ghosh ¹⁶⁰, A. Ghosh ⁷, B. Giacobbe ^{23b}, S. Giagu ^{75a,75b}, P. Giannetti ^{74a}, A. Giannini ^{62a},
 S.M. Gibson ⁹⁵, M. Gignac ¹³⁶, D.T. Gil ^{85b}, A.K. Gilbert ^{85a}, B.J. Gilbert ⁴¹, D. Gillberg ³⁴,
 G. Gilles ¹¹⁴, N.E.K. Gillwald ⁴⁸, L. Ginabat ¹²⁷, D.M. Gingrich ^{2,ai}, M.P. Giordani ^{69a,69c},
 P.F. Giraud ¹³⁵, G. Giugliarelli ^{69a,69c}, D. Giugni ^{71a}, F. Giuli ³⁶, I. Gkialas ^{9,k}, L.K. Gladilin ³⁷,
 C. Glasman ⁹⁹, G.R. Gledhill ¹²³, M. Glisic ¹²³, I. Gnesi ^{43b,g}, Y. Go ^{29,ak}, M. Goblirsch-Kolb ³⁶,
 B. Gocke ⁴⁹, D. Godin ¹⁰⁸, B. Gokturk ^{21a}, S. Goldfarb ¹⁰⁵, T. Golling ⁵⁶, M.G.D. Gololo ^{33g},
 D. Golubkov ³⁷, J.P. Gombas ¹⁰⁷, A. Gomes ^{130a,130b}, G. Gomes Da Silva ¹⁴¹,
 A.J. Gomez Delegido ¹⁶³, R. Gonçalo ^{130a,130c}, G. Gonella ¹²³, L. Gonella ²⁰, A. Gongadze ³⁸,
 F. Gonnella ²⁰, J.L. Gonski ⁴¹, R.Y. González Andana ⁵², S. González de la Hoz ¹⁶³,
 S. Gonzalez Fernandez ¹³, R. Gonzalez Lopez ⁹², C. Gonzalez Renteria ^{17a},
 R. Gonzalez Suarez ¹⁶¹, S. Gonzalez-Sevilla ⁵⁶, G.R. Gonzalvo Rodriguez ¹⁶³, L. Goossens ³⁶,
 P.A. Gorbounov ³⁷, B. Gorini ³⁶, E. Gorini ^{70a,70b}, A. Gorišek ⁹³, T.C. Gosart ¹²⁸,
 A.T. Goshaw ⁵¹, M.I. Gostkin ³⁸, S. Goswami ¹²¹, C.A. Gottardo ³⁶, M. Gouighri ^{35b},
 V. Goumarre ⁴⁸, A.G. Goussiou ¹³⁸, N. Govender ^{33c}, I. Grabowska-Bold ^{85a}, K. Graham ³⁴,
 E. Gramstad ¹²⁵, S. Grancagnolo ^{70a,70b}, M. Grandi ¹⁴⁶, V. Gratchev ^{37,*}, P.M. Gravila ^{27f},
 F.G. Gravili ^{70a,70b}, H.M. Gray ^{17a}, M. Greco ^{70a,70b}, C. Grefe ²⁴, I.M. Gregor ⁴⁸, P. Grenier ¹⁴³,
 C. Grieco ¹³, A.A. Grillo ¹³⁶, K. Grimm ^{31,n}, S. Grinstein ^{13,v}, J.-F. Grivaz ⁶⁶, E. Gross ¹⁶⁹,
 J. Grosse-Knetter ⁵⁵, C. Grud ¹⁰⁶, J.C. Grundy ¹²⁶, L. Guan ¹⁰⁶, W. Guan ¹⁷⁰, C. Gubbels ¹⁶⁴,
 J.G.R. Guerrero Rojas ¹⁶³, G. Guerrieri ^{69a,69b}, F. Guescini ¹¹⁰, R. Gugel ¹⁰⁰, J.A.M. Guhit ¹⁰⁶,

A. Guida ⁴⁸, T. Guillemin ⁴, E. Guilloton ^{167,134}, S. Guindon ³⁶, F. Guo ^{14a,14e}, J. Guo ^{62c},
 L. Guo ⁶⁶, Y. Guo ¹⁰⁶, R. Gupta ⁴⁸, S. Gurbuz ²⁴, S.S. Gurdasani ⁵⁴, G. Gustavino ³⁶,
 M. Guth ⁵⁶, P. Gutierrez ¹²⁰, L.F. Gutierrez Zagazeta ¹²⁸, C. Gutschow ⁹⁶, C. Gwenlan ¹²⁶,
 C.B. Gwilliam ⁹², E.S. Haaland ¹²⁵, A. Haas ¹¹⁷, M. Habedank ⁴⁸, C. Haber ^{17a},
 H.K. Hadavand ⁸, A. Hadeef ¹⁰⁰, S. Hadzic ¹¹⁰, J.J. Hahn ¹⁴¹, E.H. Haines ⁹⁶, M. Haleem ¹⁶⁶,
 J. Haley ¹²¹, J.J. Hall ¹³⁹, G.D. Hallewell ¹⁰², L. Halser ¹⁹, K. Hamano ¹⁶⁵, H. Hamdaoui ^{35e},
 M. Hamer ²⁴, G.N. Hamity ⁵², E.J. Hampshire ⁹⁵, J. Han ^{62b}, K. Han ^{62a}, L. Han ^{14c},
 L. Han ^{62a}, S. Han ^{17a}, Y.F. Han ¹⁵⁵, K. Hanagaki ⁸³, M. Hance ¹³⁶, D.A. Hangal ^{41,ae},
 H. Hanif ¹⁴², M.D. Hank ¹²⁸, R. Hankache ¹⁰¹, J.B. Hansen ⁴², J.D. Hansen ⁴², P.H. Hansen ⁴²,
 K. Hara ¹⁵⁷, D. Harada ⁵⁶, T. Harenberg ¹⁷¹, S. Harkusha ³⁷, Y.T. Harris ¹²⁶, N.M. Harrison ¹¹⁹,
 P.F. Harrison ¹⁶⁷, N.M. Hartman ¹⁴³, N.M. Hartmann ¹⁰⁹, Y. Hasegawa ¹⁴⁰, A. Hasib ⁵²,
 S. Haug ¹⁹, R. Hauser ¹⁰⁷, M. Havranek ¹³², C.M. Hawkes ²⁰, R.J. Hawkings ³⁶, Y. Hayashi ¹⁵³,
 S. Hayashida ¹¹¹, D. Hayden ¹⁰⁷, C. Hayes ¹⁰⁶, R.L. Hayes ¹¹⁴, C.P. Hays ¹²⁶, J.M. Hays ⁹⁴,
 H.S. Hayward ⁹², F. He ^{62a}, Y. He ¹⁵⁴, Y. He ¹²⁷, N.B. Heatley ⁹⁴, V. Hedberg ⁹⁸,
 A.L. Heggelund ¹²⁵, N.D. Hehir ⁹⁴, C. Heidegger ⁵⁴, K.K. Heidegger ⁵⁴, W.D. Heidorn ⁸¹,
 J. Heilman ³⁴, S. Heim ⁴⁸, T. Heim ^{17a}, J.G. Heinlein ¹²⁸, J.J. Heinrich ¹²³, L. Heinrich ^{110,ag},
 J. Hejbal ¹³¹, L. Helary ⁴⁸, A. Held ¹⁷⁰, S. Hellesund ¹⁶, C.M. Helling ¹⁶⁴, S. Hellman ^{47a,47b},
 C. Helsen ³⁶, R.C.W. Henderson ⁹¹, L. Henkelmann ³², A.M. Henriques Correia ³⁶, H. Herde ⁹⁸,
 Y. Hernández Jiménez ¹⁴⁵, L.M. Herrmann ²⁴, T. Herrmann ⁵⁰, G. Herten ⁵⁴, R. Hertenberger ¹⁰⁹,
 L. Hervas ³⁶, N.P. Hessey ^{156a}, H. Hibi ⁸⁴, S.J. Hillier ²⁰, F. Hinterkeuser ²⁴, M. Hirose ¹²⁴,
 S. Hirose ¹⁵⁷, D. Hirschbuehl ¹⁷¹, T.G. Hitchings ¹⁰¹, B. Hiti ⁹³, J. Hobbs ¹⁴⁵, R. Hobincu ^{27e},
 N. Hod ¹⁶⁹, M.C. Hodgkinson ¹³⁹, B.H. Hodgkinson ³², A. Hoecker ³⁶, J. Hofer ⁴⁸, T. Holm ²⁴,
 M. Holzbock ¹¹⁰, L.B.A.H. Hommels ³², B.P. Honan ¹⁰¹, J. Hong ^{62c}, T.M. Hong ¹²⁹,
 J.C. Honig ⁵⁴, B.H. Hooberman ¹⁶², W.H. Hopkins ⁶, Y. Horii ¹¹¹, S. Hou ¹⁴⁸, A.S. Howard ⁹³,
 J. Howarth ⁵⁹, J. Hoya ⁶, M. Hrabovsky ¹²², A. Hrynevich ⁴⁸, T. Hryn'ova ⁴, P.J. Hsu ⁶⁵,
 S.-C. Hsu ¹³⁸, Q. Hu ⁴¹, Y.F. Hu ^{14a,14e}, D.P. Huang ⁹⁶, S. Huang ^{64b}, X. Huang ^{14c},
 Y. Huang ^{62a}, Y. Huang ^{14a}, Z. Huang ¹⁰¹, Z. Hubacek ¹³², M. Huebner ²⁴, F. Huegging ²⁴,
 T.B. Huffman ¹²⁶, C.A. Hugli ⁴⁸, M. Huhtinen ³⁶, S.K. Huiberts ¹⁶, R. Hulsken ¹⁰⁴,
 N. Huseynov ^{12,a}, J. Huston ¹⁰⁷, J. Huth ⁶¹, R. Hyneman ¹⁴³, G. Iacobucci ⁵⁶, G. Iakovidis ²⁹,
 I. Ibragimov ¹⁴¹, L. Iconomidou-Fayard ⁶⁶, P. Iengo ^{72a,72b}, R. Iguchi ¹⁵³, T. Iizawa ⁵⁶,
 Y. Ikegami ⁸³, A. Ilg ¹⁹, N. Ilic ¹⁵⁵, H. Imam ^{35a}, T. Ingebretsen Carlson ^{47a,47b},
 G. Introzzi ^{73a,73b}, M. Iodice ^{77a}, V. Ippolito ^{75a,75b}, R.K. Irwin ⁹², M. Ishino ¹⁵³, W. Islam ¹⁷⁰,
 C. Issever ^{18,48}, S. Istin ^{21a,am}, H. Ito ¹⁶⁸, J.M. Iturbe Ponce ^{64a}, R. Iuppa ^{78a,78b}, A. Ivina ¹⁶⁹,
 J.M. Izen ⁴⁵, V. Izzo ^{72a}, P. Jacka ^{131,132}, P. Jackson ¹, R.M. Jacobs ⁴⁸, B.P. Jaeger ¹⁴²,
 C.S. Jagfeld ¹⁰⁹, P. Jain ⁵⁴, G. Jäkel ¹⁷¹, K. Jakobs ⁵⁴, T. Jakoubek ¹⁶⁹, J. Jamieson ⁵⁹,
 K.W. Janas ^{85a}, A.E. Jaspan ⁹², M. Javurkova ¹⁰³, F. Jeanneau ¹³⁵, L. Jeanty ¹²³,
 J. Jejelava ^{149a,ac}, P. Jenni ^{54,h}, C.E. Jessiman ³⁴, S. Jézéquel ⁴, C. Jia ^{62b}, J. Jia ¹⁴⁵, X. Jia ⁶¹,
 X. Jia ^{14a,14e}, Z. Jia ^{14c}, Y. Jiang ^{62a}, S. Jiggins ⁴⁸, J. Jimenez Pena ¹¹⁰, S. Jin ^{14c}, A. Jinaru ^{27b},
 O. Jinnouchi ¹⁵⁴, P. Johansson ¹³⁹, K.A. Johns ⁷, J.W. Johnson ¹³⁶, D.M. Jones ³², E. Jones ⁴⁸,
 P. Jones ³², R.W.L. Jones ⁹¹, T.J. Jones ⁹², R. Joshi ¹¹⁹, J. Jovicevic ¹⁵, X. Ju ^{17a},
 J.J. Jungburth ³⁶, T. Junkermann ^{63a}, A. Juste Rozas ^{13,v}, M.K. Juzek ⁸⁶, S. Kabana ^{137e},
 A. Kaczmarska ⁸⁶, M. Kado ¹¹⁰, H. Kagan ¹¹⁹, M. Kagan ¹⁴³, A. Kahn ⁴¹, A. Kahn ¹²⁸,
 C. Kahra ¹⁰⁰, T. Kaji ¹⁶⁸, E. Kajomovitz ¹⁵⁰, N. Kakati ¹⁶⁹, C.W. Kalderon ²⁹,
 A. Kamenshchikov ¹⁵⁵, S. Kanayama ¹⁵⁴, N.J. Kang ¹³⁶, D. Kar ^{33g}, K. Karava ¹²⁶,
 M.J. Kareem ^{156b}, E. Karentzos ⁵⁴, I. Karkanas ^{152,f}, S.N. Karpov ³⁸, Z.M. Karpova ³⁸,
 V. Kartvelishvili ⁹¹, A.N. Karyukhin ³⁷, E. Kasimi ^{152,f}, J. Katzy ⁴⁸, S. Kaur ³⁴, K. Kawade ¹⁴⁰,
 T. Kawamoto ¹³⁵, E.F. Kay ³⁶, F.I. Kaya ¹⁵⁸, S. Kazakos ¹³, V.F. Kazanin ³⁷, Y. Ke ¹⁴⁵,

J.M. Keaveney ^{id33a}, R. Keeler ^{id165}, G.V. Kehris ^{id61}, J.S. Keller ^{id34}, A.S. Kelly ^{id96}, J.J. Kempster ^{id146}, K.E. Kennedy ^{id41}, P.D. Kennedy ^{id100}, O. Kepka ^{id131}, B.P. Kerridge ^{id167}, S. Kersten ^{id171}, B.P. Kerševan ^{id93}, S. Keshri ^{id66}, L. Keszeghova ^{id28a}, S. Ketabchi Haghighat ^{id155}, M. Khandoga ^{id127}, A. Khanov ^{id121}, A.G. Kharlamov ^{id37}, T. Kharlamova ^{id37}, E.E. Khoda ^{id138}, T.J. Khoo ^{id18}, G. Khoriauli ^{id166}, J. Khubua ^{id149b}, Y.A.R. Khwaira ^{id66}, M. Kiehn ^{id36}, A. Kilgallon ^{id123}, D.W. Kim ^{id47a,47b}, Y.K. Kim ^{id39}, N. Kimura ^{id96}, A. Kirchhoff ^{id55}, C. Kirfel ^{id24}, J. Kirk ^{id134}, A.E. Kiryunin ^{id110}, D.P. Kisliuk ^{id155}, C. Kitsaki ^{id10}, O. Kivernyk ^{id24}, M. Klassen ^{id63a}, C. Klein ^{id34}, L. Klein ^{id166}, M.H. Klein ^{id106}, M. Klein ^{id92}, S.B. Klein ^{id56}, U. Klein ^{id92}, P. Klimek ^{id36}, A. Klimentov ^{id29}, T. Klioutchnikova ^{id36}, P. Kluit ^{id114}, S. Kluth ^{id110}, E. Kneringer ^{id79}, T.M. Knight ^{id155}, A. Knue ^{id54}, R. Kobayashi ^{id87}, S.F. Koch ^{id126}, M. Kocian ^{id143}, P. Kodyš ^{id133}, D.M. Koeck ^{id123}, P.T. Koenig ^{id24}, T. Koffas ^{id34}, M. Kolb ^{id135}, I. Koletsou ^{id4}, T. Komarek ^{id122}, K. Köneke ^{id54}, A.X.Y. Kong ^{id1}, T. Kono ^{id118}, N. Konstantinidis ^{id96}, B. Konya ^{id98}, R. Kopeliansky ^{id68}, S. Koperny ^{id85a}, K. Korcyl ^{id86}, K. Kordas ^{id152,f}, G. Koren ^{id151}, A. Korn ^{id96}, S. Korn ^{id55}, I. Korolkov ^{id13}, N. Korotkova ^{id37}, B. Kortman ^{id114}, O. Kortner ^{id110}, S. Kortner ^{id110}, W.H. Kostecka ^{id115}, V.V. Kostyukhin ^{id141}, A. Kotsokechagia ^{id135}, A. Kotwal ^{id51}, A. Koulouris ^{id36}, A. Kourkoumeli-Charalampidi ^{id73a,73b}, C. Kourkoumelis ^{id9}, E. Kourlitis ^{id6}, O. Kovanda ^{id146}, R. Kowalewski ^{id165}, W. Kozanecki ^{id135}, A.S. Kozhin ^{id37}, V.A. Kramarenko ^{id37}, G. Kramberger ^{id93}, P. Kramer ^{id100}, M.W. Krasny ^{id127}, A. Krasznahorkay ^{id36}, J.A. Kremer ^{id100}, T. Kresse ^{id50}, J. Kretzschmar ^{id92}, K. Kreul ^{id18}, P. Krieger ^{id155}, S. Krishnamurthy ^{id103}, M. Krivos ^{id133}, K. Krizka ^{id20}, K. Kroeninger ^{id49}, H. Kroha ^{id110}, J. Kroll ^{id131}, J. Kroll ^{id128}, K.S. Krowpman ^{id107}, U. Kruchonak ^{id38}, H. Krüger ^{id24}, N. Krumnack ^{id81}, M.C. Kruse ^{id51}, J.A. Krzysiak ^{id86}, O. Kuchinskaia ^{id37}, S. Kuday ^{id3a}, S. Kuehn ^{id36}, R. Kuesters ^{id54}, T. Kuhl ^{id48}, V. Kukhtin ^{id38}, Y. Kulchitsky ^{id37,a}, S. Kuleshov ^{id137d,137b}, M. Kumar ^{id33g}, N. Kumari ^{id102}, A. Kupco ^{id131}, T. Kupfer ^{id49}, A. Kupich ^{id37}, O. Kuprash ^{id54}, H. Kurashige ^{id84}, L.L. Kurchaninov ^{id156a}, O. Kurdysh ^{id66}, Y.A. Kurochkin ^{id37}, A. Kurova ^{id37}, M. Kuze ^{id154}, A.K. Kvam ^{id103}, J. Kvita ^{id122}, T. Kwan ^{id104}, N.G. Kyriacou ^{id106}, L.A.O. Laatu ^{id102}, C. Lacasta ^{id163}, F. Lacava ^{id75a,75b}, H. Lacker ^{id18}, D. Lacour ^{id127}, N.N. Lad ^{id96}, E. Ladygin ^{id38}, B. Laforge ^{id127}, T. Lagouri ^{id137e}, S. Lai ^{id55}, I.K. Lakomic ^{id85a}, N. Lalloue ^{id60}, J.E. Lambert ^{id120}, S. Lammers ^{id68}, W. Lampl ^{id7}, C. Lampoudis ^{id152,f}, A.N. Lancaster ^{id115}, E. Lançon ^{id29}, U. Landgraf ^{id54}, M.P.J. Landon ^{id94}, V.S. Lang ^{id54}, R.J. Langenberg ^{id103}, O.K.B. Langrekken ^{id125}, A.J. Lankford ^{id160}, F. Lanni ^{id36}, K. Lantzsck ^{id24}, A. Lanza ^{id73a}, A. Lapertosa ^{id57b,57a}, J.F. Laporte ^{id135}, T. Lari ^{id71a}, F. Lasagni Manghi ^{id23b}, M. Lassnig ^{id36}, V. Latonova ^{id131}, A. Laudrain ^{id100}, A. Laurier ^{id150}, S.D. Lawlor ^{id95}, Z. Lawrence ^{id101}, M. Lazzaroni ^{id71a,71b}, B. Le ^{id101}, E.M. Le Boulicaut ^{id51}, B. Leban ^{id93}, A. Lebedev ^{id81}, M. LeBlanc ^{id36}, F. Ledroit-Guillon ^{id60}, A.C.A. Lee ^{id96}, S.C. Lee ^{id148}, S. Lee ^{id47a,47b}, T.F. Lee ^{id92}, L.L. Leeuw ^{id33c}, H.P. Lefebvre ^{id95}, M. Lefebvre ^{id165}, C. Leggett ^{id17a}, K. Lehmann ^{id142}, G. Lehmann Miotto ^{id36}, M. Leigh ^{id56}, W.A. Leight ^{id103}, W. Leinonen ^{id113}, A. Leisos ^{id152,u}, M.A.L. Leite ^{id82c}, C.E. Leitgeb ^{id48}, R. Leitner ^{id133}, K.J.C. Leney ^{id44}, T. Lenz ^{id24}, S. Leone ^{id74a}, C. Leonidopoulos ^{id52}, A. Leopold ^{id144}, C. Leroy ^{id108}, R. Les ^{id107}, C.G. Lester ^{id32}, M. Levchenko ^{id37}, J. Levêque ^{id4}, D. Levin ^{id106}, L.J. Levinson ^{id169}, M.P. Lewicki ^{id86}, D.J. Lewis ^{id4}, A. Li ^{id5}, B. Li ^{id62b}, C. Li ^{id62a}, C-Q. Li ^{id62c}, H. Li ^{id62a}, H. Li ^{id62b}, H. Li ^{id14c}, H. Li ^{id62b}, J. Li ^{id62c}, K. Li ^{id138}, L. Li ^{id62c}, M. Li ^{id14a,14e}, Q.Y. Li ^{id62a}, S. Li ^{id14a,14e}, S. Li ^{id62d,62c,e}, T. Li ^{id62b}, X. Li ^{id104}, Z. Li ^{id126}, Z. Li ^{id104}, Z. Li ^{id92}, Z. Li ^{id14a,14e}, Z. Liang ^{id14a}, M. Liberatore ^{id48}, B. Liberti ^{id76a}, K. Lie ^{id64c}, J. Lieber Marin ^{id82b}, H. Lien ^{id68}, K. Lin ^{id107}, R.A. Linck ^{id68}, R.E. Lindley ^{id7}, J.H. Lindon ^{id2}, A. Linss ^{id48}, E. Lipeles ^{id128}, A. Lipniacka ^{id16}, A. Lister ^{id164}, J.D. Little ^{id4}, B. Liu ^{id14a}, B.X. Liu ^{id142}, D. Liu ^{id62d,62c}, J.B. Liu ^{id62a}, J.K.K. Liu ^{id32}, K. Liu ^{id62d,62c}, M. Liu ^{id62a}, M.Y. Liu ^{id62a}, P. Liu ^{id14a}, Q. Liu ^{id62d,138,62c}, X. Liu ^{id62a}, Y. Liu ^{id14d,14e}, Y.L. Liu ^{id106}, Y.W. Liu ^{id62a}, J. Llorente Merino ^{id142}, S.L. Lloyd ^{id94}, E.M. Lobodzinska ^{id48}, P. Loch ^{id7}, S. Loffredo ^{id76a,76b},

T. Lohse ¹⁸, K. Lohwasser ¹³⁹, E. Loiacono ⁴⁸, M. Lokajicek ^{131,*}, J.D. Lomas ²⁰, J.D. Long ¹⁶², I. Longarini ¹⁶⁰, L. Longo ^{70a,70b}, R. Longo ¹⁶², I. Lopez Paz ⁶⁷, A. Lopez Solis ⁴⁸, J. Lorenz ¹⁰⁹, N. Lorenzo Martinez ⁴, A.M. Lory ¹⁰⁹, O. Loseva ³⁷, X. Lou ^{47a,47b}, X. Lou ^{14a,14e}, A. Lounis ⁶⁶, J. Love ⁶, P.A. Love ⁹¹, G. Lu ^{14a,14e}, M. Lu ⁸⁰, S. Lu ¹²⁸, Y.J. Lu ⁶⁵, H.J. Lubatti ¹³⁸, C. Luci ^{75a,75b}, F.L. Lucio Alves ^{14c}, A. Lucotte ⁶⁰, F. Luehring ⁶⁸, I. Luise ¹⁴⁵, O. Lukianchuk ⁶⁶, O. Lundberg ¹⁴⁴, B. Lund-Jensen ¹⁴⁴, N.A. Luongo ¹²³, M.S. Lutz ¹⁵¹, D. Lynn ²⁹, H. Lyons ⁹², R. Lysak ¹³¹, E. Lytken ⁹⁸, V. Lyubushkin ³⁸, T. Lyubushkina ³⁸, M.M. Lyukova ¹⁴⁵, H. Ma ²⁹, L.L. Ma ^{62b}, Y. Ma ¹²¹, D.M. Mac Donell ¹⁶⁵, G. Maccarrone ⁵³, J.C. MacDonald ¹³⁹, R. Madar ⁴⁰, W.F. Mader ⁵⁰, J. Maeda ⁸⁴, T. Maeno ²⁹, M. Maerker ⁵⁰, H. Maguire ¹³⁹, A. Maio ^{130a,130b,130d}, K. Maj ^{85a}, O. Majersky ⁴⁸, S. Majewski ¹²³, N. Makovec ⁶⁶, V. Maksimovic ¹⁵, B. Malaescu ¹²⁷, Pa. Malecki ⁸⁶, V.P. Maleev ³⁷, F. Malek ⁶⁰, M. Mali ⁹³, D. Malito ^{43b,43a}, U. Mallik ⁸⁰, C. Malone ³², S. Maltezos ¹⁰, S. Malyukov ³⁸, J. Mamuzic ¹³, G. Mancini ⁵³, G. Manco ^{73a,73b}, J.P. Mandalia ⁹⁴, I. Mandić ⁹³, L. Manhaes de Andrade Filho ^{82a}, I.M. Maniatis ¹⁶⁹, J. Manjarres Ramos ^{102,ad}, D.C. Mankad ¹⁶⁹, A. Mann ¹⁰⁹, B. Mansoulie ¹³⁵, S. Manzoni ³⁶, A. Marantis ^{152,u}, G. Marchiori ⁵, M. Marcisovsky ¹³¹, C. Marcon ^{71a,71b}, M. Marinescu ²⁰, M. Marjanovic ¹²⁰, E.J. Marshall ⁹¹, Z. Marshall ^{17a}, S. Marti-Garcia ¹⁶³, T.A. Martin ¹⁶⁷, V.J. Martin ⁵², B. Martin dit Latour ¹⁶, L. Martinelli ^{75a,75b}, M. Martinez ^{13,v}, P. Martinez Agullo ¹⁶³, V.I. Martinez Outschoorn ¹⁰³, P. Martinez Suarez ¹³, S. Martin-Haugh ¹³⁴, V.S. Martoiu ^{27b}, A.C. Martyniuk ⁹⁶, A. Marzin ³⁶, D. Mascione ^{78a,78b}, L. Masetti ¹⁰⁰, T. Mashimo ¹⁵³, J. Masik ¹⁰¹, A.L. Maslennikov ³⁷, L. Massa ^{23b}, P. Massarotti ^{72a,72b}, P. Mastrandrea ^{74a,74b}, A. Mastroberardino ^{43b,43a}, T. Masubuchi ¹⁵³, T. Mathisen ¹⁶¹, J. Matousek ¹³³, N. Matsuzawa ¹⁵³, J. Maurer ^{27b}, B. Maček ⁹³, D.A. Maximov ³⁷, R. Mazini ¹⁴⁸, I. Maznas ^{152,f}, M. Mazza ¹⁰⁷, S.M. Mazza ¹³⁶, C. Mc Ginn ²⁹, J.P. Mc Gowan ¹⁰⁴, S.P. Mc Kee ¹⁰⁶, E.F. McDonald ¹⁰⁵, A.E. McDougall ¹¹⁴, J.A. Mcfayden ¹⁴⁶, R.P. McGovern ¹²⁸, G. Mchedlidze ^{149b}, R.P. Mckenzie ^{33g}, T.C. Mclachlan ⁴⁸, D.J. Mclaughlin ⁹⁶, K.D. McLean ¹⁶⁵, S.J. McMahon ¹³⁴, P.C. McNamara ¹⁰⁵, C.M. Mcpartland ⁹², R.A. McPherson ^{165,z}, T. Megy ⁴⁰, S. Mehlhase ¹⁰⁹, A. Mehta ⁹², D. Melini ¹⁵⁰, B.R. Mellado Garcia ^{33g}, A.H. Melo ⁵⁵, F. Meloni ⁴⁸, A.M. Mendes Jacques Da Costa ¹⁰¹, H.Y. Meng ¹⁵⁵, L. Meng ⁹¹, S. Menke ¹¹⁰, M. Mentink ³⁶, E. Meoni ^{43b,43a}, C. Merlassino ¹²⁶, L. Merola ^{72a,72b}, C. Meroni ^{71a}, G. Merz ¹⁰⁶, O. Meshkov ³⁷, J. Metcalfe ⁶, A.S. Mete ⁶, C. Meyer ⁶⁸, J-P. Meyer ¹³⁵, R.P. Middleton ¹³⁴, L. Mijović ⁵², G. Mikenberg ¹⁶⁹, M. Mikestikova ¹³¹, M. Mikuž ⁹³, H. Mildner ¹⁰⁰, A. Milic ³⁶, C.D. Milke ⁴⁴, D.W. Miller ³⁹, L.S. Miller ³⁴, A. Milov ¹⁶⁹, D.A. Milstead ^{47a,47b}, T. Min ^{14c}, A.A. Minaenko ³⁷, I.A. Minashvili ^{149b}, L. Mince ⁵⁹, A.I. Mincer ¹¹⁷, B. Mindur ^{85a}, M. Mineev ³⁸, Y. Mino ⁸⁷, L.M. Mir ¹³, M. Miralles Lopez ¹⁶³, M. Mironova ^{17a}, A. Mishima ¹⁵³, M.C. Missio ¹¹³, T. Mitani ¹⁶⁸, A. Mitra ¹⁶⁷, V.A. Mitsou ¹⁶³, O. Miu ¹⁵⁵, P.S. Miyagawa ⁹⁴, Y. Miyazaki ⁸⁹, A. Mizukami ⁸³, T. Mkrtychyan ^{63a}, M. Mlinarevic ⁹⁶, T. Mlinarevic ⁹⁶, M. Mlynarikova ³⁶, S. Mobius ⁵⁵, K. Mochizuki ¹⁰⁸, P. Moder ⁴⁸, P. Mogg ¹⁰⁹, A.F. Mohammed ^{14a,14e}, S. Mohapatra ⁴¹, G. Mokgatitwane ^{33g}, B. Mondal ¹⁴¹, S. Mondal ¹³², G. Monig ¹⁴⁶, K. Mönig ⁴⁸, E. Monnier ¹⁰², L. Monsonis Romero ¹⁶³, J. Montejo Berlingen ⁸³, M. Montella ¹¹⁹, F. Monticelli ⁹⁰, S. Monzani ^{69a,69c}, N. Morange ⁶⁶, A.L. Moreira De Carvalho ^{130a}, M. Moreno Llácer ¹⁶³, C. Moreno Martinez ⁵⁶, P. Morettini ^{57b}, S. Morgenstern ³⁶, M. Morii ⁶¹, M. Morinaga ¹⁵³, A.K. Morley ³⁶, F. Morodei ^{75a,75b}, L. Morvaj ³⁶, P. Moschovakos ³⁶, B. Moser ³⁶, M. Mosidze ^{149b}, T. Moskalets ⁵⁴, P. Moskvitina ¹¹³, J. Moss ^{31,o}, E.J.W. Moyses ¹⁰³, O. Mtintsilana ^{33g}, S. Muanza ¹⁰², J. Mueller ¹²⁹, D. Muenstermann ⁹¹, R. Müller ¹⁹, G.A. Mullier ¹⁶¹, A.J. Mullin ³², J.J. Mullin ¹²⁸, D.P. Mungo ¹⁵⁵, D. Munoz Perez ¹⁶³, F.J. Munoz Sanchez ¹⁰¹, M. Murin ¹⁰¹, W.J. Murray ^{167,134}, A. Murrone ^{71a,71b}, J.M. Muse ¹²⁰,

M. Muškinja ^{17a}, C. Mwewa ²⁹, A.G. Myagkov ^{37,a}, A.J. Myers ⁸, A.A. Myers ¹²⁹, G. Myers ⁶⁸,
M. Myska ¹³², B.P. Nachman ^{17a}, O. Nackenhorst ⁴⁹, A. Nag ⁵⁰, K. Nagai ¹²⁶, K. Nagano ⁸³,
J.L. Nagle ^{29,ak}, E. Nagy ¹⁰², A.M. Nairz ³⁶, Y. Nakahama ⁸³, K. Nakamura ⁸³, H. Nanjo ¹²⁴,
R. Narayan ⁴⁴, E.A. Narayanan ¹¹², I. Naryshkin ³⁷, M. Naseri ³⁴, S. Nasri ¹⁵⁹, C. Nass ²⁴,
G. Navarro ^{22a}, J. Navarro-Gonzalez ¹⁶³, R. Nayak ¹⁵¹, A. Nayaz ¹⁸, P.Y. Nechaeva ³⁷,
F. Nechansky ⁴⁸, L. Nedic ¹²⁶, T.J. Neep ²⁰, A. Negri ^{73a,73b}, M. Negrini ^{23b}, C. Nellist ¹¹⁴,
C. Nelson ¹⁰⁴, K. Nelson ¹⁰⁶, S. Nemecek ¹³¹, M. Nessi ^{36,i}, M.S. Neubauer ¹⁶², F. Neuhaus ¹⁰⁰,
J. Neundorff ⁴⁸, R. Newhouse ¹⁶⁴, P.R. Newman ²⁰, C.W. Ng ¹²⁹, Y.W.Y. Ng ⁴⁸, B. Ngair ^{35e},
H.D.N. Nguyen ¹⁰⁸, R.B. Nickerson ¹²⁶, R. Nicolaidou ¹³⁵, J. Nielsen ¹³⁶, M. Niemeyer ⁵⁵,
J. Niermann ^{55,36}, N. Nikiforou ³⁶, V. Nikolaenko ^{37,a}, I. Nikolic-Audit ¹²⁷, K. Nikolopoulos ²⁰,
P. Nilsson ²⁹, I. Ninca ⁴⁸, H.R. Nindhito ⁵⁶, G. Ninio ¹⁵¹, A. Nisati ^{75a}, N. Nishu ²,
R. Nisius ¹¹⁰, J-E. Nitschke ⁵⁰, E.K. Nkadimeng ^{33g}, S.J. Noacco Rosende ⁹⁰, T. Nobe ¹⁵³,
D.L. Noel ³², T. Nommensen ¹⁴⁷, M.A. Nomura ²⁹, M.B. Norfolk ¹³⁹, R.R.B. Norisam ⁹⁶,
B.J. Norman ³⁴, J. Novak ⁹³, T. Novak ⁴⁸, L. Novotny ¹³², R. Novotny ¹¹², L. Nozka ¹²²,
K. Ntekas ¹⁶⁰, N.M.J. Nunes De Moura Junior ^{82b}, E. Nurse ⁹⁶, J. Ocariz ¹²⁷, A. Ochi ⁸⁴,
I. Ochoa ^{130a}, S. Oerdek ¹⁶¹, J.T. Offermann ³⁹, A. Ogrodnik ^{85a}, A. Oh ¹⁰¹, C.C. Ohm ¹⁴⁴,
H. Oide ⁸³, R. Oishi ¹⁵³, M.L. Ojeda ⁴⁸, Y. Okazaki ⁸⁷, M.W. O'Keefe ⁹², Y. Okumura ¹⁵³,
L.F. Oleiro Seabra ^{130a}, S.A. Olivares Pino ^{137d}, D. Oliveira Damazio ²⁹, D. Oliveira Goncalves ^{82a},
J.L. Oliver ¹⁶⁰, M.J.R. Olsson ¹⁶⁰, A. Olszewski ⁸⁶, Ö.O. Öncel ⁵⁴, D.C. O'Neil ¹⁴²,
A.P. O'Neill ¹⁹, A. Onofre ^{130a,130e}, P.U.E. Onyisi ¹¹, M.J. Oreglia ³⁹, G.E. Orellana ⁹⁰,
D. Orestano ^{77a,77b}, N. Orlando ¹³, R.S. Orr ¹⁵⁵, V. O'Shea ⁵⁹, R. Ospanov ^{62a},
G. Otero y Garzon ³⁰, H. Otono ⁸⁹, P.S. Ott ^{63a}, G.J. Ottino ^{17a}, M. Ouchrif ^{35d}, J. Ouellette ²⁹,
F. Ould-Saada ¹²⁵, M. Owen ⁵⁹, R.E. Owen ¹³⁴, K.Y. Oyulmaz ^{21a}, V.E. Ozcan ^{21a}, N. Ozturk ⁸,
S. Ozturk ^{21d}, H.A. Pacey ³², A. Pacheco Pages ¹³, C. Padilla Aranda ¹³, G. Padovano ^{75a,75b},
S. Pagan Griso ^{17a}, G. Palacino ⁶⁸, A. Palazzo ^{70a,70b}, S. Palestini ³⁶, J. Pan ¹⁷², T. Pan ^{64a},
D.K. Panchal ¹¹, C.E. Pandini ¹¹⁴, J.G. Panduro Vazquez ⁹⁵, H. Pang ^{14b}, P. Pani ⁴⁸,
G. Panizzo ^{69a,69c}, L. Paolozzi ⁵⁶, C. Papadatos ¹⁰⁸, S. Parajuli ⁴⁴, A. Paramonov ⁶,
C. Paraskevopoulos ¹⁰, D. Paredes Hernandez ^{64b}, T.H. Park ¹⁵⁵, M.A. Parker ³², F. Parodi ^{57b,57a},
E.W. Parrish ¹¹⁵, V.A. Parrish ⁵², J.A. Parsons ⁴¹, U. Parzefall ⁵⁴, B. Pascual Dias ¹⁰⁸,
L. Pascual Dominguez ¹⁵¹, F. Pasquali ¹¹⁴, E. Pasqualucci ^{75a}, S. Passaggio ^{57b}, F. Pastore ⁹⁵,
P. Pasuwan ^{47a,47b}, P. Patel ⁸⁶, U.M. Patel ⁵¹, J.R. Pater ¹⁰¹, T. Pauly ³⁶, J. Pearkes ¹⁴³,
M. Pedersen ¹²⁵, R. Pedro ^{130a}, S.V. Peleganchuk ³⁷, O. Penc ³⁶, E.A. Pender ⁵², H. Peng ^{62a},
K.E. Pensi ¹⁰⁹, M. Penzin ³⁷, B.S. Peralva ^{82d}, A.P. Pereira Peixoto ⁶⁰, L. Pereira Sanchez ^{47a,47b},
D.V. Perepelitsa ^{29,ak}, E. Perez Codina ^{156a}, M. Perganti ¹⁰, L. Perini ^{71a,71b,*}, H. Pernegger ³⁶,
S. Perrella ³⁶, A. Perrevoort ¹¹³, O. Perrin ⁴⁰, K. Peters ⁴⁸, R.F.Y. Peters ¹⁰¹, B.A. Petersen ³⁶,
T.C. Petersen ⁴², E. Petit ¹⁰², V. Petousis ¹³², C. Petridou ^{152,f}, A. Petrukhin ¹⁴¹, M. Pettee ^{17a},
N.E. Pettersson ³⁶, A. Petukhov ³⁷, K. Petukhova ¹³³, A. Peyaud ¹³⁵, R. Pezoa ^{137f},
L. Pezzotti ³⁶, G. Pezzullo ¹⁷², T.M. Pham ¹⁷⁰, T. Pham ¹⁰⁵, P.W. Phillips ¹³⁴, M.W. Phipps ¹⁶²,
G. Piacquadio ¹⁴⁵, E. Pianori ^{17a}, F. Piazza ^{71a,71b}, R. Piegai ³⁰, D. Pietreanu ^{27b},
A.D. Pilkington ¹⁰¹, M. Pinamonti ^{69a,69c}, J.L. Pinfeld ², B.C. Pinheiro Pereira ^{130a},
A.E. Pinto Pinoargote ¹³⁵, C. Pitman Donaldson ⁹⁶, D.A. Pizzi ³⁴, L. Pizzimento ^{76a,76b},
A. Pizzini ¹¹⁴, M.-A. Pleier ²⁹, V. Plesanovs ⁵⁴, V. Pleskot ¹³³, E. Plotnikova ³⁸, G. Poddar ⁴,
R. Poettgen ⁹⁸, L. Poggioli ¹²⁷, D. Pohl ²⁴, I. Pokharel ⁵⁵, S. Polacek ¹³³, G. Polesello ^{73a},
A. Poley ^{142,156a}, R. Polifka ¹³², A. Polini ^{23b}, C.S. Pollard ¹⁶⁷, Z.B. Pollock ¹¹⁹,
V. Polychronakos ²⁹, E. Pompa Pacchi ^{75a,75b}, D. Ponomarenko ¹¹³, L. Pontecorvo ³⁶, S. Popa ^{27a},
G.A. Popeneciu ^{27d}, D.M. Portillo Quintero ^{156a}, S. Pospisil ¹³², P. Postolache ^{27c},
K. Potamianos ¹²⁶, P.A. Potepa ^{85a}, I.N. Potrap ³⁸, C.J. Potter ³², H. Potti ¹, T. Poulsen ⁴⁸,

J. Poveda ¹⁶³, M.E. Pozo Astigarraga ³⁶, A. Prades Ibanez ¹⁶³, M.M. Prapa ⁴⁶, J. Pretel ⁵⁴, D. Price ¹⁰¹, M. Primavera ^{70a}, M.A. Principe Martin ⁹⁹, R. Privara ¹²², T. Procter ⁵⁹, M.L. Proffitt ¹³⁸, N. Proklova ¹²⁸, K. Prokofiev ^{64c}, G. Proto ^{76a,76b}, S. Protopopescu ²⁹, J. Proudfoot ⁶, M. Przybycien ^{35a}, W.W. Przygoda ^{85b}, J.E. Puddefoot ¹³⁹, D. Pudzha ³⁷, D. Pyatiizbyantseva ³⁷, J. Qian ¹⁰⁶, D. Qichen ¹⁰¹, Y. Qin ¹⁰¹, T. Qiu ⁵², A. Quadt ⁵⁵, M. Queitsch-Maitland ¹⁰¹, G. Quetant ⁵⁶, G. Rabanal Bolanos ⁶¹, D. Rafanoharana ⁵⁴, F. Ragusa ^{71a,71b}, J.L. Rainbolt ³⁹, J.A. Raine ⁵⁶, S. Rajagopalan ²⁹, E. Ramakoti ³⁷, K. Ran ^{48,14e}, N.P. Rapheeha ^{33g}, H. Rasheed ^{27b}, V. Raskina ¹²⁷, D.F. Rassloff ^{63a}, S. Rave ¹⁰⁰, B. Ravina ⁵⁵, I. Ravinovich ¹⁶⁹, M. Raymond ³⁶, A.L. Read ¹²⁵, N.P. Readioff ¹³⁹, D.M. Rebuzzi ^{73a,73b}, G. Redlinger ²⁹, A.S. Reed ¹¹⁰, K. Reeves ²⁶, J.A. Reidelsturz ¹⁷¹, D. Reikher ¹⁵¹, A. Rej ¹⁴¹, C. Rembser ³⁶, A. Renardi ⁴⁸, M. Renda ^{27b}, M.B. Rendel ¹¹⁰, F. Renner ⁴⁸, A.G. Rennie ⁵⁹, S. Resconi ^{71a}, M. Ressegotti ^{57b,57a}, E.D. Resseguie ^{17a}, S. Rettie ³⁶, J.G. Reyes Rivera ¹⁰⁷, B. Reynolds ¹¹⁹, E. Reynolds ^{17a}, M. Rezaei Estabragh ¹⁷¹, O.L. Rezanova ³⁷, P. Reznicek ¹³³, N. Ribaric ⁹¹, E. Ricci ^{78a,78b}, R. Richter ¹¹⁰, S. Richter ^{47a,47b}, E. Richter-Was ^{85b}, M. Ridel ¹²⁷, S. Ridouani ^{35d}, P. Rieck ¹¹⁷, P. Riedler ³⁶, M. Rijssenbeek ¹⁴⁵, A. Rimoldi ^{73a,73b}, M. Rimoldi ⁴⁸, L. Rinaldi ^{23b,23a}, T.T. Rinn ²⁹, M.P. Rinnagel ¹⁰⁹, G. Ripellino ¹⁶¹, I. Riu ¹³, P. Rivadeneira ⁴⁸, J.C. Rivera Vergara ¹⁶⁵, F. Rizatdinova ¹²¹, E. Rizvi ⁹⁴, C. Rizzi ⁵⁶, B.A. Roberts ¹⁶⁷, B.R. Roberts ^{17a}, S.H. Robertson ^{104,z}, M. Robin ⁴⁸, D. Robinson ³², C.M. Robles Gajardo ^{137f}, M. Robles Manzano ¹⁰⁰, A. Robson ⁵⁹, A. Rocchi ^{76a,76b}, C. Roda ^{74a,74b}, S. Rodriguez Bosca ^{63a}, Y. Rodriguez Garcia ^{22a}, A. Rodriguez Rodriguez ⁵⁴, A.M. Rodríguez Vera ^{156b}, S. Roe ³⁶, J.T. Roemer ¹⁶⁰, A.R. Roepe-Gier ¹³⁶, J. Roggel ¹⁷¹, O. Røhne ¹²⁵, R.A. Rojas ¹⁰³, C.P.A. Roland ⁶⁸, J. Roloff ²⁹, A. Romaniouk ³⁷, E. Romano ^{73a,73b}, M. Romano ^{23b}, A.C. Romero Hernandez ¹⁶², N. Rompotis ⁹², L. Roos ¹²⁷, S. Rosati ^{75a}, B.J. Rosser ³⁹, E. Rossi ¹²⁶, E. Rossi ^{72a,72b}, L.P. Rossi ^{57b}, L. Rossini ⁴⁸, R. Rosten ¹¹⁹, M. Rotaru ^{27b}, B. Rottler ⁵⁴, C. Rougier ^{102,ad}, D. Rousseau ⁵⁶, D. Rousso ³², A. Roy ¹⁶², S. Roy-Garand ¹⁵⁵, A. Rozanov ¹⁰², Y. Rozen ¹⁵⁰, X. Ruan ^{33g}, A. Rubio Jimenez ¹⁶³, A.J. Ruby ⁹², V.H. Ruelas Rivera ¹⁸, T.A. Ruggeri ¹, A. Ruggiero ¹²⁶, A. Ruiz-Martinez ¹⁶³, A. Rummler ³⁶, Z. Rurikova ⁵⁴, N.A. Rusakovich ³⁸, H.L. Russell ¹⁶⁵, G. Russo ^{75a,75b}, J.P. Rutherford ⁷, S. Rutherford Colmenares ³², K. Rybacki ⁹¹, M. Rybar ¹³³, E.B. Rye ¹²⁵, A. Ryzhov ³⁷, J.A. Sabater Iglesias ⁵⁶, P. Sabatini ¹⁶³, L. Sabetta ^{75a,75b}, H.F-W. Sadrozinski ¹³⁶, F. Safai Tehrani ^{75a}, B. Safarzadeh Samani ¹⁴⁶, M. Safdari ¹⁴³, S. Saha ¹⁰⁴, M. Sahinsoy ¹¹⁰, M. Saimpert ¹³⁵, M. Saito ¹⁵³, T. Saito ¹⁵³, D. Salamani ³⁶, A. Salnikov ¹⁴³, J. Salt ¹⁶³, A. Salvador Salas ¹³, D. Salvatore ^{43b,43a}, F. Salvatore ¹⁴⁶, A. Salzburger ³⁶, D. Sammel ⁵⁴, D. Sampsonidis ^{152,f}, D. Sampsonidou ^{123,62c}, J. Sánchez ¹⁶³, A. Sanchez Pineda ⁴, V. Sanchez Sebastian ¹⁶³, H. Sandaker ¹²⁵, C.O. Sander ⁴⁸, J.A. Sandesara ¹⁰³, M. Sandhoff ¹⁷¹, C. Sandoval ^{22b}, D.P.C. Sankey ¹³⁴, T. Sano ⁸⁷, A. Sansoni ⁵³, L. Santi ^{75a,75b}, C. Santoni ⁴⁰, H. Santos ^{130a,130b}, S.N. Santpur ^{17a}, A. Santra ¹⁶⁹, K.A. Saoucha ¹³⁹, J.G. Saraiva ^{130a,130d}, J. Sardain ⁷, O. Sasaki ⁸³, K. Sato ¹⁵⁷, C. Sauer ^{63b}, F. Sauerburger ⁵⁴, E. Sauvan ⁴, P. Savard ^{155,ai}, R. Sawada ¹⁵³, C. Sawyer ¹³⁴, L. Sawyer ⁹⁷, I. Sayago Galvan ¹⁶³, C. Sbarra ^{23b}, A. Sbrizzi ^{23b,23a}, T. Scanlon ⁹⁶, J. Schaarschmidt ¹³⁸, P. Schacht ¹¹⁰, D. Schaefer ³⁹, U. Schäfer ¹⁰⁰, A.C. Schaffer ^{66,44}, D. Schaile ¹⁰⁹, R.D. Schamberger ¹⁴⁵, E. Schanet ¹⁰⁹, C. Scharf ¹⁸, M.M. Schefer ¹⁹, V.A. Schegelsky ³⁷, D. Scheirich ¹³³, F. Schenck ¹⁸, M. Schernau ¹⁶⁰, C. Scheulen ⁵⁵, C. Schiavi ^{57b,57a}, E.J. Schioppa ^{70a,70b}, M. Schioppa ^{43b,43a}, B. Schlag ^{143,q}, K.E. Schleicher ⁵⁴, S. Schlenker ³⁶, J. Schmeing ¹⁷¹, M.A. Schmidt ¹⁷¹, K. Schmieden ¹⁰⁰, C. Schmitt ¹⁰⁰, S. Schmitt ⁴⁸, L. Schoeffel ¹³⁵, A. Schoening ^{63b}, P.G. Scholer ⁵⁴, E. Schopf ¹²⁶, M. Schott ¹⁰⁰, J. Schovancova ³⁶, S. Schramm ⁵⁶,

F. Schroeder ¹⁷¹, H-C. Schultz-Coulon ^{63a}, M. Schumacher ⁵⁴, B.A. Schumm ¹³⁶, Ph. Schune ¹³⁵, A.J. Schuy ¹³⁸, H.R. Schwartz ¹³⁶, A. Schwartzman ¹⁴³, T.A. Schwarz ¹⁰⁶, Ph. Schwemling ¹³⁵, R. Schwienhorst ¹⁰⁷, A. Sciandra ¹³⁶, G. Sciolla ²⁶, F. Scuri ^{74a}, F. Scutti ¹⁰⁵, C.D. Sebastiani ⁹², K. Sedlaczek ¹¹⁵, P. Seema ¹⁸, S.C. Seidel ¹¹², A. Seiden ¹³⁶, B.D. Seidlitz ⁴¹, C. Seitz ⁴⁸, J.M. Seixas ^{82b}, G. Sekhniaidze ^{72a}, S.J. Sekula ⁴⁴, L. Selem ⁴, N. Semprini-Cesari ^{23b,23a}, S. Sen ⁵¹, D. Sengupta ⁵⁶, V. Senthilkumar ¹⁶³, L. Serin ⁶⁶, L. Serkin ^{69a,69b}, M. Sessa ^{76a,76b}, H. Severini ¹²⁰, F. Sforza ^{57b,57a}, A. Sfyrta ⁵⁶, E. Shabalina ⁵⁵, R. Shaheen ¹⁴⁴, J.D. Shahinian ¹²⁸, D. Shaked Renous ¹⁶⁹, L.Y. Shan ^{14a}, M. Shapiro ^{17a}, A. Sharma ³⁶, A.S. Sharma ¹⁶⁴, P. Sharma ⁸⁰, S. Sharma ⁴⁸, P.B. Shatalov ³⁷, K. Shaw ¹⁴⁶, S.M. Shaw ¹⁰¹, Q. Shen ^{62c,5}, P. Sherwood ⁹⁶, L. Shi ⁹⁶, X. Shi ^{14a}, C.O. Shimmin ¹⁷², Y. Shimogama ¹⁶⁸, J.D. Shinner ⁹⁵, I.P.J. Shipsey ¹²⁶, S. Shirabe ⁶⁰, M. Shiyakova ^{38,x}, J. Shlomi ¹⁶⁹, M.J. Shochet ³⁹, J. Shojaii ¹⁰⁵, D.R. Shope ¹²⁵, S. Shrestha ^{119,al}, E.M. Shrif ^{33g}, M.J. Shroff ¹⁶⁵, P. Sicho ¹³¹, A.M. Sickles ¹⁶², E. Sideras Haddad ^{33g}, A. Sidoti ^{23b}, F. Siegert ⁵⁰, Dj. Sijacki ¹⁵, R. Sikora ^{85a}, F. Sili ⁹⁰, J.M. Silva ²⁰, M.V. Silva Oliveira ³⁶, S.B. Silverstein ^{47a}, S. Simion ⁶⁶, R. Simoniello ³⁶, E.L. Simpson ⁵⁹, H. Simpson ¹⁴⁶, L.R. Simpson ¹⁰⁶, N.D. Simpson ⁹⁸, S. Simsek ^{21d}, S. Sindhu ⁵⁵, P. Sinervo ¹⁵⁵, S. Singh ¹⁴², S. Singh ¹⁵⁵, S. Sinha ⁴⁸, S. Sinha ^{33g}, M. Sioli ^{23b,23a}, I. Siral ³⁶, E. Sitnikova ⁴⁸, S.Yu. Sivoklov ^{37,*}, J. Sjölin ^{47a,47b}, A. Skaf ⁵⁵, E. Skorda ⁹⁸, P. Skubic ¹²⁰, M. Slawinska ⁸⁶, V. Smakhtin ¹⁶⁹, B.H. Smart ¹³⁴, J. Smiesko ³⁶, S.Yu. Smirnov ³⁷, Y. Smirnov ³⁷, L.N. Smirnova ^{37,a}, O. Smirnova ⁹⁸, A.C. Smith ⁴¹, E.A. Smith ³⁹, H.A. Smith ¹²⁶, J.L. Smith ⁹², R. Smith ¹⁴³, M. Smizanska ⁹¹, K. Smolek ¹³², A.A. Snesarev ³⁷, S.R. Snider ¹⁵⁵, H.L. Snoek ¹¹⁴, S. Snyder ²⁹, R. Sobie ^{165,z}, A. Soffer ¹⁵¹, C.A. Solans Sanchez ³⁶, E.Yu. Soldatov ³⁷, U. Soldevila ¹⁶³, A.A. Solodkov ³⁷, S. Solomon ²⁶, A. Soloshenko ³⁸, K. Solovieva ⁵⁴, O.V. Solovyanov ⁴⁰, V. Solovyev ³⁷, P. Sommer ³⁶, A. Sonay ¹³, W.Y. Song ^{156b}, J.M. Sonneveld ¹¹⁴, A. Sopcak ¹³², A.L. Sopio ⁹⁶, F. Sopkova ^{28b}, V. Sothilingam ^{63a}, S. Sottocornola ⁶⁸, R. Soualah ^{116b}, Z. Soumami ^{35e}, D. South ⁴⁸, S. Spagnolo ^{70a,70b}, M. Spalla ¹¹⁰, D. Sperlich ⁵⁴, G. Spigo ³⁶, M. Spina ¹⁴⁶, S. Spinali ⁹¹, D.P. Spiteri ⁵⁹, M. Spousta ¹³³, E.J. Staats ³⁴, A. Stabile ^{71a,71b}, R. Stamen ^{63a}, M. Stamenkovic ¹¹⁴, A. Stampekis ²⁰, M. Standke ²⁴, E. Stanecka ⁸⁶, M.V. Stange ⁵⁰, B. Stanislaus ^{17a}, M.M. Stanitzki ⁴⁸, M. Stankaityte ¹²⁶, B. Stapf ⁴⁸, E.A. Starchenko ³⁷, G.H. Stark ¹³⁶, J. Stark ^{102,ad}, D.M. Starke ^{156b}, P. Staroba ¹³¹, P. Starovoitov ^{63a}, S. Stärz ¹⁰⁴, R. Staszewski ⁸⁶, G. Stavropoulos ⁴⁶, J. Steentoft ¹⁶¹, P. Steinberg ²⁹, B. Stelzer ^{142,156a}, H.J. Stelzer ¹²⁹, O. Stelzer-Chilton ^{156a}, H. Stenzel ⁵⁸, T.J. Stevenson ¹⁴⁶, G.A. Stewart ³⁶, J.R. Stewart ¹²¹, M.C. Stockton ³⁶, G. Stoica ^{27b}, M. Stolarski ^{130a}, S. Stonjek ¹¹⁰, A. Straessner ⁵⁰, J. Strandberg ¹⁴⁴, S. Strandberg ^{47a,47b}, M. Strauss ¹²⁰, T. Strebler ¹⁰², P. Strizenc ^{28b}, R. Ströhmer ¹⁶⁶, D.M. Strom ¹²³, L.R. Strom ⁴⁸, R. Stroynowski ⁴⁴, A. Strubig ^{47a,47b}, S.A. Stucci ²⁹, B. Stugu ¹⁶, J. Stupak ¹²⁰, N.A. Styles ⁴⁸, D. Su ¹⁴³, S. Su ^{62a}, W. Su ^{62d,138,62c}, X. Su ^{62a,66}, K. Sugizaki ¹⁵³, V.V. Sulim ³⁷, M.J. Sullivan ⁹², D.M.S. Sultan ^{78a,78b}, L. Sultanaliyeva ³⁷, S. Sultansoy ^{3b}, T. Sumida ⁸⁷, S. Sun ¹⁰⁶, S. Sun ¹⁷⁰, O. Sunneborn Gudnadottir ¹⁶¹, M.R. Sutton ¹⁴⁶, M. Svatos ¹³¹, M. Swiatlowski ^{156a}, T. Swirski ¹⁶⁶, I. Sykora ^{28a}, M. Sykora ¹³³, T. Sykora ¹³³, D. Ta ¹⁰⁰, K. Tackmann ^{48,w}, A. Taffard ¹⁶⁰, R. Tafirout ^{156a}, J.S. Tafoya Vargas ⁶⁶, R.H.M. Taibah ¹²⁷, R. Takashima ⁸⁸, E.P. Takeva ⁵², Y. Takubo ⁸³, M. Talby ¹⁰², A.A. Talyshev ³⁷, K.C. Tam ^{64b}, N.M. Tamir ¹⁵¹, A. Tanaka ¹⁵³, J. Tanaka ¹⁵³, R. Tanaka ⁶⁶, M. Tanasini ^{57b,57a}, Z. Tao ¹⁶⁴, S. Tapia Araya ^{137f}, S. Tapprogge ¹⁰⁰, A. Tarek Abouelfadl Mohamed ¹⁰⁷, S. Tarem ¹⁵⁰, K. Tariq ^{62b}, G. Tarna ^{102,27b}, G.F. Tartarelli ^{71a}, P. Tas ¹³³, M. Tasevsky ¹³¹, E. Tassi ^{43b,43a}, A.C. Tate ¹⁶², G. Tateno ¹⁵³, Y. Tayalati ^{35e,y}, G.N. Taylor ¹⁰⁵, W. Taylor ^{156b}, H. Teagle ⁹², A.S. Tee ¹⁷⁰, R. Teixeira De Lima ¹⁴³, P. Teixeira-Dias ⁹⁵, J.J. Teoh ¹⁵⁵, K. Terashi ¹⁵³, J. Terron ⁹⁹,

S. Terzo ¹³, M. Testa ⁵³, R.J. Teuscher ^{155,z}, A. Thaler ⁷⁹, O. Theiner ⁵⁶, N. Themistokleous ⁵²,
 T. Thevenaux-Pelzer ¹⁰², O. Thielmann ¹⁷¹, D.W. Thomas ⁹⁵, J.P. Thomas ²⁰, E.A. Thompson ^{17a},
 P.D. Thompson ²⁰, E. Thomson ¹²⁸, Y. Tian ⁵⁵, V. Tikhomirov ^{37,a}, Yu.A. Tikhonov ³⁷,
 S. Timoshenko ³⁷, E.X.L. Ting ¹, P. Tipton ¹⁷², S.H. Tlou ^{33g}, A. Tnourji ⁴⁰, K. Todome ^{23b,23a},
 S. Todorova-Nova ¹³³, S. Todt ⁵⁰, M. Togawa ⁸³, J. Tojo ⁸⁹, S. Tokár ^{28a}, K. Tokushuku ⁸³,
 O. Toldaiev ⁶⁸, R. Tombs ³², M. Tomoto ^{83,111}, L. Tompkins ^{143,q}, K.W. Topolnicki ^{85b},
 E. Torrence ¹²³, H. Torres ^{102,ad}, E. Torró Pastor ¹⁶³, M. Toscani ³⁰, C. Tosciri ³⁹, M. Tost ¹¹,
 D.R. Tovey ¹³⁹, A. Traeet ¹⁶, I.S. Trandafir ^{27b}, T. Trefzger ¹⁶⁶, A. Tricoli ²⁹, I.M. Trigger ^{156a},
 S. Trincaz-Duvoid ¹²⁷, D.A. Trischuk ²⁶, B. Trocmé ⁶⁰, C. Troncon ^{71a}, L. Truong ^{33c},
 M. Trzebinski ⁸⁶, A. Trzupiek ⁸⁶, F. Tsai ¹⁴⁵, M. Tsai ¹⁰⁶, A. Tsiamis ^{152,f}, P.V. Tsiareshka ³⁷,
 S. Tsigaridas ^{156a}, A. Tsirigotis ^{152,u}, V. Tsiskaridze ¹⁵⁵, E.G. Tskhadadze ^{149a}, M. Tsopoulou ^{152,f},
 Y. Tsujikawa ⁸⁷, I.I. Tsukerman ³⁷, V. Tsulaia ^{17a}, S. Tsuno ⁸³, O. Tsur ¹⁵⁰, K. Tsur ¹¹⁸,
 D. Tsybychev ¹⁴⁵, Y. Tu ^{64b}, A. Tudorache ^{27b}, V. Tudorache ^{27b}, A.N. Tuna ³⁶, S. Turchikhin ³⁸,
 I. Turk Cakir ^{3a}, R. Turra ^{71a}, T. Turtuvshin ^{38,aa}, P.M. Tuts ⁴¹, S. Tzamarias ^{152,f}, P. Tzanis ¹⁰,
 E. Tzovara ¹⁰⁰, K. Uchida ¹⁵³, F. Ukegawa ¹⁵⁷, P.A. Ulloa Poblete ^{137c}, E.N. Umaka ²⁹,
 G. Unal ³⁶, M. Unal ¹¹, A. Undrus ²⁹, G. Unel ¹⁶⁰, J. Urban ^{28b}, P. Urquijo ¹⁰⁵, G. Usai ⁸,
 R. Ushioda ¹⁵⁴, M. Usman ¹⁰⁸, Z. Uysal ^{21b}, L. Vacavant ¹⁰², V. Vacek ¹³², B. Vachon ¹⁰⁴,
 K.O.H. Vadla ¹²⁵, T. Vafeiadis ³⁶, A. Vaitkus ⁹⁶, C. Valderanis ¹⁰⁹, E. Valdes Santurio ^{47a,47b},
 M. Valente ^{156a}, S. Valentineti ^{23b,23a}, A. Valero ¹⁶³, E. Valiente Moreno ¹⁶³, A. Vallier ^{102,ad},
 J.A. Valls Ferrer ¹⁶³, D.R. Van Arneman ¹¹⁴, T.R. Van Daalen ¹³⁸, P. Van Gemmeren ⁶,
 M. Van Rijnbach ^{125,36}, S. Van Stroud ⁹⁶, I. Van Vulpen ¹¹⁴, M. Vanadia ^{76a,76b}, W. Vandelli ³⁶,
 M. Vandenbroucke ¹³⁵, E.R. Vandewall ¹²¹, D. Vannicola ¹⁵¹, L. Vannoli ^{57b,57a}, R. Vari ^{75a},
 E.W. Varnes ⁷, C. Varni ^{17a}, T. Varol ¹⁴⁸, D. Varouchas ⁶⁶, L. Varriale ¹⁶³, K.E. Varvell ¹⁴⁷,
 M.E. Vasile ^{27b}, L. Vaslin ⁴⁰, G.A. Vasquez ¹⁶⁵, F. Vazeille ⁴⁰, T. Vazquez Schroeder ³⁶,
 J. Veatch ³¹, V. Vecchio ¹⁰¹, M.J. Veen ¹⁰³, I. Veliscek ¹²⁶, L.M. Veloce ¹⁵⁵, F. Veloso ^{130a,130c},
 S. Veneziano ^{75a}, A. Ventura ^{70a,70b}, A. Verbytskyi ¹¹⁰, M. Verducci ^{74a,74b}, C. Vergis ²⁴,
 M. Verissimo De Araujo ^{82b}, W. Verkerke ¹¹⁴, J.C. Vermeulen ¹¹⁴, C. Vernieri ¹⁴³,
 P.J. Verschuuren ⁹⁵, M. Vessella ¹⁰³, M.C. Vetterli ^{142,ai}, A. Vgenopoulos ^{152,f},
 N. Viaux Maira ^{137f}, T. Vickey ¹³⁹, O.E. Vickey Boeriu ¹³⁹, G.H.A. Viehhauser ¹²⁶, L. Vignani ^{63b},
 M. Villa ^{23b,23a}, M. Villaplana Perez ¹⁶³, E.M. Villhauer ⁵², E. Vilucchi ⁵³, M.G. Vincter ³⁴,
 G.S. Virdee ²⁰, A. Vishwakarma ⁵², C. Vittori ³⁶, I. Vivarelli ¹⁴⁶, V. Vladimirov ¹⁶⁷,
 E. Voevodina ¹¹⁰, F. Vogel ¹⁰⁹, P. Vokac ¹³², J. Von Ahnen ⁴⁸, E. Von Toerne ²⁴,
 B. Vormwald ³⁶, V. Vorobel ¹³³, K. Vorobev ³⁷, M. Vos ¹⁶³, K. Voss ¹⁴¹, J.H. Vosseveld ⁹²,
 M. Vozak ¹¹⁴, L. Vozdecky ⁹⁴, N. Vranjes ¹⁵, M. Vranjes Milosavljevic ¹⁵, M. Vreeswijk ¹¹⁴,
 R. Vuillermet ³⁶, O. Vujinovic ¹⁰⁰, I. Vukotic ³⁹, S. Wada ¹⁵⁷, C. Wagner ¹⁰³, J.M. Wagner ^{17a},
 W. Wagner ¹⁷¹, S. Wahdan ¹⁷¹, H. Wahlberg ⁹⁰, R. Wakasa ¹⁵⁷, M. Wakida ¹¹¹, J. Walder ¹³⁴,
 R. Walker ¹⁰⁹, W. Walkowiak ¹⁴¹, A. Wall ¹²⁸, A.Z. Wang ¹⁷⁰, C. Wang ¹⁰⁰, C. Wang ^{62c},
 H. Wang ^{17a}, J. Wang ^{64a}, R.-J. Wang ¹⁰⁰, R. Wang ⁶¹, R. Wang ⁶, S.M. Wang ¹⁴⁸,
 S. Wang ^{62b}, T. Wang ^{62a}, W.T. Wang ⁸⁰, X. Wang ^{14c}, X. Wang ¹⁶², X. Wang ^{62c},
 Y. Wang ^{62d}, Y. Wang ^{14c}, Z. Wang ¹⁰⁶, Z. Wang ^{62d,51,62c}, Z. Wang ¹⁰⁶, A. Warburton ¹⁰⁴,
 R.J. Ward ²⁰, N. Warrack ⁵⁹, A.T. Watson ²⁰, H. Watson ⁵⁹, M.F. Watson ²⁰, G. Watts ¹³⁸,
 B.M. Waugh ⁹⁶, C. Weber ²⁹, H.A. Weber ¹⁸, M.S. Weber ¹⁹, S.M. Weber ^{63a}, C. Wei ^{62a},
 Y. Wei ¹²⁶, A.R. Weidberg ¹²⁶, E.J. Weik ¹¹⁷, J. Weingarten ⁴⁹, M. Weirich ¹⁰⁰, C. Weiser ⁵⁴,
 C.J. Wells ⁴⁸, T. Wenaus ²⁹, B. Wendland ⁴⁹, T. Wengler ³⁶, N.S. Wenke ¹¹⁰, N. Wermes ²⁴,
 M. Wessels ^{63a}, K. Whalen ¹²³, A.M. Wharton ⁹¹, A.S. White ⁶¹, A. White ⁸, M.J. White ¹,
 D. Whiteson ¹⁶⁰, L. Wickremasinghe ¹²⁴, W. Wiedenmann ¹⁷⁰, C. Wiel ⁵⁰, M. Wielers ¹³⁴,
 C. Wiglesworth ⁴², L.A.M. Wiik-Fuchs ⁵⁴, D.J. Wilbern ¹²⁰, H.G. Wilkens ³⁶, D.M. Williams ⁴¹,

H.H. Williams¹²⁸, S. Williams³², S. Willocq¹⁰³, B.J. Wilson¹⁰¹, P.J. Windischhofer³⁹, F. Winklmeier¹²³, B.T. Winter⁵⁴, J.K. Winter¹⁰¹, M. Wittgen¹⁴³, M. Wobisch⁹⁷, Z. Wolfs¹¹⁴, R. Wölker¹²⁶, J. Wollrath¹⁶⁰, M.W. Wolter⁸⁶, H. Wolters^{130a,130c}, V.W.S. Wong¹⁶⁴, A.F. Wongel⁴⁸, S.D. Worm⁴⁸, B.K. Wosiek⁸⁶, K.W. Woźniak⁸⁶, K. Wraight⁵⁹, J. Wu^{14a,14e}, M. Wu^{64a}, M. Wu¹¹³, S.L. Wu¹⁷⁰, X. Wu⁵⁶, Y. Wu^{62a}, Z. Wu¹³⁵, J. Wuerzinger¹¹⁰, T.R. Wyatt¹⁰¹, B.M. Wynne⁵², S. Xella⁴², L. Xia^{14c}, M. Xia^{14b}, J. Xiang^{64c}, X. Xiao¹⁰⁶, M. Xie^{62a}, X. Xie^{62a}, S. Xin^{14a,14e}, J. Xiong^{17a}, D. Xu^{14a}, H. Xu^{62a}, H. Xu^{62a}, L. Xu^{62a}, R. Xu¹²⁸, T. Xu¹⁰⁶, Y. Xu^{14b}, Z. Xu⁵², Z. Xu^{14a}, B. Yabsley¹⁴⁷, S. Yacoob^{33a}, N. Yamaguchi⁸⁹, Y. Yamaguchi¹⁵⁴, E. Yamashita¹⁵³, H. Yamauchi¹⁵⁷, T. Yamazaki^{17a}, Y. Yamazaki⁸⁴, J. Yan^{62c}, S. Yan¹²⁶, Z. Yan²⁵, H.J. Yang^{62c,62d}, H.T. Yang^{62a}, S. Yang^{62a}, T. Yang^{64c}, X. Yang^{62a}, X. Yang^{14a}, Y. Yang⁴⁴, Y. Yang^{62a}, Z. Yang^{62a,106}, W-M. Yao^{17a}, Y.C. Yap⁴⁸, H. Ye^{14c}, H. Ye⁵⁵, J. Ye⁴⁴, S. Ye²⁹, X. Ye^{62a}, Y. Yeh⁹⁶, I. Yeletsikh³⁸, B.K. Yeo^{17a}, M.R. Yexley⁹¹, P. Yin⁴¹, K. Yorita¹⁶⁸, S. Younas^{27b}, C.J.S. Young⁵⁴, C. Young¹⁴³, Y. Yu^{62a}, M. Yuan¹⁰⁶, R. Yuan^{62b,1}, L. Yue⁹⁶, M. Zaazoua^{35e}, B. Zabinski⁸⁶, E. Zaid⁵², T. Zakareishvili^{149b}, N. Zakharchuk³⁴, S. Zambito⁵⁶, J.A. Zamora Saa^{137d,137b}, J. Zang¹⁵³, D. Zanzi⁵⁴, O. Zaplatilek¹³², C. Zeitnitz¹⁷¹, H. Zeng^{14a}, J.C. Zeng¹⁶², D.T. Zenger Jr²⁶, O. Zenin³⁷, T. Ženiš^{28a}, S. Zenz⁹⁴, S. Zerradi^{35a}, D. Zerwas⁶⁶, M. Zhai^{14a,14e}, B. Zhang^{14c}, D.F. Zhang¹³⁹, J. Zhang^{62b}, J. Zhang⁶, K. Zhang^{14a,14e}, L. Zhang^{14c}, P. Zhang^{14a,14e}, R. Zhang¹⁷⁰, S. Zhang¹⁰⁶, T. Zhang¹⁵³, X. Zhang^{62c}, X. Zhang^{62b}, Y. Zhang^{62c,5}, Y. Zhang⁹⁶, Z. Zhang^{17a}, Z. Zhang⁶⁶, H. Zhao¹³⁸, P. Zhao⁵¹, T. Zhao^{62b}, Y. Zhao¹³⁶, Z. Zhao^{62a}, A. Zhemchugov³⁸, K. Zheng¹⁶², X. Zheng^{62a}, Z. Zheng¹⁴³, D. Zhong¹⁶², B. Zhou¹⁰⁶, H. Zhou⁷, N. Zhou^{62c}, Y. Zhou⁷, C.G. Zhu^{62b}, J. Zhu¹⁰⁶, Y. Zhu^{62c}, Y. Zhu^{62a}, X. Zhuang^{14a}, K. Zhukov³⁷, V. Zhulanov³⁷, N.I. Zimine³⁸, J. Zinsser^{63b}, M. Ziolkowski¹⁴¹, L. Živković¹⁵, A. Zoccoli^{23b,23a}, K. Zoch⁵⁶, T.G. Zorbas¹³⁹, O. Zormpa⁴⁶, W. Zou⁴¹, L. Zwalinski³⁶.

¹Department of Physics, University of Adelaide, Adelaide; Australia.

²Department of Physics, University of Alberta, Edmonton AB; Canada.

³(^a)Department of Physics, Ankara University, Ankara; (^b)Division of Physics, TOBB University of Economics and Technology, Ankara; Türkiye.

⁴LAPP, Université Savoie Mont Blanc, CNRS/IN2P3, Annecy; France.

⁵APC, Université Paris Cité, CNRS/IN2P3, Paris; France.

⁶High Energy Physics Division, Argonne National Laboratory, Argonne IL; United States of America.

⁷Department of Physics, University of Arizona, Tucson AZ; United States of America.

⁸Department of Physics, University of Texas at Arlington, Arlington TX; United States of America.

⁹Physics Department, National and Kapodistrian University of Athens, Athens; Greece.

¹⁰Physics Department, National Technical University of Athens, Zografou; Greece.

¹¹Department of Physics, University of Texas at Austin, Austin TX; United States of America.

¹²Institute of Physics, Azerbaijan Academy of Sciences, Baku; Azerbaijan.

¹³Institut de Física d'Altes Energies (IFAE), Barcelona Institute of Science and Technology, Barcelona; Spain.

¹⁴(^a)Institute of High Energy Physics, Chinese Academy of Sciences, Beijing; (^b)Physics Department, Tsinghua University, Beijing; (^c)Department of Physics, Nanjing University, Nanjing; (^d)School of Science, Shenzhen Campus of Sun Yat-sen University; (^e)University of Chinese Academy of Science (UCAS), Beijing; China.

¹⁵Institute of Physics, University of Belgrade, Belgrade; Serbia.

¹⁶Department for Physics and Technology, University of Bergen, Bergen; Norway.

- ^{17(a)}Physics Division, Lawrence Berkeley National Laboratory, Berkeley CA;^(b)University of California, Berkeley CA; United States of America.
- ¹⁸Institut für Physik, Humboldt Universität zu Berlin, Berlin; Germany.
- ¹⁹Albert Einstein Center for Fundamental Physics and Laboratory for High Energy Physics, University of Bern, Bern; Switzerland.
- ²⁰School of Physics and Astronomy, University of Birmingham, Birmingham; United Kingdom.
- ^{21(a)}Department of Physics, Bogazici University, Istanbul;^(b)Department of Physics Engineering, Gaziantep University, Gaziantep;^(c)Department of Physics, Istanbul University, Istanbul;^(d)Istinye University, Sariyer, Istanbul; Türkiye.
- ^{22(a)}Facultad de Ciencias y Centro de Investigaciones, Universidad Antonio Nariño, Bogotá;^(b)Departamento de Física, Universidad Nacional de Colombia, Bogotá;^(c)Pontificia Universidad Javeriana, Bogota; Colombia.
- ^{23(a)}Dipartimento di Fisica e Astronomia A. Righi, Università di Bologna, Bologna;^(b)INFN Sezione di Bologna; Italy.
- ²⁴Physikalisches Institut, Universität Bonn, Bonn; Germany.
- ²⁵Department of Physics, Boston University, Boston MA; United States of America.
- ²⁶Department of Physics, Brandeis University, Waltham MA; United States of America.
- ^{27(a)}Transilvania University of Brasov, Brasov;^(b)Horia Hulubei National Institute of Physics and Nuclear Engineering, Bucharest;^(c)Department of Physics, Alexandru Ioan Cuza University of Iasi, Iasi;^(d)National Institute for Research and Development of Isotopic and Molecular Technologies, Physics Department, Cluj-Napoca;^(e)University Politehnica Bucharest, Bucharest;^(f)West University in Timisoara, Timisoara;^(g)Faculty of Physics, University of Bucharest, Bucharest; Romania.
- ^{28(a)}Faculty of Mathematics, Physics and Informatics, Comenius University, Bratislava;^(b)Department of Subnuclear Physics, Institute of Experimental Physics of the Slovak Academy of Sciences, Kosice; Slovak Republic.
- ²⁹Physics Department, Brookhaven National Laboratory, Upton NY; United States of America.
- ³⁰Universidad de Buenos Aires, Facultad de Ciencias Exactas y Naturales, Departamento de Física, y CONICET, Instituto de Física de Buenos Aires (IFIBA), Buenos Aires; Argentina.
- ³¹California State University, CA; United States of America.
- ³²Cavendish Laboratory, University of Cambridge, Cambridge; United Kingdom.
- ^{33(a)}Department of Physics, University of Cape Town, Cape Town;^(b)iThemba Labs, Western Cape;^(c)Department of Mechanical Engineering Science, University of Johannesburg, Johannesburg;^(d)National Institute of Physics, University of the Philippines Diliman (Philippines);^(e)University of South Africa, Department of Physics, Pretoria;^(f)University of Zululand, KwaDlangezwa;^(g)School of Physics, University of the Witwatersrand, Johannesburg; South Africa.
- ³⁴Department of Physics, Carleton University, Ottawa ON; Canada.
- ^{35(a)}Faculté des Sciences Ain Chock, Réseau Universitaire de Physique des Hautes Energies - Université Hassan II, Casablanca;^(b)Faculté des Sciences, Université Ibn-Tofail, Kénitra;^(c)Faculté des Sciences Semlalia, Université Cadi Ayyad, LPHEA-Marrakech;^(d)LPMR, Faculté des Sciences, Université Mohamed Premier, Oujda;^(e)Faculté des sciences, Université Mohammed V, Rabat;^(f)Institute of Applied Physics, Mohammed VI Polytechnic University, Ben Guerir; Morocco.
- ³⁶CERN, Geneva; Switzerland.
- ³⁷Affiliated with an institute covered by a cooperation agreement with CERN.
- ³⁸Affiliated with an international laboratory covered by a cooperation agreement with CERN.
- ³⁹Enrico Fermi Institute, University of Chicago, Chicago IL; United States of America.
- ⁴⁰LPC, Université Clermont Auvergne, CNRS/IN2P3, Clermont-Ferrand; France.
- ⁴¹Nevis Laboratory, Columbia University, Irvington NY; United States of America.

- ⁴²Niels Bohr Institute, University of Copenhagen, Copenhagen; Denmark.
- ⁴³(^a)Dipartimento di Fisica, Università della Calabria, Rende; (^b)INFN Gruppo Collegato di Cosenza, Laboratori Nazionali di Frascati; Italy.
- ⁴⁴Physics Department, Southern Methodist University, Dallas TX; United States of America.
- ⁴⁵Physics Department, University of Texas at Dallas, Richardson TX; United States of America.
- ⁴⁶National Centre for Scientific Research "Demokritos", Agia Paraskevi; Greece.
- ⁴⁷(^a)Department of Physics, Stockholm University; (^b)Oskar Klein Centre, Stockholm; Sweden.
- ⁴⁸Deutsches Elektronen-Synchrotron DESY, Hamburg and Zeuthen; Germany.
- ⁴⁹Fakultät Physik , Technische Universität Dortmund, Dortmund; Germany.
- ⁵⁰Institut für Kern- und Teilchenphysik, Technische Universität Dresden, Dresden; Germany.
- ⁵¹Department of Physics, Duke University, Durham NC; United States of America.
- ⁵²SUPA - School of Physics and Astronomy, University of Edinburgh, Edinburgh; United Kingdom.
- ⁵³INFN e Laboratori Nazionali di Frascati, Frascati; Italy.
- ⁵⁴Physikalisches Institut, Albert-Ludwigs-Universität Freiburg, Freiburg; Germany.
- ⁵⁵II. Physikalisches Institut, Georg-August-Universität Göttingen, Göttingen; Germany.
- ⁵⁶Département de Physique Nucléaire et Corpusculaire, Université de Genève, Genève; Switzerland.
- ⁵⁷(^a)Dipartimento di Fisica, Università di Genova, Genova; (^b)INFN Sezione di Genova; Italy.
- ⁵⁸II. Physikalisches Institut, Justus-Liebig-Universität Giessen, Giessen; Germany.
- ⁵⁹SUPA - School of Physics and Astronomy, University of Glasgow, Glasgow; United Kingdom.
- ⁶⁰LPSC, Université Grenoble Alpes, CNRS/IN2P3, Grenoble INP, Grenoble; France.
- ⁶¹Laboratory for Particle Physics and Cosmology, Harvard University, Cambridge MA; United States of America.
- ⁶²(^a)Department of Modern Physics and State Key Laboratory of Particle Detection and Electronics, University of Science and Technology of China, Hefei; (^b)Institute of Frontier and Interdisciplinary Science and Key Laboratory of Particle Physics and Particle Irradiation (MOE), Shandong University, Qingdao; (^c)School of Physics and Astronomy, Shanghai Jiao Tong University, Key Laboratory for Particle Astrophysics and Cosmology (MOE), SKLPPC, Shanghai; (^d)Tsung-Dao Lee Institute, Shanghai; China.
- ⁶³(^a)Kirchhoff-Institut für Physik, Ruprecht-Karls-Universität Heidelberg, Heidelberg; (^b)Physikalisches Institut, Ruprecht-Karls-Universität Heidelberg, Heidelberg; Germany.
- ⁶⁴(^a)Department of Physics, Chinese University of Hong Kong, Shatin, N.T., Hong Kong; (^b)Department of Physics, University of Hong Kong, Hong Kong; (^c)Department of Physics and Institute for Advanced Study, Hong Kong University of Science and Technology, Clear Water Bay, Kowloon, Hong Kong; China.
- ⁶⁵Department of Physics, National Tsing Hua University, Hsinchu; Taiwan.
- ⁶⁶IJCLab, Université Paris-Saclay, CNRS/IN2P3, 91405, Orsay; France.
- ⁶⁷Centro Nacional de Microelectrónica (IMB-CNM-CSIC), Barcelona; Spain.
- ⁶⁸Department of Physics, Indiana University, Bloomington IN; United States of America.
- ⁶⁹(^a)INFN Gruppo Collegato di Udine, Sezione di Trieste, Udine; (^b)ICTP, Trieste; (^c)Dipartimento Politecnico di Ingegneria e Architettura, Università di Udine, Udine; Italy.
- ⁷⁰(^a)INFN Sezione di Lecce; (^b)Dipartimento di Matematica e Fisica, Università del Salento, Lecce; Italy.
- ⁷¹(^a)INFN Sezione di Milano; (^b)Dipartimento di Fisica, Università di Milano, Milano; Italy.
- ⁷²(^a)INFN Sezione di Napoli; (^b)Dipartimento di Fisica, Università di Napoli, Napoli; Italy.
- ⁷³(^a)INFN Sezione di Pavia; (^b)Dipartimento di Fisica, Università di Pavia, Pavia; Italy.
- ⁷⁴(^a)INFN Sezione di Pisa; (^b)Dipartimento di Fisica E. Fermi, Università di Pisa, Pisa; Italy.
- ⁷⁵(^a)INFN Sezione di Roma; (^b)Dipartimento di Fisica, Sapienza Università di Roma, Roma; Italy.
- ⁷⁶(^a)INFN Sezione di Roma Tor Vergata; (^b)Dipartimento di Fisica, Università di Roma Tor Vergata, Roma; Italy.
- ⁷⁷(^a)INFN Sezione di Roma Tre; (^b)Dipartimento di Matematica e Fisica, Università Roma Tre, Roma;

Italy.

^{78(a)}INFN-TIFPA;^(b)Università degli Studi di Trento, Trento; Italy.

⁷⁹Universität Innsbruck, Department of Astro and Particle Physics, Innsbruck; Austria.

⁸⁰University of Iowa, Iowa City IA; United States of America.

⁸¹Department of Physics and Astronomy, Iowa State University, Ames IA; United States of America.

^{82(a)}Departamento de Engenharia Elétrica, Universidade Federal de Juiz de Fora (UFJF), Juiz de Fora;^(b)Universidade Federal do Rio De Janeiro COPPE/EE/IF, Rio de Janeiro;^(c)Instituto de Física, Universidade de São Paulo, São Paulo;^(d)Rio de Janeiro State University, Rio de Janeiro; Brazil.

⁸³KEK, High Energy Accelerator Research Organization, Tsukuba; Japan.

⁸⁴Graduate School of Science, Kobe University, Kobe; Japan.

^{85(a)}AGH University of Science and Technology, Faculty of Physics and Applied Computer Science, Krakow;^(b)Marian Smoluchowski Institute of Physics, Jagiellonian University, Krakow; Poland.

⁸⁶Institute of Nuclear Physics Polish Academy of Sciences, Krakow; Poland.

⁸⁷Faculty of Science, Kyoto University, Kyoto; Japan.

⁸⁸Kyoto University of Education, Kyoto; Japan.

⁸⁹Research Center for Advanced Particle Physics and Department of Physics, Kyushu University, Fukuoka ; Japan.

⁹⁰Instituto de Física La Plata, Universidad Nacional de La Plata and CONICET, La Plata; Argentina.

⁹¹Physics Department, Lancaster University, Lancaster; United Kingdom.

⁹²Oliver Lodge Laboratory, University of Liverpool, Liverpool; United Kingdom.

⁹³Department of Experimental Particle Physics, Jožef Stefan Institute and Department of Physics, University of Ljubljana, Ljubljana; Slovenia.

⁹⁴School of Physics and Astronomy, Queen Mary University of London, London; United Kingdom.

⁹⁵Department of Physics, Royal Holloway University of London, Egham; United Kingdom.

⁹⁶Department of Physics and Astronomy, University College London, London; United Kingdom.

⁹⁷Louisiana Tech University, Ruston LA; United States of America.

⁹⁸Fysiska institutionen, Lunds universitet, Lund; Sweden.

⁹⁹Departamento de Física Teórica C-15 and CIAFF, Universidad Autónoma de Madrid, Madrid; Spain.

¹⁰⁰Institut für Physik, Universität Mainz, Mainz; Germany.

¹⁰¹School of Physics and Astronomy, University of Manchester, Manchester; United Kingdom.

¹⁰²CPPM, Aix-Marseille Université, CNRS/IN2P3, Marseille; France.

¹⁰³Department of Physics, University of Massachusetts, Amherst MA; United States of America.

¹⁰⁴Department of Physics, McGill University, Montreal QC; Canada.

¹⁰⁵School of Physics, University of Melbourne, Victoria; Australia.

¹⁰⁶Department of Physics, University of Michigan, Ann Arbor MI; United States of America.

¹⁰⁷Department of Physics and Astronomy, Michigan State University, East Lansing MI; United States of America.

¹⁰⁸Group of Particle Physics, University of Montreal, Montreal QC; Canada.

¹⁰⁹Fakultät für Physik, Ludwig-Maximilians-Universität München, München; Germany.

¹¹⁰Max-Planck-Institut für Physik (Werner-Heisenberg-Institut), München; Germany.

¹¹¹Graduate School of Science and Kobayashi-Maskawa Institute, Nagoya University, Nagoya; Japan.

¹¹²Department of Physics and Astronomy, University of New Mexico, Albuquerque NM; United States of America.

¹¹³Institute for Mathematics, Astrophysics and Particle Physics, Radboud University/Nikhef, Nijmegen; Netherlands.

¹¹⁴Nikhef National Institute for Subatomic Physics and University of Amsterdam, Amsterdam; Netherlands.

- ¹¹⁵Department of Physics, Northern Illinois University, DeKalb IL; United States of America.
- ¹¹⁶^(a)New York University Abu Dhabi, Abu Dhabi;^(b)University of Sharjah, Sharjah; United Arab Emirates.
- ¹¹⁷Department of Physics, New York University, New York NY; United States of America.
- ¹¹⁸Ochanomizu University, Otsuka, Bunkyo-ku, Tokyo; Japan.
- ¹¹⁹Ohio State University, Columbus OH; United States of America.
- ¹²⁰Homer L. Dodge Department of Physics and Astronomy, University of Oklahoma, Norman OK; United States of America.
- ¹²¹Department of Physics, Oklahoma State University, Stillwater OK; United States of America.
- ¹²²Palacký University, Joint Laboratory of Optics, Olomouc; Czech Republic.
- ¹²³Institute for Fundamental Science, University of Oregon, Eugene, OR; United States of America.
- ¹²⁴Graduate School of Science, Osaka University, Osaka; Japan.
- ¹²⁵Department of Physics, University of Oslo, Oslo; Norway.
- ¹²⁶Department of Physics, Oxford University, Oxford; United Kingdom.
- ¹²⁷LPNHE, Sorbonne Université, Université Paris Cité, CNRS/IN2P3, Paris; France.
- ¹²⁸Department of Physics, University of Pennsylvania, Philadelphia PA; United States of America.
- ¹²⁹Department of Physics and Astronomy, University of Pittsburgh, Pittsburgh PA; United States of America.
- ¹³⁰^(a)Laboratório de Instrumentação e Física Experimental de Partículas - LIP, Lisboa;^(b)Departamento de Física, Faculdade de Ciências, Universidade de Lisboa, Lisboa;^(c)Departamento de Física, Universidade de Coimbra, Coimbra;^(d)Centro de Física Nuclear da Universidade de Lisboa, Lisboa;^(e)Departamento de Física, Universidade do Minho, Braga;^(f)Departamento de Física Teórica y del Cosmos, Universidad de Granada, Granada (Spain);^(g)Departamento de Física, Instituto Superior Técnico, Universidade de Lisboa, Lisboa; Portugal.
- ¹³¹Institute of Physics of the Czech Academy of Sciences, Prague; Czech Republic.
- ¹³²Czech Technical University in Prague, Prague; Czech Republic.
- ¹³³Charles University, Faculty of Mathematics and Physics, Prague; Czech Republic.
- ¹³⁴Particle Physics Department, Rutherford Appleton Laboratory, Didcot; United Kingdom.
- ¹³⁵IRFU, CEA, Université Paris-Saclay, Gif-sur-Yvette; France.
- ¹³⁶Santa Cruz Institute for Particle Physics, University of California Santa Cruz, Santa Cruz CA; United States of America.
- ¹³⁷^(a)Departamento de Física, Pontificia Universidad Católica de Chile, Santiago;^(b)Millennium Institute for Subatomic physics at high energy frontier (SAPHIR), Santiago;^(c)Instituto de Investigación Multidisciplinario en Ciencia y Tecnología, y Departamento de Física, Universidad de La Serena;^(d)Universidad Andres Bello, Department of Physics, Santiago;^(e)Instituto de Alta Investigación, Universidad de Tarapacá, Arica;^(f)Departamento de Física, Universidad Técnica Federico Santa María, Valparaíso; Chile.
- ¹³⁸Department of Physics, University of Washington, Seattle WA; United States of America.
- ¹³⁹Department of Physics and Astronomy, University of Sheffield, Sheffield; United Kingdom.
- ¹⁴⁰Department of Physics, Shinshu University, Nagano; Japan.
- ¹⁴¹Department Physik, Universität Siegen, Siegen; Germany.
- ¹⁴²Department of Physics, Simon Fraser University, Burnaby BC; Canada.
- ¹⁴³SLAC National Accelerator Laboratory, Stanford CA; United States of America.
- ¹⁴⁴Department of Physics, Royal Institute of Technology, Stockholm; Sweden.
- ¹⁴⁵Departments of Physics and Astronomy, Stony Brook University, Stony Brook NY; United States of America.
- ¹⁴⁶Department of Physics and Astronomy, University of Sussex, Brighton; United Kingdom.

- ¹⁴⁷School of Physics, University of Sydney, Sydney; Australia.
- ¹⁴⁸Institute of Physics, Academia Sinica, Taipei; Taiwan.
- ¹⁴⁹^(a)E. Andronikashvili Institute of Physics, Iv. Javakhishvili Tbilisi State University, Tbilisi;^(b)High Energy Physics Institute, Tbilisi State University, Tbilisi;^(c)University of Georgia, Tbilisi; Georgia.
- ¹⁵⁰Department of Physics, Technion, Israel Institute of Technology, Haifa; Israel.
- ¹⁵¹Raymond and Beverly Sackler School of Physics and Astronomy, Tel Aviv University, Tel Aviv; Israel.
- ¹⁵²Department of Physics, Aristotle University of Thessaloniki, Thessaloniki; Greece.
- ¹⁵³International Center for Elementary Particle Physics and Department of Physics, University of Tokyo, Tokyo; Japan.
- ¹⁵⁴Department of Physics, Tokyo Institute of Technology, Tokyo; Japan.
- ¹⁵⁵Department of Physics, University of Toronto, Toronto ON; Canada.
- ¹⁵⁶^(a)TRIUMF, Vancouver BC;^(b)Department of Physics and Astronomy, York University, Toronto ON; Canada.
- ¹⁵⁷Division of Physics and Tomonaga Center for the History of the Universe, Faculty of Pure and Applied Sciences, University of Tsukuba, Tsukuba; Japan.
- ¹⁵⁸Department of Physics and Astronomy, Tufts University, Medford MA; United States of America.
- ¹⁵⁹United Arab Emirates University, Al Ain; United Arab Emirates.
- ¹⁶⁰Department of Physics and Astronomy, University of California Irvine, Irvine CA; United States of America.
- ¹⁶¹Department of Physics and Astronomy, University of Uppsala, Uppsala; Sweden.
- ¹⁶²Department of Physics, University of Illinois, Urbana IL; United States of America.
- ¹⁶³Instituto de Física Corpuscular (IFIC), Centro Mixto Universidad de Valencia - CSIC, Valencia; Spain.
- ¹⁶⁴Department of Physics, University of British Columbia, Vancouver BC; Canada.
- ¹⁶⁵Department of Physics and Astronomy, University of Victoria, Victoria BC; Canada.
- ¹⁶⁶Fakultät für Physik und Astronomie, Julius-Maximilians-Universität Würzburg, Würzburg; Germany.
- ¹⁶⁷Department of Physics, University of Warwick, Coventry; United Kingdom.
- ¹⁶⁸Waseda University, Tokyo; Japan.
- ¹⁶⁹Department of Particle Physics and Astrophysics, Weizmann Institute of Science, Rehovot; Israel.
- ¹⁷⁰Department of Physics, University of Wisconsin, Madison WI; United States of America.
- ¹⁷¹Fakultät für Mathematik und Naturwissenschaften, Fachgruppe Physik, Bergische Universität Wuppertal, Wuppertal; Germany.
- ¹⁷²Department of Physics, Yale University, New Haven CT; United States of America.
- ^a Also Affiliated with an institute covered by a cooperation agreement with CERN.
- ^b Also at An-Najah National University, Nablus; Palestine.
- ^c Also at Borough of Manhattan Community College, City University of New York, New York NY; United States of America.
- ^d Also at Bruno Kessler Foundation, Trento; Italy.
- ^e Also at Center for High Energy Physics, Peking University; China.
- ^f Also at Center for Interdisciplinary Research and Innovation (CIRI-AUTH), Thessaloniki ; Greece.
- ^g Also at Centro Studi e Ricerche Enrico Fermi; Italy.
- ^h Also at CERN, Geneva; Switzerland.
- ⁱ Also at Département de Physique Nucléaire et Corpusculaire, Université de Genève, Genève; Switzerland.
- ^j Also at Departament de Física de la Universitat Autònoma de Barcelona, Barcelona; Spain.
- ^k Also at Department of Financial and Management Engineering, University of the Aegean, Chios; Greece.
- ^l Also at Department of Physics and Astronomy, Michigan State University, East Lansing MI; United States of America.
- ^m Also at Department of Physics, Ben Gurion University of the Negev, Beer Sheva; Israel.

- ⁿ Also at Department of Physics, California State University, East Bay; United States of America.
- ^o Also at Department of Physics, California State University, Sacramento; United States of America.
- ^p Also at Department of Physics, King's College London, London; United Kingdom.
- ^q Also at Department of Physics, Stanford University, Stanford CA; United States of America.
- ^r Also at Department of Physics, University of Fribourg, Fribourg; Switzerland.
- ^s Also at Department of Physics, University of Thessaly; Greece.
- ^t Also at Department of Physics, Westmont College, Santa Barbara; United States of America.
- ^u Also at Hellenic Open University, Patras; Greece.
- ^v Also at Institutio Catalana de Recerca i Estudis Avancats, ICREA, Barcelona; Spain.
- ^w Also at Institut für Experimentalphysik, Universität Hamburg, Hamburg; Germany.
- ^x Also at Institute for Nuclear Research and Nuclear Energy (INRNE) of the Bulgarian Academy of Sciences, Sofia; Bulgaria.
- ^y Also at Institute of Applied Physics, Mohammed VI Polytechnic University, Ben Guerir; Morocco.
- ^z Also at Institute of Particle Physics (IPP); Canada.
- ^{aa} Also at Institute of Physics and Technology, Ulaanbaatar; Mongolia.
- ^{ab} Also at Institute of Physics, Azerbaijan Academy of Sciences, Baku; Azerbaijan.
- ^{ac} Also at Institute of Theoretical Physics, Ilia State University, Tbilisi; Georgia.
- ^{ad} Also at L2IT, Université de Toulouse, CNRS/IN2P3, UPS, Toulouse; France.
- ^{ae} Also at Lawrence Livermore National Laboratory, Livermore; United States of America.
- ^{af} Also at National Institute of Physics, University of the Philippines Diliman (Philippines); Philippines.
- ^{ag} Also at Technical University of Munich, Munich; Germany.
- ^{ah} Also at The Collaborative Innovation Center of Quantum Matter (CICQM), Beijing; China.
- ^{ai} Also at TRIUMF, Vancouver BC; Canada.
- ^{aj} Also at Università di Napoli Parthenope, Napoli; Italy.
- ^{ak} Also at University of Colorado Boulder, Department of Physics, Colorado; United States of America.
- ^{al} Also at Washington College, Chestertown, MD; United States of America.
- ^{am} Also at Yeditepe University, Physics Department, Istanbul; Türkiye.
- * Deceased